# New imaging strategies in neuroendocrine tumors

van Asselt, Sophie

*DOI:*
10.1016/j.gie.2014.09.037

# New imaging strategies in neuroendocrine tumors

Sophie van Asselt

Financially support for printing of this thesis is kindly provided by:
The Endocrinology Fund, as part of the Ubbo Emmius Fund
Stichting Werkgroep Interne Oncologie
Graduate School for Drug Exploration (GUIDE)
Rijksuniversiteit Groningen
Dutch Cancer Society.

The research presented in this thesis was financially supported by a grant of the Dutch Cancer Society (RUG 2008-4188).

Cover and layout: Johan de Jong & Sophie van Asselt
Groningen, The Netherlands

Printed by: Ipskamp Drukkers
Enschede, The Netherlands

ISBN: 978-90-367-6870-2

New imaging strategies in neuroendocrine tumors.

rijksuniversiteit
groningen

# New imaging strategies in neuroendocrine tumors

**Proefschrift**

ter verkrijging van de graad van doctor aan de
Rijksuniversiteit Groningen
op gezag van de
rector magnificus prof. dr. E. Sterken
en volgens besluit van het College voor Promoties.

De openbare verdediging zal plaatsvinden op

maandag 14 april 2014 om 12.45 uur

door

**Sophie Josephien van Asselt**

geboren op 4 juli 1984
te Hoogeveen

**Promotores:**
Prof. dr. T.P. Links
Prof. dr. E.G.E. de Vries

**Copromotores:**
Dr. A.H. Brouwers
Dr. H.M. van Dullemen

**Beoordelingscommissie:**
Prof. dr. B.H.R. Wolffenbuttel
Prof. dr. R.A.J.O. Dierckx
Prof. dr. C.J. Lips

# Contents

**Paranimfen:**
K.Y. Heida
A. van der Heide

# Chapter 1

## General introduction

# General introduction

Neuroendocrine tumors comprise tumors, which originate from (neuro)endocrine cells throughout the body. They are rare tumors with a reported incidence of 5/100,000.[1] Neuroendocrine tumors can produce biogenic amines, peptides or proteins with endocrine activity, and are called functional neuroendocrine tumors if overproduction causes clinical symptoms. Neuroendocrine tumors can be divided in low-grade, intermediate-grade and high-grade tumors. This grading system depends on the mitotic count and Ki-67 index which reflect growth rate of the tumor. Low-grade and intermediate-grade are also called well-differentiated neuroendocrine tumors. In general, these tumors have a better prognosis than their high-grade counterparts.[2-3] In this thesis only well-differentiated neuroendocrine tumors have been addressed. Neuroendocrine tumors can occur sporadically, but can also be part of the hereditary tumor syndromes von Hippel-Lindau (VHL) disease and Multiple Endocrine Neoplasia type 1 (MEN1). In both tumor syndromes, patients are prone to develop pancreatic neuroendocrine tumors.

VHL patients have a germline mutation in the *VHL* tumor suppressor gene, located on the short arm of chromosome 3 (3p25-26).[4] A second hit in the corresponding gene leads to development of VHL-related manifestations. Loss of functional VHL protein can result in increased production of vascular endothelial growth factor A (VEGF-A). VEGF-A induces angiogenesis. The prevalence of VHL disease is about 1-2/100,000 with an estimated birth incidence of 1 per 36,000-43,000 live births.[5-6] Next to pancreatic neuroendocrine tumors, VHL patients are also at risk to develop hemangioblastomas in the central nervous system, endolymphatic sac tumors of the middle ear, pheochromocytomas, clear cell renal cell cancer, renal cysts and pancreatic cysts.[7] Mortality in VHL patients is often the result of metastasized renal cell cancer and neurological complications caused by (progressive) hemangioblastomas.[8-9] VHL patients have a shorter life expectancy compared to the general population.[10] Currently, no biomarkers are available that can predict disease progression.

In patients in whom VHL was diagnosed after 1990, life expectancy was increased with 16 years compared to VHL patients diagnosed before 1985.[10] This is probably the result of improved screening and treatment options in the last decades. An increased survival in VHL patients might result in an increasing prevalence of pancreatic neuroendocrine tumors.

MEN1 is caused by a mutation in the *MEN1* tumor suppressor gene located at chromosome 11 (11q13). The prevalence of MEN1 is 1-10/100,000.[11] In MEN1 patients, the prevalence of pancreatic neuroendocrine tumors is 30-75%.[11-12] In MEN1 both non-functional as well as functional pancreatic neuroendocrine tumors can occur, of which gastrinomas and insulinomas are most common. In addition to pancreatic neuroendocrine tumors, MEN1 patients are also prone to develop other tumors, including parathyroid and pituitary adenomas. In MEN1 patients, 33% of the mortality is MEN1-related, of which pancreatic neuroendocrine tumors are the leading cause of death.[13-15]

For localization of pancreatic neuroendocrine tumors, different anatomical and molecular imaging techniques are available. Anatomical imaging includes computed tomography (CT), magnetic resonance imaging (MRI), transabdominal ultrasound and endoscopic ultrasound (EUS). For molecular imaging tracers are available specific for neuroendocrine tumors, including somatostatin receptor scintigraphy (SRS). Positron emission tomography (PET) is available for pancreatic neuroendocrine tumors with the specific tracers 6-[F-18]fluoro-L-dihydrophenylalanin ($^{18}$F-DOPA) and $^{11}$C-5-hydroytryptophan ($^{11}$C-5-HTP), based on the ability of amine precursor uptake and decarboxylation of neuroendocrine tumor cells. $^{11}$C-5-HTP PET combined with CT is superior for detection of pancreatic neuroendocrine tumors in patients known with advanced disease.[16] Based on the available literature, EUS seems a promising method for early detection of pancreatic neuroendocrine tumors.[17]

Screening is recommended in both VHL disease and MEN1 for early tumor lesion detection. For screening of the kidneys, adrenal gland and pancreas, the international VHL guideline recommends a high quality transabdominal ultrasound every year and MRI at least every other year.[18] For pancreatic neuroendocrine tumor localization, the recently revised expert opinion based MEN1 guideline recommends MRI, CT or EUS once every year.[19] The earlier MEN1 guideline recommended MRI or CT, and SRS once every 3 years.[12] Unfortunately, the level of evidence of these recommendations is low. It is unknown which imaging technique is best for early detection of pancreatic neuroendocrine tumors in both VHL and MEN1 patients.

The only curative treatment of neuroendocrine tumors is surgery. Compared to epithelial tumors, neuroendocrine tumors often behave indolent, but can also act more aggressive and/or become resistant to treatment. Currently, more treatment options consisting of targeted agents are becoming available for patients with advanced/metastasized disease.[20] These are the consequences of the increasing knowledge on cell biological behavior of these tumors. Neuroendocrine tumors often are hypervascular. The VEGF-A receptor tyrosine kinase inhibitor sunitinib and the mTOR inhibitor everolimus have beneficial effect in patients with advanced pancreatic neuroendocrine tumors.[21-22] Bevacizumab is an antibody which binds VEGF-A. Currently, VEGF-A can be imaged with PET by zirconium-89 ($^{89}Zr$) labeled bevacizumab. Imaging with $^{89}Zr$-bevacizumab PET can potentially provide information about VEGF-A status at the tumor site non-invasively.

## Aim of the thesis

The aim of this thesis is to evaluate EUS and $^{11}C$-5-HTP PET for the early detection of pancreatic neuroendocrine tumors in VHL and MEN1 patients. Moreover, in VHL patients and patients with advanced progressive neuroendocrine tumors, we evaluated the feasibility of $^{89}Zr$-bevacizumab PET to visualize VEGF-A in lesions.

## Outline of the thesis

VHL disease is the only hereditary tumor syndrome with a high prevalence (~70%) of cysts located in the pancreas.[23] Using the monogenetic disorder VHL disease as a model might give insight in the pathophysiology of pancreatic cysts in general from a VHL point of view. In **chapter 2** we reviewed the literature to explain pancreatic cyst development. We searched the literature for *in vitro* and *in vivo* VHL models for (pancreatic) cyst development. PubMed search terms included von Hippel-Lindau and pancreatic cysts or cystadenoma, pancreatic serous cystic neoplasms, pancreatic neuroendocrine tumors or neoplasms, histopathology, *VHL*, pVHL, extracellular matrix, cytoskeleton and cilia. Due to the limited number articles of pancreatic cysts in VHL disease, no time restrictions were made. No studies could be retrieved on the role of *VHL* mutations in pancreatic cell lines, so we reviewed other VHL-related *in vitro* studies. Only articles in English were included. Relevant references from the selected articles were also reviewed.

In VHL patients the prevalence of pancreatic neuroendocrine tumors is 10-17%.[23-24] Unlike MEN1, only non-functional pancreatic neuroendocrine tumors occur in VHL disease. Next to pancreatic neuroendocrine tumors, pancreatic cysts occur in VHL, with some mimicking neuroendocrine tumors, since they can harbor a solid appearance on imaging. Since it is unknown which imaging method is best, the aim of the study reported in **chapter 3** was to evaluate the value of linear EUS and $^{11}C$-5-HTP PET versus CT/MRI+ SRS for detection of pancreatic solid lesions suspected for neuroendocrine tumors in VHL patients. Eligible patients were those with genetically proven VHL or patients with clinically proven VHL with a 1$^{st}$ grade family member with genetically confirmed VHL, with an age of ≥ 18 years. Excluded were pregnant patients and patients known with alcohol abuses and/or chronic pancreatitis. CT/MRI+ SRS were performed in patients' own center, before patients underwent linear EUS and $^{11}$C-5-HTP PET at the University Medical Center of Groningen. Patient and lesion-based positivity for pancreatic solid lesions were calculated for all imaging techniques, by using the total outcome of the four imaging techniques as a composite reference standard.

Since evidence is limited for the best imaging method for MEN1 screening, we report in **chapter 4** a prospective study in MEN1 patients in which the value was assessed of linear EUS and $^{11}$C-5-HTP-PET versus CT/MRI+ SRS for early detection of pancreatic lesions. Eligible were patients with ≥ 18 years of age, with genetically proven MEN1 or patients with clinically proven MEN1 with a 1$^{st}$ grade family member with genetically confirmed MEN1. CT/MRI+ SRS were performed in patients' own center, before patients underwent EUS and $^{11}$C-5-HTP PET at the University Medical Center of Groningen. Patient and lesion-based positivity for pancreatic lesions were calculated for all imaging techniques, by using the total outcome of the four imaging techniques as a composite reference standard.

The *VHL* gene encodes for the VHL protein. The VHL protein is part of an E3-ubiquitin ligase complex in the cell, responsible for degradation of the α-subunit of the transcription factor hypoxia inducible factor (HIF) in normoxic conditions. During hypoxia, HIF-α will not be degraded, resulting in transport of HIF-α to the nucleus. Together with the ß-subunit HIF is formed, resulting in gene transcription that enhances cell survival. This includes expression of VEGF-A. If the VHL protein function is lost, HIF-α accumulates which subsequently can result in development of both benign and malignant lesions.[5]

Currently in VHL disease, no biomarkers are available to predict disease progression. Overexpression of VEGF-A has been shown in VHL-related hemangioblastomas and renal cell cancer.[25] Bevacizumab is an IgG1 antibody which binds VEGF-A. The aim of the study described in **chapter 5** was to assess if $^{89}$Zr-bevacizumab PET can visualize manifestations in VHL patients, and if $^{89}$Zr-bevacizumab uptake in non-malignant lesions can predict progression. Included were VHL patients known with hemangioblastomas located in the central nervous system, visualized on MRI. In addition to the recent VHL screening, a PET scan was performed 4 days after administration of the tracer $^{89}$Zr-bevacizumab. VHL conventional screening was repeated within 12 months. $^{89}$Zr-bevacizumab PET and MRI scans were fused in order to identify the specific VHL manifestations that were imaged with $^{89}$Zr-bevacizumab PET. Lesion growth and/or presence of new VHL manifestations were assessed and it was evaluated if $^{89}$Zr-bevacizumab positive manifestations was associated with progressive disease based on conventional imaging and/or clinical progression.

More treatment options are becoming available for patients with advanced progressive neuroendocrine tumors.[20] Neuroendocrine tumors are hypervascular and VEGF-A is often present in tumor lesions.[26] In preclinical models, a down-stream effect of everolimus is VEGF-A inhibition.[27-28] Everolimus is effective in patients with advanced neuroendocrine tumors. [22, 29] Tumor VEGF-A production might lower during everolimus treatment in these patients. Therefore, in the feasibility study described in **chapter 6** we evaluated if tumor lesions can be visualized with $^{89}$Zr-bevacizumab PET in patients with advanced progressive neuroendocrine tumors. Moreover, we assessed if $^{89}$Zr-bevacizumab uptake in tumor lesions lowered after start of everolimus treatment. Included were patients > 18 years with well-differentiated neuroendocrine tumors progressive over the past year according to response evaluation criteria in solid tumors (RECIST) 1.1. At baseline, 2 weeks and 12 weeks a PET scan was performed 4 days after administration of the tracer $^{89}$Zr-bevacizumab. After the baseline PET scan, everolimus therapy was started and continued until occurrence of progression of disease or intolerable toxicity. A CT scan was performed at baseline and every 3 months for response evaluation according to RECIST1.1. The number of visualized lesions on $^{89}$Zr-bevacizumab PET was assessed and the maximum standardized uptake value ($SUV_{max}$) was calculated at baseline, 2 weeks and 12 weeks. Next to disease evaluation according to RECIST1.1, serum chromogranin A, serum VEGF-A and whole blood everolimus levels were assessed and correlated with $^{89}$Zr-bevacizumab PET outcomes.

**Chapter 7** gives a summary of the findings and addresses future perspectives and **chapter 8** gives a summary of this thesis in Dutch.

# References


1. Yao JC, Eisner MP, Leary C, et al. Population-based study of islet cell carcinoma. Ann Surg Oncol 2007;14:3492-3500.
2. Rindi G, Klöppel G, Alhman H, et al. TNM staging of foregut (neuro)endocrine tumors: a consensus proposal including a grading system. Vichows Arch 2006;449:395-401.
3. Rindi G, Klöppel G, Coulevard A, et al. TNM staging of midgut and hindgut (neuro) endocrine tumors: a consensus proposal including a grading system. Virchows Arch 2007;451:757-762.
4. Latif F, Tory K, Gnarra J, et al. Identification of the von Hippel-Lindau disease tumor suppressor gene. Science 1993;260:1317-1320.
5. Maher ER, Iselius L, Yates JR, et al. Von Hippel-Lindau disease: a genetic study. J Med Genet 1991;28:443-447.
6. Evans DG, Howard E, Giblin C, et al. Birth incidence and prevalence of tumor-prone syndromes: estimates from a UK family genetic register service. Am J Genet A 2010;152A:327-323.
7. Lonser RR, Glenn GM, Walther M, et al. Von Hippel-Lindau disease. Lancet 2003;361:2059-2067.
8. Maher ER, Yates JR, Harries R, et al. Clinical features and natural history of von Hippel-Lindau disease. Q J Med 1990;77:1151-1163.
9. Neumann HP, Eggert HR, Scheremet R, et al. Central nervous system lesions in von Hippel-Lindau syndrome. J Neurol Neurosurg Psychiatry 1992;55:898-901.
10. Wilding A, Ingham SL, Lalloo F, et al. Life expectancy in hereditary cancer predisposing diseases: an observational study. J Med Genet 2012;49;264-269.
11. Pieterman CR, Vriens MR, Dreijerink KM, et al. Care for patients with multiple endocrine neoplasia type 1: the current evidence base. Fam Cancer 2011;10:157-171.
12. Brandi ML, Gagel RF, Angeli A, et al. Guidelines for diagnosis and therapy of MEN type 1 and type 2. J Clin Endocrinol Metab 2001;86:5658-5671.
13. Doherty GM, Olson JA, Frisella MM, et al. Lethality of multiple endocrine neoplasia type 1. World J Surg 1998;22:581-586.
14. Dean PG, van Heerden JA, Farley DR, et al. Are patients with multiple endocrine neoplasia type I prone to premature death? World J Surg 2000;24:1437-1441.
15. Goudet P, Murat A, Binquet C, et al. Risk factors and causes of death in MEN1 disease. A GTE (Groupe d'Etude des Tumeurs Endocrines) cohort study among 758 patients. World J Surg 2010;34:249-255.
16. Koopmans KP, Neels OC, Kema IP, et al. Improved staging of patients with carcinoid and islet cell tumors with $^{18}$F-dihydroxy-phenyl-alanine and $^{11}$C-5-hydroxy-tryptophan positron emission tomography. J Clin Oncol 2008;26:1489-1495.
17. Fiebrich HB, van Asselt SJ, Brouwers AH, et al. Tailored imaging of islet cell tumors of the pancreas amidst increasing options. Crit Rev Oncol Hematol 2012; 82:213-226.
18. http://www.vhl.org/handbook/vhlhb4.php#Suggested (Access date: 2 January 2014)
19. Thakker RV, Newey PJ, Walls GV, et al. Clinical practice guidelines for Multiple Endocrine Neoplasia Type 1 (MEN1). J Clin Endocrin Metab 2012;97:2990-3011.

20. Dong M, Phan AT, Yao JC. New strategies for advanced neuroendocrine tumors in the era of targeted therapy. Clin Cancer Res 2012;18:1830-1836.
21. Raymond E, Dahan L, Raoul JL, et al. Sunitinib malate for the treatment of pancreatic neuroendocrine tumors. N Engl J Med 2011;364:501-513.
22. Yao JC, Shah MH, Ito T, et al. RAD001 in advanced neuroendocrine tumors, Third (RADIANT-3) Study Group. Everolimus for advanced pancreatic neuroendocrine tumors. N Engl J Med 2011;364:514-523.
23. Hammel PR, Vilgrain V, Terris B, et al. Pancreatic involvement in von Hippel-Lindau disease. The Groupe Francophone d’Etude de la Maladie de von Hippel-Lindau. Gastroenterology 2000;119:1087-1095.
24. Blansfield JA, Choyke L, Morita SY, et al. Clinical, genetic and radiographic analysis of 108 patients with von Hippel-Lindau disease (VHL) manifested by pancreatic neuroendocrine neoplasms (PNETs). Surgery 2007;142:814-818.
25. Kim WY, Kaelin WG. Role of *VHL* gene mutation in human cancer. J Clin Oncol 2004;22:4991-5004.
26. Zhang J, Jia Z, Li Q, et al. Elevated expression of vascular endothelial growth factor correlates with increased angiogenesis and decreased progression-free survival among patients with low-grade neuroendocrine tumors. Cancer 2007;109:437-48.
27. Villaume K, Blanc M, Gouysse G, et al. VEGF secretion by neuroendocrine tumor cells is inhibited by octreotide and by inhibitors of the PI3K/AKT/mTOR pathway. Neuroendocrinology 2010;91:268-78.
28. Thomas GV, Tran C, Mellinghoff IK, et al. Hypoxia-inducible factor determines sensitivity to inhibitors of mTOR in kidney cancer. Nat Med 2006;12:122-7.
29. Pavel ME, Hainsworth JD, Baudin E, et al. Everolimus plus octreotide long-acting repeatable for the treatment of advanced neuroendocrine tumours associated with carcinoid syndrome (RADIANT-2): a randomised, placebo-controlled, phase 3 study. Lancet 2011;378:2005-2012.

# Chapter 2

## Pancreatic cyst development: insights from von Hippel-Lindau disease

Sophie J. van Asselt
Elisabeth G.E. de Vries
Hendrik M. van Dullemen
Adrienne H. Brouwers
Annemiek M.E. Walenkamp
Rachel H. Giles
Thera P. Links

***Published in Cilia 2013;2:3***

# Abstract

Pancreatic cysts are a heterogeneous group of lesions, which can be benign or malignant. Due to improved imaging techniques, physicians are more often confronted with pancreatic cysts. Little is known about the origin of pancreatic cysts in general. Von Hippel-Lindau (VHL) disease is an atypical ciliopathy and inherited tumor syndrome, caused by a mutation in the *VHL* tumor suppressor gene encoding the VHL protein (pVHL). VHL patients are prone to develop cysts and neuroendocrine tumors in the pancreas in addition to several other benign and malignant neoplasms. Remarkably, pancreatic cysts occur in approximately 70% of VHL patients, making it the only hereditary tumor syndrome with such a discernible expression of pancreatic cysts. Cellular loss of pVHL due to biallelic mutation can model pancreatic cystogenesis in other organisms, suggesting a causal relationship. Here, we give a comprehensive overview of various pVHL functions, focusing on those that can potentially explain pancreatic cyst development in VHL disease. Based on preclinical studies, cilia loss in ductal cells is probably an important early event in pancreatic cyst development.

# Introduction

Pancreatic cysts are frequent, with a prevalence of 2.4 to 13.5% in patients without known pancreatic disease. Due to increased use of cross-sectional imaging techniques, physicians are more frequently confronted with pancreatic cysts.[1] Various types of pancreatic cysts can occur, which can be benign or have malignant potential. An expectative policy is accepted for benign cysts and surgery is indicated for malignant lesions. Currently, accurate diagnostics are not available to identify malignant cysts.[1] Despite the need for mechanistic insight, little is known about the origin and pathophysiology of pancreatic cysts in general.

Von Hippel-Lindau (VHL) disease (MIM #193300) is a rare hereditary tumor syndrome that results from a germline mutation in the *VHL* gene. The reported incidence is 1 per 36,000 live births and a >90% penetrance is present by the age of 65 years.[2] VHL disease can lead to the development of hemangioblastomas of the central nervous system, retinal angiomas, endolymphatic sac tumors, epididymis or broad ligament cystadenomas, renal cysts and renal cell carcinomas (RCCs), pheochromocytomas, pancreatic cysts and pancreatic neuroendocrine tumors (pNETs)[3] (Figure 1). Currently, RCC and hemangioblastomas are the main causes of death.[4-5] VHL patients undergo screening for early detection of manifestations.[6] Understanding the role of the *VHL* gene in the oxygen-sensing pathway in the tumor micro-environment of RCC has led to major pharmaceutical successes through targeted therapies for many cancer types, such as humanized antibodies targeting vascular endothelial growth factor (VEGF), mTOR- and VEGF receptor tyrosine kinase inhibitors.[7] As a result, first-line treatment of metastasized RCCs has entirely changed in the last decade.

pNETs are present in 10 to 17% of VHL patients [8-9] and pancreatic cysts occur in about 70%.[10-11] Because of this high prevalence, it is worthwhile examining the early cellular events that result in pancreatic cysts in VHL disease, reflecting insight into pancreatic cystic disorders in general. In this review, we conduct a complete overview of pVHL functions to explain cellular events involved in cyst development in the context of VHL. Based on knock-out mouse models, we discuss the consequences of *Vhlh* loss in the pancreas and the origin of pancreatic cysts.

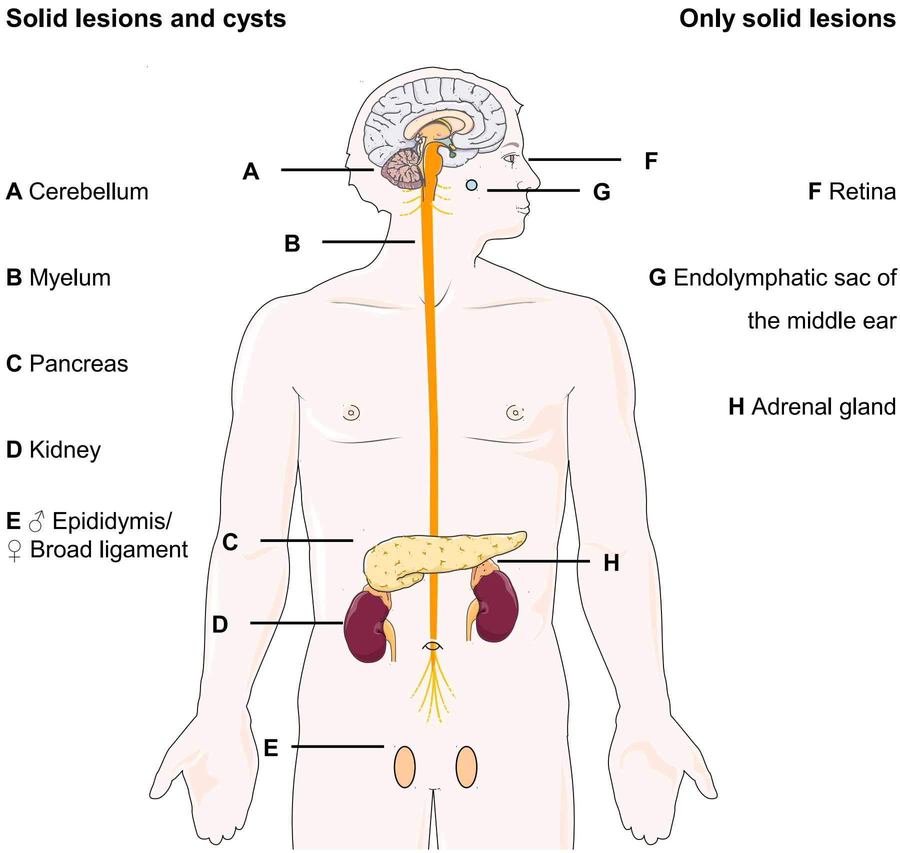


***Figure 1.*** *VHL disease can affect various organs. On the left, the organs in which cysts as well as solid lesions occur, have been listed and on the right are the locations in which only hypervascular solid lesions occur. (Constructed using Servier Medical art).*

## Pancreatic involvement in VHL disease

VHL pancreatic cysts include simple cysts and serous cystadenomas. In addition to these cysts pNETs occur in VHL patients, which can have malignant potential.[10] One autopsy series of 50 VHL patients showed a prevalence of 72% for pancreatic cysts.[11] In the largest clinical study describing pancreatic involvement, 158 VHL patients underwent abdominal computed tomography scan at least once. Pancreatic involvement was observed in 77% of patients: 71% had simple cysts, 15% had serous cystadenomas and 10% had pNETs, which coincided with pancreatic cysts in 11 cases (69%).[10] In VHL patients, a broad heterogeneity is present regarding pancreatic cyst involvement: isolated cystadenomas and small cysts occur, whereas in some patients cystic growth replaces almost the entire pancreas [10, 12-16] (Figure 2).

Data is limited about clinical consequences of VHL pancreatic cysts. One study [10] and numerous case-reports [12-13, 17-23] have recorded clinical problems, of which compression of the biliary tract was most frequently reported (Table 1). Intervention was indicated in only 3% of VHL patients.[10] No evidence exists for an association between endocrine or exocrine pancreatic insufficiency and cyst involvement. Moreover, no cases have been described of malignant pancreatic cysts in VHL disease. Nineteen cases with a pancreatic serous cystadenoma mixed with a pNET were reported,[10, 14-16, 24-25] but no relationship exists between presence of pancreatic cysts and pNETs. Conclusively, pancreatic cysts in VHL disease are not associated with malignancy and sporadically cause problems.[26]

**Table 1. Complications caused by pancreatic cysts in VHL disease**

| Reference [no] | No of patients | Symptoms | Diagnosis | Therapeutic intervention |
|---|---|---|---|---|
| [17] | 1 | Jaundice | Bile duct obstruction | Surgery |
| [19] | 1 | Jaundice | Bile duct obstruction | Biliary stent |
| [20] | 2 | Jaundice | Bile duct obstruction | Surgery |
| [12] | 2 | Jaundice | Bile duct obstruction | Surgery |
| [22] | 1 | Abdominal pain, jaundice and fever | Bile duct obstruction | Surgery |
| [23] | 1 | Pruritis | Bile duct obstruction | Surgery |
| [10] | 1 | Not reported | Necrotizing pancreatitis | Expectative |
| [10] | 2 | Abdominal pain | Pressure/ obstruction | 1 Drainage<br>1 Surgery |
| [21] | 1 | Vomiting | Pressure on stomach and duodenum | Surgery |
| [13] | 1 | Abdominal swelling | *Hemosuccus pancreaticus* | Surgery |
| [18] | 1 | Abdominal swelling | Duodenal compression | Surgery |

## VHL disease classification

The clearest genotype-phenotype correlation is exemplified by type 2 VHL, typically characterized by a *VHL* missense mutation and presence of pheochromocytomas.[27-28] Type 1 VHL is more frequently characterized by a *VHL* truncating mutation and absence or rare occurrence of pheochromocytomas. Type 2 *VHL* alleles can be further subdivided based on absence or presence of RCC; called VHL type 2A and type 2B, respectively.[28-29] A pheochromocytoma-only subtype has also been described:

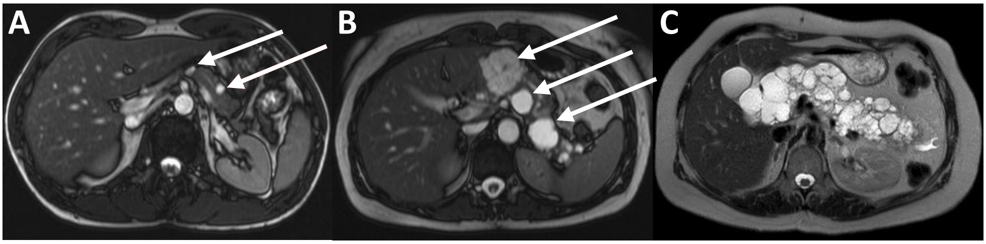


***Figure 2**. Axial MRI images of pancreatic involvement in three VHL patients. None of these patients had pancreas-related symptoms or exocrine/endocrine insufficiency. **A** Simple cysts (arrows) with size <1 cm in a 32 year old man; **B** A 4 cm sized serous microcystic cystadenoma (top arrow) is present next to multiple simple cysts (arrows) in a 39 year old woman; **C** Shows replacement of almost the entire pancreas by multiple cysts in a 47 year old woman.*

VHL type 2C.[30] Pancreatic involvement occurs in both VHL type 1 and type 2B, although it is unclear whether it occurs in the rare VHL types 2A and 2C.[31]

## The *VHL* gene

The *VHL* gene was identified in 1993 [32] and is a tumor suppressor gene; somatic inactivation of the wild-type allele or loss of heterozygosity (LOH) of the *VHL* gene is often observed prior to development of VHL-associated lesions.[33-34] Consisting of three exons, the human *VHL* gene is located on chromosome 3 (3p26-p25), encoding a 213-amino acid pVHL (30 kDa VHLp30) and a 160-amino acid shorter form (19 kDa VHLp19).[35-36] The role of *VHL* in the oxygen-sensing pathway is its best-characterized function: cellular normoxic conditions enable the pVHL E3 ubiquitin ligase complex to target the α-subunit of hypoxia inducible factor (HIF) for proteosomal degradation. During hypoxia, pVHL is not able to bind HIF-α, resulting in accumulation of un-ubiquitinated HIF-α, which then translocates to the nucleus. This stimulates the transcription of various genes, including *VEGF*.[37]

Since pVHL is still capable of functioning within the E3 ubiquitin ligase complex in VHL type 2C,[38] other pVHL functions must be present to induce tumorigenesis. Indeed, *VHL* also regulates the assembly of the extracellular matrix (ECM),[39-45] and recent studies have shown that pVHL regulates the microtubule cytoskeleton, particularly plus-end stability.[46-54]

## Sporadic pancreatic serous cystadenomas

Data suggest that *VHL* loss through LOH of chromosome 3p might be a common mechanism initiating cystogenesis in sporadic pancreatic cystadenomas.[55-56] Recently, whole-exome sequencing was performed in various sporadic pancreatic cysts.[57] Seven out of eight serous cystadenomas lost chromosome 3p alleles, and in four, *VHL* gene mutations were found. This further supports that *VHL* loss initiates cystogenesis in pancreatic cystadenomas. Given that loss of the *VHL* locus was the only recurrent lesion identified, these data indicate that *VHL* loss alone could be sufficient for this development. Interestingly, in this same study, intraductal papillary mucinous neoplasms, mucinous cystic neoplasms, and solid pseudopapillary neoplasms did not show alterations in 3p alleles. In these lesions other genes encoding E3 ubiquitin ligases were involved, pointing to protein turnover as an underlying mechanistic theme.[57]

## pVHL regulates cellular architecture

Most *in vitro* studies exploring the influence of pVHL on the cytoskeleton have been performed in RCC cell lines. To the best of our knowledge, no comparable studies have been performed with pancreatic cell lines. Since somatic LOH of wild-type *VHL* allele has been verified in pancreatic cysts in VHL,[58] we reviewed the existing literature based on RCC cell line studies to gain insight into the effect of pVHL on pancreatic cell regulation and cyst development. Figure 3 represents a schematic overview of pVHL functions which might also explain pancreatic cyst development in VHL disease.

### *pVHL and the extracellular matrix*

The ECM consists of proteins including collagen, fibronectin and laminin. Fibronectin plays a major role in the spread and migration of cells by binding them to the ECM. Integrins are cell surface receptors that mediate cell-cell and cell-ECM attachment.[59] pVHL promotes cell adhesion to the ECM.[40] *VHL* inactivation in RCC cells, mouse embryos and mouse embryo fibroblasts impair the ability to form a fibronectin assembly.[39] Fibrillar adhesions are essential to form a fibronectin assembly. Despite sufficient fibronectin, *VHL−/−* RCC cells fail to construct β1-integrin fibrillar adhesions due to deficient integrin regulation.[41] In RCC cell lines with wild-type *VHL*, collagen IV interacts with pVHL.[42] More specifically, pVHL binds the collagen IVα2 chain, part of the triple helix collagen IV; whereas in RCC cells with

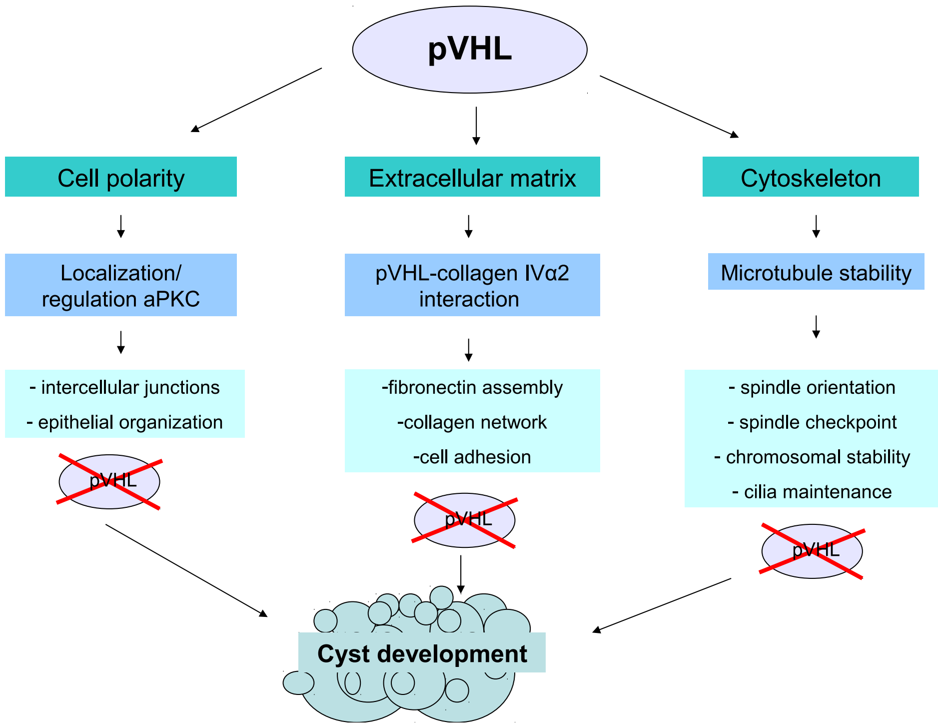


***Figure 3**. Schematic overview of functions of pVHL.*

mutant pVHL this interaction fails.[43] This results in loss of collagen network *in vitro* and collagen remodeling *in vivo* [42] (Figure 4). Collagen IV associates with fibronectin, suggesting that the previously observed interaction between pVHL and fibronectin is indirect.[43]

In a xenograft model using RCC cell lines, VHL-ECM, VHL-HIF or both pathways were inactivated. *VHL−/−* 786–0 cells expressing HIF-2α failed to assemble an ECM. *VHL+/+* cells retrovirally infected to produce proteasome-resistant HIF-2α, were still able to assemble an ECM, indicating that it is independent of VHL-HIF regulation. Alternatively in VHL type 2C cells, mutant pVHL regulates HIF normally, but interferes with ECM assembly.[45] Xenograft tumors from VHL type 2C cells were hypervascular and invasive, similar to tumors originating from *VHL−/−* 786–0 cells. In contrast, xenografts derived from *VHL+/+* cells engineered to stabilize HIF-2α resulted in tumors with lower microvessel density and invasiveness, despite higher VEGF expression.[45] Thus, upregulation of VEGF alone is not sufficient for hypervascularization of tumors. Kurban *et al.* suggested that a strong collagen IV network, dependent on pVHL, naturally suppresses tumorigenesis.[45]

### *pVHL and cell polarity*

Epithelial cells have asymmetric specification of membrane domains. Asymmetry and polarization are regulated by partitioning defective proteins (PAR) and atypical protein kinase C (aPKC). The PAR3-PAR6-aPKC complex is essential for establishing the apical membrane domain and junction structures of epithelial cells.[60] In addition, this complex is involved in formation of the apical lumen in three-dimensional cultures.[61]

The pVHL ubiquitin ligase complex targets the active form of aPKC for degradation, analogous to HIF-α.[62] *VHL* mutant cells fail to form intercellular junctions, resulting in lost polarity.[44] This may be due to deregulation of active aPKC. Moreover, pVHL associates with the PAR3-PAR6-aPKC complex.[50] In a follicular epithelial model in *Drosophila,* loss of wild-type *vhl* resulted in epithelial disorganization, microtubule destabilization and subsequent aPKC mislocalization [63] (Figure 4). Duchi *et al.* concluded that loss of *VHL in vivo* can destabilize strict planar cell polarity control, resulting in architectural changes permissive to cyst development.[63]

### *pVHL and microtubule dynamics*

Microtubules are polymerized filaments composed of α- and β-tubulin monomers. Microtubules continuously shrink at their "minus-ends" and grow at their "plus-ends".[64] pVHL promotes microtubule stabilization by reducing tubulin turnover;[46-47, 54] it binds microtubules through kinesin-2.[48] *In vitro* inhibition of tubulin GTP-ase activity by pVHL at microtubule plus-ends contributes to this stability, which is compromised by *VHL* patient-associated mutant alleles.[54] Furthermore, cellular inactivation of pVHL results in spindle misorientation, spindle checkpoint weakening and chromosomal instability attributed to microtubule instability.[53] Interestingly, pVHL directs growth of microtubule orientation towards the outer plasma membrane.[50]

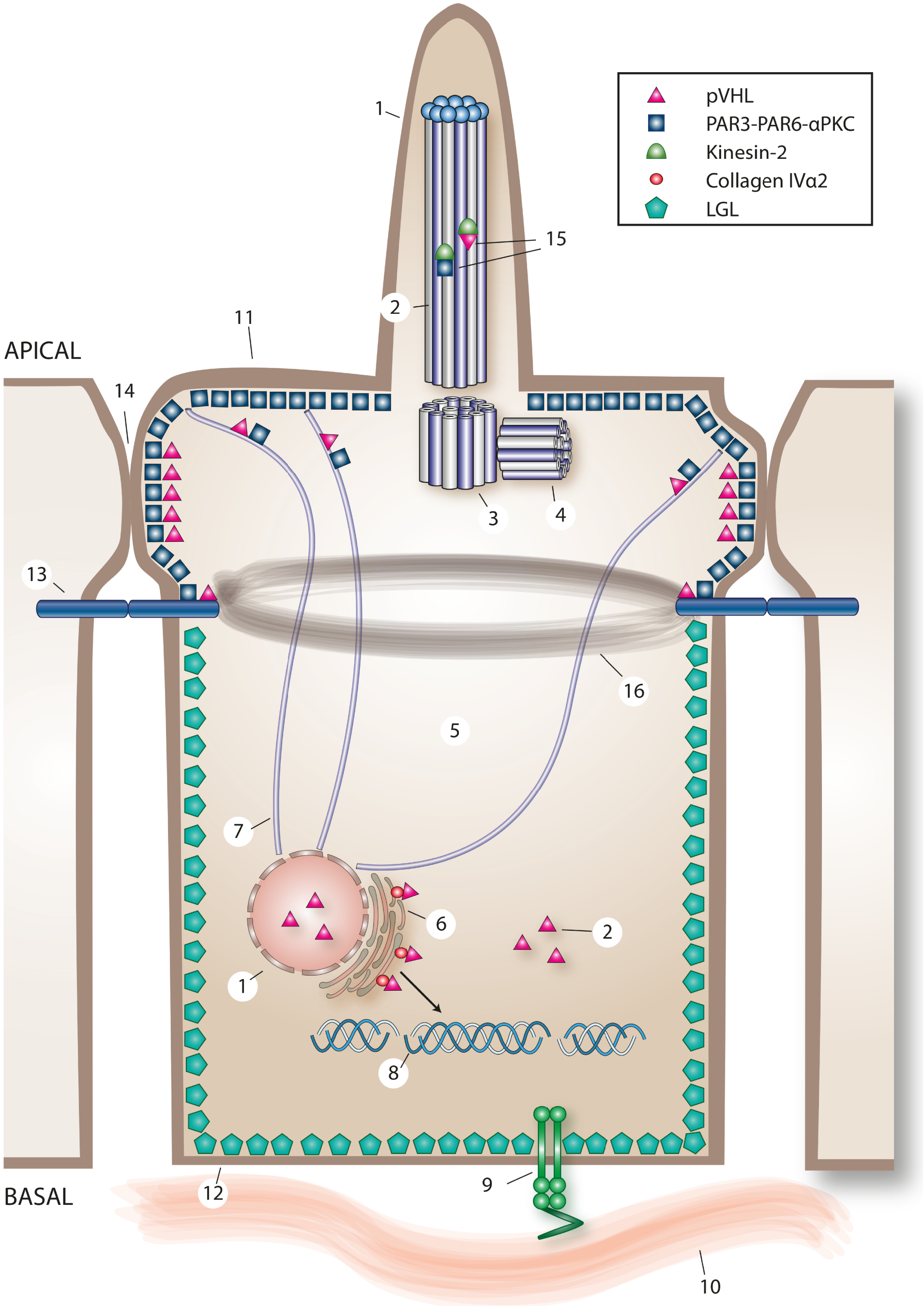


***Figure 4.*** *Overview of direct and indirect pVHL-regulated cell processes in an epithelial cell.*

***Figure 4.*** *Overview of direct and indirect pVHL-regulated cell processes in an epithelial cell. The cilium (1) consists a microtubule-based axoneme (2), and a mother (3) and a daughter centriole (4). In the cell, pVHL is located in the cilium (1), the cytoplasm (5), the endoplasmic reticulum (6) and microtubules (7). The endoplasmic reticulum is the cellular compartment where trihelical collagen IV (8) is produced. pVHL binds collagen IVα2 in the endoplasmic reticulum. When pVHL-collagen IVα2 binding is perturbed, defects in the collagen network results. Integrins (9) facilitate cell-ECM (10) adhesion. Upon loss of pVHL function, misregulation of β1-integrin disturbs the fibronectin matrix assembly. The epithelial cell polarity complex PAR3-PAR6-aPKC is located at the apical membrane (11) and LGL2 at the basolateral membrane (12). Moreover, pVHL and PAR3-PAR6-aPKC are necessary for the formation of adherens junctions (13) and tight junctions (14). PAR3-PAR6-aPKC and pVHL play a role in regulation of the cilium, each capable of binding kinesin-2 (15). Functional loss of pVHL destabilizes cell polarity, partially attributable to abnormal adherens junctions [with consequent effects on the actin belt (16)] and unstable tight junctions. The relevant literature supports a scenario whereby microtubule instability as a result of pVHL dysfunction might affect PAR3-PAR6-aPKC localization, subsequently destabilizing cell polarity and cilia maintenance.*

### *pVHL and cilia*

Microtubules form the backbone of cilia, which project from the apical cell surface. Cilia sense outside the cell and are involved in signaling pathways. Intraflagellar transport of ciliary components is required for ciliary functions, which is powered by kinesin-2. The heterotrimeric motor kinesin-2 comprises motor subunits of kinesin superfamily protein 3 (KIF3A, KIF3B) and kinesin-associated protein 3 (KAP3).[65] pVHL binds KIF3A and KAP3 of kinesin-2,[48] and in the cell, mobility of pVHL is at least partially regulated by kinesin-2.[49]

In renal tissue from VHL patients, cilia are lost in cysts, while cilia are still present in normal tissue.[51] Accordingly, RCC cell lines with or without reconstitution of wild-type *VHL*, show that pVHL contributes to ciliary maintenance and stability.[51-52] Cilia loss in kidney tubules due to pVHL dysfunction likely results from disoriented microtubule growth and decreased microtubule stability,[50] and is associated with renal cyst development [51] (Figure 4). It has not been confirmed that pancreatic cysts in VHL patients are the consequence of cilia loss. However, in a pancreatic-specific *Kif3a* knock-out mouse model, cyst development was attributed to cilia loss (see "Cilia loss in pancreatic cells *in vivo*").[66] Therefore, it is likely that pancreatic cysts in VHL are a result of similar consequences.

## **Histopathology of the pancreas in VHL**

Embryonic epithelial cells that express the transcription factor pancreatic and duodenal homeobox 1 (Pdx1) give rise to pancreatic tissue, consisting of exocrine (acinar and duct) and endocrine (islet) cells.[67] Centro-acinar cells are duct cells, which connect acini with intralobular ducts. Recently centro-acinar cells were isolated based on specific expression of aldehyde dehydrogenase 1. *In vitro*, centro-acinar cell suspensions were able to proliferate with a capacity to differentiate into both exocrine and endocrine cells.[68] Centro-acinar cells might therefore act as facultative progenitor cells in the mature pancreas for acinar, duct and islet cells (Figure 5).

### *Histology of pancreatic cysts and pNETs*

Pancreatic cysts and pNETs in VHL disease have distinct features. pNETs have a solid, trabecular and/or glandular architecture with stromal collagen bands and neurosecretory dense core granules,[69] which are absent in VHL pancreatic cysts.[58] Immunohistochemical staining for chromogranin A, S-100, synaptophysin and neuron-specific enolase showed positive expression in VHL pNETs.[69] Pancreatic cysts stained negative for chromogranin A and S-100.[58] The histology of 119 pancreatic cysts was examined in detail from nine VHL patients.[58] All demonstrated a mixture of clear and/or amphophilic glycogen-rich epithelial cells, endothelial cells and smooth muscle cells. Cysts contained and were surrounded by fibrous tissue. In both pNETs and pancreatic cysts, LOH of *VHL* wild-type allele was confirmed.[58, 69]

### *The pancreas in VHL mouse models*

Constitutional inactivation of *Vhlh* results in embryonic lethality at 10.5 to 12.5 days of gestation, due to placental vasculogenesis defects.[70] To investigate the development of VHL-associated pancreatic manifestations, conditional mouse models have been generated using *Cre/LoxP* technology.[71] In other mouse models *Vhlh, Hif-1α* or both, were conditionally inactivated in pancreatic β-cells in order to investigate the role of pVHL in glucose metabolism.[72-75]

In the first study,[71] the *Vhlh* gene was inactivated in pancreatic progenitor cells by driving *Cre* recombinase with the *Pdx-1* promoter. Postnatal death was observed in the *Pdx1-Cre;Vhlh f/f* mice (n = 22), of which 18 were dead within five days. Histological analyses by pathologists blinded for genotypes showed no abnormalities. However, five individual *Pdx1-Cre;Vhlh f/f* mice survived longer. At 6 to 7 months of age, no pancreatic abnormalities were found in two *Pdx1-Cre;Vhlh f/f* mice. The remaining three were sacrificed at 16 to 18 months of age. At this time point, pancreatic tissue was replaced by fat deposition and pancreatic cysts, and microcystic adenomas were present. The epithelial lining and endothelial cells of the microcystic adenomas expressed cytokeratin MAK6 and CD31, respectively, comparable to findings of pancreatic cysts in VHL patients.[58] In *Pdx1-Cre;Vhlh f/f* mice, all pancreatic islets were characterized by complex and dilated hypervascularity. Some

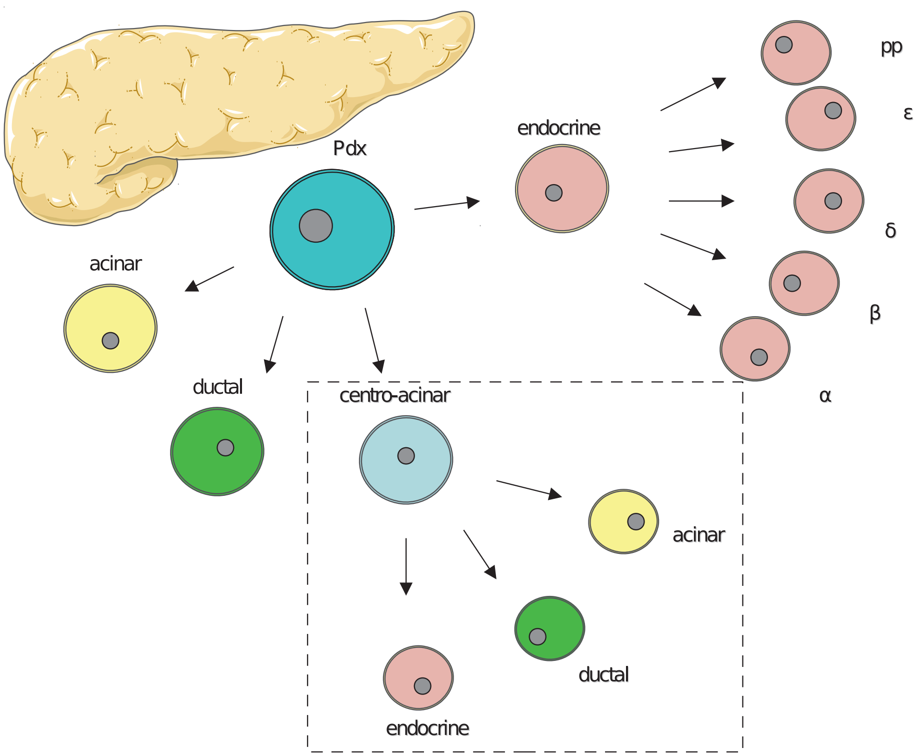


***Figure 5.*** *Pancreatic progenitor or Pdx-cells can differentiate into endocrine or exocrine cells, including acinar, ductal and centro-acinar cells. Strong evidence supports the assertion that centro-acinar cells, similar to Pdx-cells, can differentiate into both endocrine and exocrine cells (Constructed using Servier Medical art).*

islets had a small, abnormally shaped appearance and others were hyperplastic.[71] In another study *Pdx1-Cre;Vhlh f/f* mice were born in the normal Mendelian frequencies. At 12 months of age no cysts or tumors were seen, but a slightly increased pancreatic vascularization was present, compared to control mice.[73]

In other knock-out mouse models the *Vhlh* gene was inactivated by targeting endocrine pancreatic cells for *Cre* recombinase.[71] In mice with conditional *Vhlh* inactivation of endocrine α-cells or β-cells, no pancreatic abnormalities were observed (n = 16). Deletion of *Vhlh* alleles in α- or β-cells was confirmed by polymerase chain reaction analysis.[71] However, others did find increased vascularization in islets in conditional *Vhlh* knock-out mice in β-cells.[73-75] Additionally, disrupted islet morphology with α-cells scattered throughout the islets were found in *Vhlh* knock-out mice in β-cells.[75] In all these models, no pNETs were observed. Table 2 shows an overview of knock-out mouse models, serving as a VHL pancreatic model.

**Table 2. VHL (related) pancreatic knock-out mouse models**

| Ref. [no] | Knock-out gene(s) | Target cells | Age (months) | Pancreatic manifestations |
|---|---|---|---|---|
| [71] | *Vhlh* | Progenitor | 6-8 | None |
| [73] | *Vhlh* | Progenitor | 12 | Increased pancreatic vascularization |
| [71] | *Vhlh* | Progenitor | 16-18 | Cysts, microcystic adenomas, fat depositions, abnormal shaped and hyper-vascular islet cells |
| [71] | *Vhlh* | Endocrine α | 10-23 | None |
| [71] | *Vhlh* | Endocrine β | 15 | None |
| [73] | *Vhlh* | Endocrine β | 12 | Increased vascularization in islets |
| [72] | *Vhlh* | Endocrine β | 6.5 | None |
| [72] | *Vhlh; Hif-1α* | Endocrine β | 6.5 | None |
| [72] | *Hif-1α* | Endocrine β | 6.5 | None |
| [74] | *Vhlh* | Endocrine β | ? | Increased vascularization in islets |
| [75] | *Vhlh* | Endocrine β | 2 | Increased vascularization and α-cells scattered throughout the islets |
| [66] | *Kif3a* | Progenitor | 2 | Compromised acinar tissue |
| [66] | *Kif3a* | Progenitor | 12 | Fibrosis, ductal dilation, cysts |

### *Origin of pancreatic lesions in VHL*

Whether pNETs originate from exocrine or endocrine cells remains unknown.[76] In pancreatic tissue of 13 VHL patients who underwent surgery because of pNETs, microadenomas were found ranging from 1 to 25 per patient. Expression of cyclin D1, carbonic anhydrase 9 and HIF-1α suggests that these microadenomas occur due to LOH of *VHL* in clonal lesions, which might be an early stage of pNETs. Most microadenomas were located close to acinar cells, but were also found close to duct or islet cells.[76]

In contrast, evidence exists that pancreatic serous cystadenomas originate from duct cells. In these cysts and duct cells, co-expression of cytokeratin patterns is present, as determined immunohistochemically.[77-78] Moreover, of 38 serous cysts including two VHL-related, 70% stained positive for mucin 6,[79] which is also expressed in duct and essentially centro-acinar cells.[80] This suggests a ductal/centro-acinar origin for pancreatic serous cysts.[79]

### Cilia loss in pancreatic cells in vivo

A study with conditionally inactivated *Kif3a* in pancreatic tissue in mice suggests that pancreatic cysts originate from duct cells, as a result of cilia loss.[66] *Pdx1-Cre*$^{early}$*;Kif3a f/f* mice were sacrificed at different time points: at two days postnatal, loss of acini was observed and enhancement of lumen between acinar cells and interstitial cells in acini; at 15 days progressive lumen between acini and duct dilation were found. These pathologies all progressed with age and led to acinar tissue being replaced by adipose tissue, severe fibroses, fluid-filled cysts and extensive ductal dilation (age 6 to 12 months). Cilia were lacking in all pancreatic cells. To further identify the cells of origin, conditional knock-out mice were developed for *Kif3a* inactivation in islet cells only, as well as in islet and acinar cells. In mice lacking *Kif3a* in islet cells, no morphological abnormalities were observed. Cilia were only present in duct and reduced in islet cells, suggesting that pancreatic cysts originate from ductal cells.[66]

# Conclusions

We argue that VHL disease can serve as an excellent model to improve the understanding of pathophysiology of pancreatic cysts in general. *In vitro* studies support a role for pVHL in microtubule stabilization and subsequent cilia maintenance. Loss of cilia is directly related to renal cyst development in VHL and in other renal cystic syndromes.[51] Other cell aspects are also involved; pVHL influences assembly of the extracellular matrix as well as the cytoskeleton, including cell polarity.

In *Pdx1-Cre*;*Vhlh f/f* mice with pancreatic-specific loss of *Vhlh*, pancreatic cysts were observed after 16 to 18 months.[71] Conditional *Kif3a* knock-out in pancreatic duct cells in mice also resulted in cysts, but changes were already observed after 2 days.[66] Assuming that cysts mainly result from cilia loss, these data suggest that loss of additional alleles might be necessary for *Vhlh*-driven pancreatic cyst development. In contrast, exome sequencing of sporadic human pancreatic serous cysts only found chromosome 3p loss/*VHL* mutations as recurrent genetic lesions, suggesting that *VHL* loss is sufficient for pancreatic cyst development. The high prevalence of pancreatic cysts in patients with VHL disease supports this notion. Differences in findings might be attributed to differences in species, since in general mice seem to be relatively resistant to *VHL* loss when compared to humans,[81] indicating that in humans *VHL* loss alone might be sufficient for pancreatic serous cyst development.

Monogenetic diseases like VHL provide insights which can be translated to pancreatic cysts in general. Better understanding and identification of genes regarding pancreatic cyst development will probably provide new directions for diagnostics, follow-up and treatment options. Future studies should focus more on *VHL* and also other E3 ubiquitin ligase genes, which appear to be involved in pancreatic cysts.

**Acknowledgments** Supported by Grant 2008-4188 from the Dutch Cancer Society and a grant from the VHL Family Alliance. RHG acknowledges support from EU FP7/2009 241955 "SYSCILIA". The work was independent of the funding. We would like to thank Esther M van Straten for assistance of illustration of Figure 4.

# References


1. de Jong K, Bruno MJ, Fockens P. Epidemiology, diagnosis, and management of cystic lesions of the pancreas. Gastroenterol Res Pract 2012;2012:147465.
2. Maher ER, Iselius L, Yates JR, et al. Von Hippel-Lindau disease: a genetic study. J Med Genet 1991;28:443-447.
3. Lonser RR, Glenn GM, Walther M, et al. Von Hippel-Lindau disease. Lancet 2003;361:2059-2067.
4. Maher ER, Yates JR, Harries R, et al. Clinical features and natural history of von Hippel-Lindau disease. Q J Med 1990;77:1151-1163.
5. Neumann HP, Eggert HR, Scheremet R, et al. Central nervous system lesions in von Hippel-Lindau syndrome. J Neurol Neurosurg Psychiatry 1992;55:898-901.
6. The VHL Handbook [http://www.vhl.org/handbook/vhlhb4.php#Suggested].
7. Baldewijns MM, van Vlodrop IJ, Vermeulen PB, et al. VHL and HIF signalling in renal cell carcinogenesis. J Pathol 2010;221:125-138.
8. Blansfield JA, Choyke L, Morita SY, et al. Clinical, genetic and radiographic analysis of 108 patients with von Hippel-Lindau disease (VHL) manifested by pancreatic neuroendocrine neoplasms (PNETs). Surgery 2007;142:814-818.
9. Erlic Z, Ploeckinger U, Cascon A, et al. VHL-ICT Consortium, German NET Registry. Systematic comparison of sporadic and syndromic pancreatic islet cell tumors. Endocr Relat Cancer 2010;17:875-883.
10. Hammel PR, Vilgrain V, Terris B, et al. Pancreatic involvement in von Hippel-Lindau disease. The Groupe Francophone d'Etude de la Maladie de von Hippel-Lindau. Gastroenterology 2000;119:1087-1095.
11. Horton WA, Wong V, Eldridge R. Von Hippel-Lindau disease: clinical and pathological manifestations in nine families with 50 affected members. Arch Intern Med 1976;136:769-777.
12. Cheng TY, Su CH, Shyr YM, et al. Management of pancreatic lesions in von Hippel-Lindau disease. World J Surg 1997;21:307-312.
13. Kanno A, Satoh K, Hamada S, et al. Serous cystic neoplasms of the whole pancreas in a patient with von hippel-lindau disease. Intern Med 2011;50:1293-1298.
14. Hough DM, Stephens DH, Johnson CD, et al. Pancreatic lesions in von Hippel-Lindau disease: prevalence, clinical significance, and CT findings. AJR Am J Roentgenol 1994;162:1091-1094.
15. Mukhopadhyay B, Sahdev A, Monson JP, et al. Pancreatic lesions in von Hippel-Lindau disease. Clin Endocrinol (Oxf) 2002;57:603-608.
16. Delman KA, Shapiro SE, Jonasch EW, et al. Abdominal visceral lesions in von Hippel-Lindau disease: incidence and clinical behavior of pancreatic and adrenal lesions at a single center. World J Surg 2006;30:665-669.
17. Beerman MH, Fromkes JJ, Carey LC, et al. Pancreatic cystadenoma in Von Hippel-Lindau disease: an unusual cause of pancreatic and common bile duct obstruction. J Clin Gastroenterol 1982;4:537-540.

18. Jackaman FR. Polycystic pancreas: Lindau's disease. J R Coll Surg Edinb 1984;29:121-122.
19. Deboever G, Dewulf P, Maertens J. Common bile duct obstruction due to pancreatic involvement in the von Hippel-Lindau syndrome. Am J Gastroenterol 1992;87:1866-1868.
20. Issar SK, Kumar N, Sachdeva AK, et al. Von Hippel Lindau syndrome presenting as obstructive jaundice with involvement of pancreas in two siblings. Trop Gastroenterol 1996;17:30-32.
21. Kunzli BM, Shrikhande SV, Buchler MW, et al. Pancreatic lesions in von Hippel-Lindau syndrome: report of a case. Surg Today 2004;34:626-629.
22. Boujaoude J, Samaha E, Honein K, et al. A benign cause of obstructive jaundice with von Hippel-Lindau disease. A case report and review of the literature. JOP 2007;8:790-794.
23. Gupta R, Chettri D, Sharma A, et al. Pancreatic cysts causing biliary obstruction in von Hippel Lindau syndrome. JOP 2008;9:313-316.
24. Baek SY, Kang BC, Choi HY, et al. Pancreatic serous cystadenoma associated with islet cell tumour. Br J Radiol 2000;73:83-86.
25. Agarwal N, Kumar S, Dass J, et al. Diffuse pancreatic serous cystadenoma associated with neuroendocrine carcinoma: a case report and review of literature. JOP 2009;10:55-58.
26. Charlesworth M, Verbeke CS, Falk GA, et al. Pancreatic lesions in von Hippel-Lindau disease? A systematic review and meta-synthesis of the literature. J Gastrointest Surg 2012;16:1422-1428.
27. Crossey PA, Richards FM, Foster K, et al. Identification of intragenic mutations in the von Hippel-Lindau disease tumour suppressor gene and correlation with disease phenotype. Hum Mol Genet 1994;3:1303-1308.
28. Chen F, Kishida T, Yao M, et al. Germline mutations in the von Hippel-Lindau disease tumor suppressor gene: correlations with phenotype. Hum Mutat 1995;5:66-75.
29. Zbar B, Kishida T, Chen F, et al. Germline mutations in the Von Hippel-Lindau disease (VHL) gene in families from North America, Europe, and Japan. Hum Mutat 1996;8:348-357.
30. Ritter MM, Frilling A, Crossey PA, et al. Isolated familial pheochromocytoma as a variant of von Hippel-Lindau disease. J Clin Endocrinol Metab 1996;81:1035-1037.
31. Nordstrom-O'Brien M, van der Luijt RB, van Rooijen E, et al. Genetic analysis of von Hippel-Lindau disease. Hum Mutat 2010;31:521-537.
32. Latif F, Tory K, Gnarra J, et al. Identification of the von Hippel-Lindau disease tumor suppressor gene. Science 1993;260:1317-1320.
33. Maher ER, Yates JR, Ferguson-Smith MA. Statistical analysis of the two stage mutation model in von Hippel-Lindau disease, and in sporadic cerebellar haemangioblastoma and renal cell carcinoma. J Med Genet 1990;27:311-314.
34. Crossey PA, Foster K, Richards FM, et al. Molecular genetic investigations of the mechanism of tumourigenesis in von Hippel-Lindau disease: analysis of allele loss in VHL tumours. Hum Genet 1994;93:53-58.

35. Schoenfeld A, Davidowitz EJ, Burk RD. A second major native von Hippel-Lindau gene product, initiated from an internal translation start site, functions as a tumor suppressor. Proc Natl Acad Sci U S A 1998;95:8817-8822.
36. Iliopoulos O, Ohh M, Kaelin WG,Jr. pVHL19 is a biologically active product of the von Hippel-Lindau gene arising from internal translation initiation. Proc Natl Acad Sci U S A 1998;95:11661-11666.
37. Haase VH. The VHL/HIF oxygen-sensing pathway and its relevance to kidney disease. Kidney Int 2006;69:1302-1307.
38. Clifford SC, Cockman ME, Smallwood AC, et al. Contrasting effects on HIF-1alpha regulation by disease-causing pVHL mutations correlate with patterns of tumourigenesis in von Hippel-Lindau disease. Hum Mol Genet 2001;10:1029-1038.
39. Ohh M, Yauch RL, Lonergan KM, et al. The von Hippel-Lindau tumor suppressor protein is required for proper assembly of an extracellular fibronectin matrix. Mol Cell 1998;1:959-968.
40. Kamada M, Suzuki K, Kato Y, et al. Von Hippel-Lindau protein promotes the assembly of actin and vinculin and inhibits cell motility. Cancer Res 2001;61:4184-4189.
41. Esteban-Barragan MA, Avila P, Alvarez-Tejado M, et al. Role of the von Hippel-Lindau tumor suppressor gene in the formation of beta1-integrin fibrillar adhesions. Cancer Res 2002;62:2929-2936.
42. Grosfeld A, Stolze IP, Cockman ME, et al. Interaction of hydroxylated collagen IV with the von hippel-lindau tumor suppressor. J Biol Chem 2007;282:13264-13269.
43. Kurban G, Duplan E, Ramlal N, et al. Collagen matrix assembly is driven by the interaction of von Hippel-Lindau tumor suppressor protein with hydroxylated collagen IV alpha 2. Oncogene 2008;27:1004-1012.
44. Calzada MJ, Esteban MA, Feijoo-Cuaresma M, et al. Von Hippel-Lindau tumor suppressor protein regulates the assembly of intercellular junctions in renal cancer cells through hypoxia-inducible factor-independent mechanisms. Cancer Res 2006;66:1553-1560.
45. Kurban G, Hudon V, Duplan E, et al. Characterization of a von Hippel Lindau pathway involved in extracellular matrix remodeling, cell invasion, and angiogenesis. Cancer Res 2006;66:1313-1319.
46. Hergovich A, Lisztwan J, Barry R, et al. Regulation of microtubule stability by the von Hippel-Lindau tumour suppressor protein pVHL. Nat Cell Biol 2003;5:64-70.
47. Lolkema MP, Mehra N, Jorna AS, et al. The von Hippel-Lindau tumor suppressor protein influences microtubule dynamics at the cell periphery. Exp Cell Res 2004;301:139-146.
48. Lolkema MP, Mans DA, Snijckers CM, et al. The von Hippel-Lindau tumour suppressor interacts with microtubules through kinesin-2. FEBS Lett 2007;581:4571-4576.
49. Mans DA, Lolkema MP, van Beest M, et al. Mobility of the von Hippel-Lindau tumour suppressor protein is regulated by kinesin-2. Exp Cell Res 2008;314:1229-1236.
50. Schermer B, Ghenoiu C, Bartram M, et al. The von Hippel-Lindau tumor suppressor protein controls ciliogenesis by orienting microtubule growth. J Cell Biol 2006;175:547-554.

51. Esteban MA, Harten SK, Tran MG, et al. Formation of primary cilia in the renal epithelium is regulated by the von Hippel-Lindau tumor suppressor protein. J Am Soc Nephrol 2006;17:1801-1806.
52. Lutz MS, Burk RD. Primary cilium formation requires von hippel-lindau gene function in renal-derived cells. Cancer Res 2006;66:6903-6907.
53. Thoma CR, Toso A, Gutbrodt KL, et al. VHL loss causes spindle misorientation and chromosome instability. Nat Cell Biol 2009;11:994-1001.
54. Thoma CR, Matov A, Gutbrodt KL, et al. Quantitative image analysis identifies pVHL as a key regulator of microtubule dynamic instability. J Cell Biol 2010;190:991-1003.
55. Vortmeyer AO, Lubensky IA, Fogt F, et al. Allelic deletion and mutation of the von Hippel-Lindau (VHL) tumor suppressor gene in pancreatic microcystic adenomas. Am J Pathol 1997;151:951-956.
56. Moore PS, Zamboni G, Brighenti A, et al. Molecular characterization of pancreatic serous microcystic adenomas: evidence for a tumor suppressor gene on chromosome 10q. Am J Pathol 2001;158:317-321.
57. Wu J, Jiao Y, Dal Molin M, et al. Whole-exome sequencing of neoplastic cysts of the pancreas reveals recurrent mutations in components of ubiquitin-dependent pathways. Proc Natl Acad Sci U S A 2011;108:21188-21193.
58. Mohr VH, Vortmeyer AO, Zhuang Z, et al. Histopathology and molecular genetics of multiple cysts and microcystic (serous) adenomas of the pancreas in von Hippel-Lindau patients. Am J Pathol 2000;157:1615-1621.
59. Cotran RS, Kumar V, Collins T. Tissue repair: cellular growth, fibrosis and wound healing. In Robbins pathologic basis of disease. 6th edition. Edited by Cotran RS, Kumar V, Collins T. Philadelphia, NJ: WB Saunders Company; 1999:89-112.
60. Suzuki A, Ohno S. The PAR-aPKC system: lessons in polarity. J Cell Sci 2006;119:979-987.
61. Martin-Belmonte F, Gassama A, Datta A, et al. PTEN-mediated apical segregation of phosphoinositides controls epithelial morphogenesis through Cdc42. Cell 2007;128:383-397.
62. Okuda H, Saitoh K, Hirai S, et al. The von Hippel-Lindau tumor suppressor protein mediates ubiquitination of activated atypical protein kinase C. J Biol Chem 2001;276:43611-43617.
63. Duchi S, Fagnocchi L, Cavaliere V, et al. Drosophila VHL tumor-suppressor gene regulates epithelial morphogenesis by promoting microtubule and aPKC stability. Development 2010;137:1493-1503.
64. Mofrad MR, Kamm RD. Introduction, with the biological basis for cell mechanics. In Cytoskeletal mechanics : models and measurements. 1st edition. Edited by Mofrad MR, Kamm RD. Cambridge: Cambridge University Press; 2006:1-17.
65. D'Angelo A, Franco B. The dynamic cilium in human diseases. Pathogenetics 2009;2:3.
66. Cano DA, Sekine S, Hebrok M. Primary cilia deletion in pancreatic epithelial cells results in cyst formation and pancreatitis. Gastroenterology 2006;131:1856-1869.
67. Pan FC, Wright C. Pancreas organogenesis: from bud to plexus to gland. Dev Dyn 2011;240:530-565.

68. Rovira M, Scott SG, Liss AS, et al. Isolation and characterization of centroacinar/terminal ductal progenitor cells in adult mouse pancreas. Proc Natl Acad Sci U S A 2010;107:75-80.
69. Lubensky IA, Pack S, Ault D, et al. Multiple neuroendocrine tumors of the pancreas in von Hippel-Lindau disease patients: histopathological and molecular genetic analysis. Am J Pathol 1998;153:223-231.
70. Gnarra JR, Ward JM, Porter FD, et al. Defective placental vasculogenesis causes embryonic lethality in VHL-deficient mice. Proc Natl Acad Sci U S A 1997;94:9102-9107.
71. Shen HC, Adem A, Ylaya K, et al. Deciphering von Hippel-Lindau (VHL/Vhl)-associated pancreatic manifestations by inactivating Vhl in specific pancreatic cell populations. PLoS One 2009;4:e4897.
72. Zehetner J, Danzer C, Collins S, et al. PVHL is a regulator of glucose metabolism and insulin secretion in pancreatic beta cells. Genes Dev 2008;22:3135-3146.
73. Cantley J, Selman C, Shukla D, et al. Deletion of the von Hippel-Lindau gene in pancreatic beta cells impairs glucose homeostasis in mice. J Clin Invest 2009;119:125-135.
74. Puri S, Cano DA, Hebrok M. A role for von Hippel-Lindau protein in pancreatic beta-cell function. Diabetes 2009;58:433-441.
75. Choi D, Cai EP, Schroer SA, et al. Vhl is required for normal pancreatic beta cell function and the maintenance of beta cell mass with age in mice. Lab Invest 2011;91:527-538.
76. Perigny M, Hammel P, Corcos O, et al. Pancreatic endocrine microadenomatosis in patients with von Hippel-Lindau disease: characterization by VHL/HIF pathway proteins expression. Am J Surg Pathol 2009;33:739-748.
77. Alpert LC, Truong LD, Bossart MI, et al. Microcystic adenoma (serous cystadenoma) of the pancreas. A study of 14 cases with immunohistochemical and electron-microscopic correlation. Am J Surg Pathol 1988;12:251-263.
78. Egawa N, Maillet B, Schroder S, et al. Serous oligocystic and ill-demarcated adenoma of the pancreas: a variant of serous cystic adenoma. Virchows Arch 1994;424:13-17.
79. Buisine MP, Devisme L, Degand P, et al. Developmental mucin gene expression in the gastroduodenal tract and accessory digestive glands. II. Duodenum and liver, gallbladder, and pancreas. J Histochem Cytochem 2000;48:1667-1676.
80. Kosmahl M, Wagner J, Peters K, et al. Serous cystic neoplasms of the pancreas: an immunohistochemical analysis revealing alpha-inhibin, neuron-specific enolase, and MUC6 as new markers. Am J Surg Pathol 2004;28:339-346.
81. Hsu T. Complex cellular functions of the von Hippel-Lindau tumor suppressor gene: insights from model organisms. Oncogene 2012;31:2247-2257.

# Chapter 3

## Endoscopic ultrasound is superior compared to standard imaging for detection of pancreatic solid lesions in von Hippel-Lindau patients

Sophie J. van Asselt
Adrienne H. Brouwers*
Hendrik M. van Dullemen*
Eric J. van der Jagt
Alfons H.H. Bongaerts
Klaas P. Koopmans
Ido P. Kema
Bernard A. Zonnenberg
Henri J.L.M. Timmers
Wouter W. de Herder
Wim J. Sluiter
Elisabeth G.E. de Vries
Thera P. Links

***Those authors contributed equally and are both second author**

***Submitted***

# Abstract

**Background** Patients with von Hippel-Lindau (VHL) disease are prone to develop pancreatic neuroendocrine tumors (pNETs). However, the best imaging technique for detection of pNETs in VHL is currently unknown.

**Aim** In a head-to-head comparison we evaluated endoscopic ultrasound (EUS) and $^{11}$C-5-hydroxytryptophan positron emission tomography ($^{11}$C-5-HTP PET) relative to standard screening for pancreatic solid lesion detection.

**Design** We conducted a cross-sectional study in 22 patients at a tertiary care university medical center. Patients with a VHL mutation or with one VHL manifestation and a mutation carrier as 1$^{st}$ grade family member, with recent screening by abdominal computed tomography (CT) or magnetic resonance imaging (MRI) and somatostatin receptor scintigraphy (SRS), were eligible. Patients underwent linear EUS combined with power Doppler and $^{11}$C-5-HTP PET. Patient and lesion-based positivity for pancreatic solid lesions were calculated for all imaging techniques with a composite reference standard.

**Results** In 10 of the 22 patients, 20 pancreatic solid lesions were detected: 17 with EUS ($P < .05$ versus CT/MRI+ SRS), 3 with $^{11}$C-5-HTP PET, 3 with SRS, 9 with CT/MRI and 9 with CT/MRI+ SRS. With EUS, the solid lesions had a median size of 9.7 mm (range 2.9-55 mm) and most were homogeneous, hypoechoic, iso-elastic and hypervascular. Moreover, EUS detected multiple pancreatic cysts in 18 patients with a median of 4 cysts (range 1-30) per patient.

**Conclusions** EUS is superior to CT/MRI+ SRS for detecting pancreatic solid lesions in VHL disease. $^{11}$C-5-HTP PET has no value.

# Introduction

Pancreatic neuroendocrine tumors (pNETs) are uncommon neoplasms with an incidence of 1-10 per 1 million in the general population.[1-2] pNETs can occur sporadically or as part of the hereditary multiple tumor syndromes von Hippel-Lindau (VHL) disease and Multiple Endocrine Neoplasia type 1. VHL disease is a dominantly inherited multiple tumor syndrome that results from a germline mutation in the *VHL* gene, located on chromosome 3 (3p25-26).[3] The incidence is 1 per 36,000 live births.[4] VHL disease can lead to the development of benign and malignant tumors in various organ systems, including hemangioblastomas in the central nervous system, renal cysts and clear cell renal cell carcinomas, pheochromocytomas, pancreatic cysts and pNETs. VHL patients have a shorter life expectancy compared to the general population, and 73% of deaths are VHL disease-related.[5] Therefore, VHL patients undergo screening to detect manifestations at an early stage.[6]

Non-functional pNETs are present in 10-17% of the VHL patients.[7-9] In addition, 71% of the VHL patients have pancreatic cysts including serous microcystic cystadenomas, which are benign lesions that rarely require intervention.[7] Since the only curative treatment for pNETs is surgery, timely detection is critical. Surgery should be considered based on one of the following: germline mutation in the *VHL* gene located on exon 3, tumor doubling rate < 500 days and/or tumor size > 3 cm.[8,10] For screening of the kidneys, adrenals and pancreas yearly abdominal computed tomography (CT) is recommended from 18 years of age.[6] The VHL handbook, revised in 2012, recommends high-quality abdominal ultrasound yearly and magnetic resonance imaging (MRI) at least every other year from 16 years of age onwards.[10] In case of suspicion of a sporadic pNET, the National Comprehensive Cancer Network (NCCN) guideline recommends multiphase CT or MRI, and suggests that somatostatin receptor scintigraphy (SRS) plus circulating tumor markers (serum chromogranin A and plasma pancreatic polypeptide) can be considered.[11]

Currently, the best imaging technique for early detection of pNETs in VHL disease is unknown. Moreover, differentiation between serous microcystic cystadenomas and pNETs on radiological imaging can be difficult.[6, 8-9, 12] In 69 VHL patients with pancreatic solid lesions, abdominal CT was more sensitive for detection of pancreatic lesions than MRI, 6-[F-18]fluoro-L-dihydroxyphenylalanin ($^{18}$F-DOPA) and $^{18}$F-fluordeoxyglucose ($^{18}$F-FDG) positron emission tomography (PET).[12] The disadvantage of CT, however, is its radiation burden, which may be even more undesirable in genetically vulnerable VHL patients.

Two new imaging strategies are available for detection of pNETs: endoscopic ultrasound (EUS) and $^{11}$C-5-hydroxytryptophan ($^{11}$C-5-HTP) PET. In a retrospective control study in patients without a hereditary multiple tumor syndrome, EUS identified 82% of histological proven functional pNETs, undetectable by trans-abdominal ultrasound and CT.[13] No such studies are available in VHL patients. $^{11}$C-5-HTP is a precursor of serotonin which neuroendocrine cells can take up, decarboxylate into $^{11}$C-serotonin and store in vesicles.[14] A PET scan with this tracer could potentially provide insight into the neuroendocrine nature of a pancreatic lesion. $^{11}$C-5-HTP PET was more sensitive to detect lesions in patients with advanced pNETs than SRS and $^{18}$F-DOPA PET.[15] The aim of this study was therefore to evaluate EUS and $^{11}$C-5-HTP PET in a head-to-head comparison relative to standard screening for the detection of pNETs in VHL patients.

# Patients and methods

## Patients

In this prospective study, patients under standard surveillance in the VHL centers of the Erasmus MC Rotterdam, University Medical Centers Utrecht and Groningen were referred to the University Medical Center Groningen for study participation. Patients were included between February 2009 and August 2011. Eligible were patients with a VHL mutation or with one VHL-manifestation and a mutation carrier as 1$^{st}$ grade family member, with an age of ≥ 18 years. Excluded were pregnant patients or patients with known alcohol abuse and/or chronic pancreatitis. The study was approved by the Medical Ethics Committee of Groningen, and all patients gave written informed consent. The study was registered at the Dutch trial registry under http://www.trialregister.nl/trialreg/index.asp (NTR1668).

Before study entry, standard work-up screening had to be performed in the patient's own center, consisting of SRS within 6 months, and abdominal CT or MRI and serum/plasma tumor markers within 4 months. With radio-immunoassays, serum levels of chromogranin A (CgA-React, Cis Bio International, Gif-sur-Yvette, France, upper limit of normal 100 µg/L) and plasma levels of pancreatic polypeptide (Eurodiagnostica, Nijmegen, the Netherlands, upper limit of normal 100 pmol/L) were determined. Since the use of proton pump inhibitors can lead to spurious elevation of chromogranin A,[16] patients on proton pump inhibitors were excluded from analysis of these levels. Values > upper limit of normal were considered as overproduction.

## CT/MRI

Patients underwent abdominal CT or MRI, depending on the preference of the treating physician. CT scans were performed with a multidetector CT scanner, before and after intravenous (IV) administration of iodine-containing contrast agent. MRI scans were performed in T1 and T2-weighted sequences, with and without IV administration of gadolinium-containing contrast agent.

The reconstruction interval varied between 0.75 and 5.0 mm. Lesions were recorded as pancreatic solid lesions when they were hyperattenuating lesions on contrast images during the arterial or portal venous phase. On MRI, lesions with low intensity on T1 sequences and high intensity on T2 sequences compared to pancreatic tissue were considered as solid.[17] CT and MRI scans were reviewed by a radiologist (EJvdJ) blinded for clinical information. In case of discrepancy between the radiologist of the referral and research center, a second radiologist (AHHB) reviewed these particular scans and consensus between EJvdJ and AHHB was reached after discussion.

## SRS

Twenty-four hours after IV administration of ~200 MBq $^{111}$In-pentetreotide (Octreoscan; Mallinckrodt, Petten, the Netherlands), planar total-body and 3D single photon emission computed tomography (SPECT) images were obtained.[18] SRS scans were reviewed by a nuclear medicine physician (AHB). In case of discrepancy between the nuclear medicine physician of the referral and research center, a second nuclear medicine physician (KPK) reviewed the SRS, and after discussion between AHB and KPK, consensus was reached.

## EUS and $^{11}$C-5-HTP PET

If possible, EUS and $^{11}$C-5-HTP PET were executed on the same day. EUS was performed with a linear ultrasound endoscope (FG-34UX, Pentax GmbH, Hamburg, Germany) and a scanner system (EUB-525, Hitachi Ultrasound BV, Reeuwijk, the Netherlands). The endoscope had a 60º forward oblique viewing video camera, a 120º scanning ultrasound transducer with a 105º field of view, and a 2.0 mm working channel. The scanning frequency could be switched between 5 and 10 MHz. With power Doppler presence of vascularity was assessed and with elastography imaging,[19] elasticity or rigidity was demonstrated. Patients underwent conscious sedation, and EUS was performed by one endoscopist (HMvD) blinded for other imaging results.

Number and location of pancreatic findings were recorded on a standardized record form. Pancreatic lesions with an-echogenic appearances plus an enhanced ultrasound signal were interpreted as simple cysts. Lesions with a honeycomb pattern were classified as serous microcystic cystadenomas.[20] Other focal lesions in the pancreas were considered solid lesions. Fine needle aspiration with a 22 or 25 G needle with a stylet (Sono Tip II 22 or 25 Gauge Medi-Globe GmbH, Germany) was performed on solid lesions if cytological confirmation of pNET was desired by the referred physician. A cytotechnologist was present during the FNA procedure for on-site assessment of the obtained material.

$^{11}$C-5-HTP PET scans were performed as described previously,[15] either on an ECAT HR+ PET camera (n=11) or on a Siemens Biograph mCT camera (PET/CT 64 slices) (Siemens, Knoxville, TN) (n=11). Maximum standardized uptake value ($SUV_{max}$) was assessed for each lesion. PET scans were independently and randomly interpreted by two nuclear medicine physicians (AHB, KPK) blinded for all clinical information and other imaging. Number and location of positive lesions were recorded on a standardized record form. In discrepant cases, consensus was reached between AHB and KPK.

The results of the four imaging modalities were discussed in a multidisciplinary team, consisting of a radiologist (EJvdJ), nuclear medicine physician (AHB), gastroenterologist (HMvD), endocrinologist (TPL) and the clinical trial doctor (SJvA). The pancreatic lesions found on both EUS and $^{11}$C-5-HTP PET were matched with the CT/MRI+ SRS.

## Statistical analysis

A total of 20 patients were estimated to be required to demonstrate additional or new lesions in 25% of the patients with $^{11}$C-5-HTP PET and/or EUS. McNemar's test was used for comparison with 80% power and 5% two-sided significance levels.

Analysis was performed at the levels of individual patients and individual lesions. SRS and $^{11}$C-5-HTP PET scan are whole body modalities, whereas CT/ MRI cover the abdominal area and EUS the pancreatic region only. Therefore, EUS was compared with other modalities for the pancreatic region only. The percentage of visualized solid lesions was calculated for all four imaging techniques by using a composite reference standard. This standard included the sum of the four imaging outcomes. McNemar's test was used to compare the yield of the four imaging techniques. A $P$ value $< .05$ was considered statistically significant. All authors had access to the study data and had reviewed and approved the final manuscript.

# Results

## Patient characteristics

Of the 31 eligible patients, 9 declined participation. Patient characteristics of the remaining 22 VHL patients included in this study are presented in Table 1.

**Table 1.** Patient characteristics (n=22)

| Characteristics | Value |
|---|---|
| Female/Male (n) | 12/10 |
| Age in years median/(range) | 41/(21-64) |
| VHL germline mutation (n): | |
| c.-89-?_c.297+?del | 11 |
| c.500G>A | 3 |
| c.-213-?_463+?del | 2 |
| c.463+2T>C p.(?) | 1 |
| c.259_260insA | 1 |
| c.497T>C | 1 |
| c.509T>A | 1 |
| c.241C>T | 1 |
| *46,XX.ish del(3)(p25-26p25-26)(cos11-) | 1 |
| Earlier pancreatic surgery (n) | |
| Yes/no | 0/22 |
| Abdominal conventional imaging (n) | |
| MRI | 11 |
| CT | 11 |
| Serum chromogranin A (µg/L) (n=19) | |
| Median/range | 38/(23-118) |
| Plasma pancreatic polypeptide (pmol/L) (n=22) | |
| Median/range | 58/(22-234) |

Abbreviations: VHL, von Hippel-Lindau; MRI, magnetic resonance imaging; CT, computed tomography.
*According to archaic mutation analysis.

## Conventional screening

CT/MRI was positive in 7 patients and detected 9 pancreatic solid lesions. Focal pancreatic uptake on SRS was present in 3 patients, visualizing 3 lesions with increased uptake corresponding with 3 pancreatic solid lesions detected with CT/MRI.

Of the 22 patients, 6 had elevated plasma pancreatic polypeptide with a median of 131 pmol/L (range 115-234 pmol/L). Of the 19 patients evaluable for serum chromogranin A, one had a marginally elevated level of 118 µg/L. In total, 7 patients

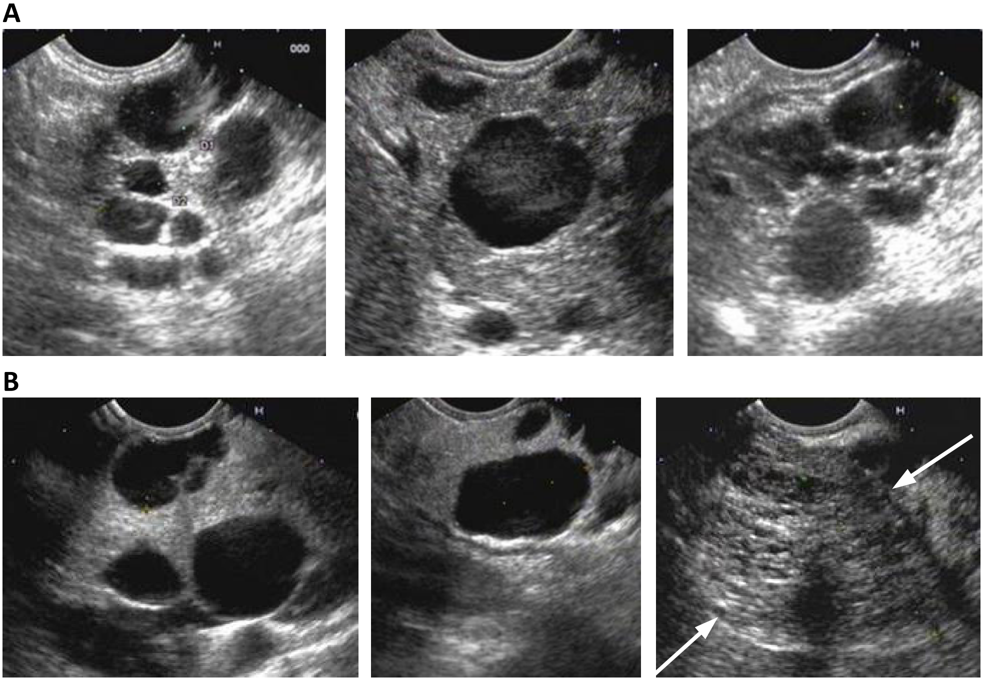


***Figure 1**. EUS images of pancreatic cysts of two VHL patients. **A** 28 year old man with multiple pancreatic cysts in the entire pancreas, ranging in size from 0.5-1.2 cm. The strongly enhanced ultrasound signal (white regions) is characteristic for cysts. **B** A 36 year old woman with multiple cysts in the entire pancreas and (red arrows) a 4.5 cm microcystic serous cystadenoma with characteristic honeycomb structure in the pancreatic body-tail region.*

had elevated tumor markers with 6 not more than a 2-fold elevation. Of these 7 patients, 3 (43%) had pancreatic solid lesions on conventional imaging.

## EUS and $^{11}$C-5-HTP PET

EUS detected 17 pancreatic solid lesions in 10 patients with a median size of 9.7 mm (range 2.9-55 mm). Most lesions were homogeneous and hypoechoic on EUS with an iso-elastic consistency and hypervascular. In addition, in 18 patients 169 pancreatic cysts were found. See Supplemental Table 1 for EUS characteristics of both cystic and solid lesions.

Only 4 patients had no pancreatic simple cysts or serous microcystic cystadenomas, 12 had 1-10 simple cysts, 4 had > 10 simple cysts, 3 had serous microcystic cystadenoma(s) and 1 patient had almost the complete pancreas replaced by at least 30 cysts. In patients with cysts, the median number of cysts was 4 (range 1-30) per

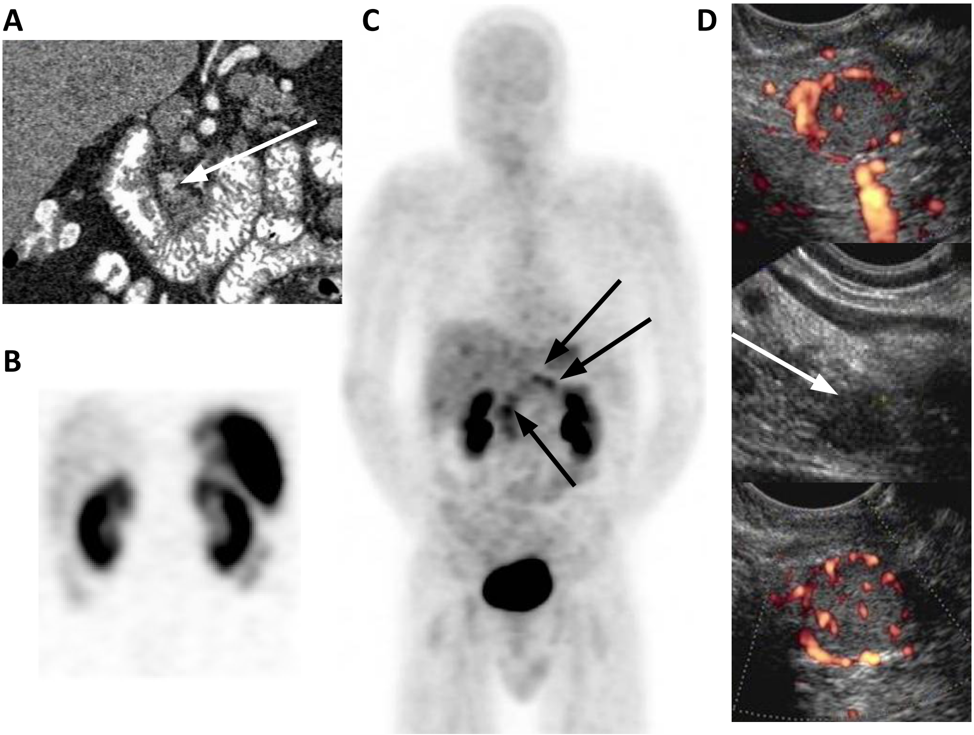


***Figure 2.*** ***A*** *Coronal images of CT scan,* ***B*** *SRS SPECT image,* ***C*** *maximum intensity projection image of* $^{11}$*C-5-HTP PET and* ***D*** *ultrasound images of pancreatic lesions visualized with EUS. In total 4 pancreatic solid lesions were detected. With CT, 1 lesion was found. The SRS was negative.* $^{11}$*C-5-HTP PET detected 3 lesions: 1 in the pancreatic head and 2 in the body-tail region. EUS detected 2 hypoechoic solid lesions in the pancreatic head and 1 in the body-tail region ranging 9.7-14.1 mm. Two solid lesions showed hypervascularity with power Doppler.*

patient (Figure 1). In patients with pancreatic solid lesions, the median number of cysts was 1 (range 0-9).

$^{11}$C-5-HTP PET detected pancreatic lesions in only 1 patient. In this patient 3 pancreatic lesions were visualized with $^{11}$C-5-HTP PET with a $SUV_{max}$ ranging from 4.3-4.9. One lesion was confirmed by CT and 2 lesions by EUS (Figure 2).

During the EUS procedure, FNA was performed in 7 solid lesions of 6 patients with a median of 2 passes (range 2-6). The median size was 17 mm (range 7.2-55), of which 3 lesions were < 10 mm. In cell material from 2 lesions of 2 patients, tumor cells were detected. One of these patients was offered for surgery and the other patient remained for follow-up in the VHL surveillance.

In total, 3 patients underwent pancreatic surgery because of large solid lesions suspicious of pNET: the first patient had 1 solid lesion of 5 cm visible on MRI, SRS and EUS, the second patient had 1 lesion of 2 cm visible on MRI, SRS and EUS +

confirmation by cytology, and the third patient had 2 lesions of 4 and 2 cm, both visible on CT and 1 lesion visible on EUS. All 3 patients underwent pylorus preserving pancreaticoduodenectomy. All lesions were hypervascular and inhomogeneous based on EUS. In the first 2 patients histology confirmed the diagnosis of NET. However in the third patient, histology showed that both lesions were serous microcystic cystadenomas.

## EUS and $^{11}$C-5-HTP PET compared to conventional screening

At a patient-based level, pancreatic solid lesions were found in 10 patients: EUS was positive in 100%, $^{11}$C-5-HTP PET in 10%, SRS in 30% and CT/MRI in 70%. At a lesion-based level, 20 pancreatic solid lesions were found with a median size of 9.0 mm (range 2.9-55 mm). EUS detected 17 pancreatic solid lesions, $^{11}$C-5-HTP PET 3, CT/MRI 9, SRS 3 and CT/MRI+ SRS found 9. EUS detected the most solid lesions compared to CT/MRI, SRS and CT/MRI+ SRS ($P < .05$) (Table 2). In total, 12 solid lesions were found in the pancreatic head and 8 in the body-tail region, of which EUS detected 11 in the pancreatic head (92%) and 6 in the body-tail region (75%).

**Table 2.** All patients with pancreatic solid lesions on imaging (n=10)

| Imaging modality | n (%) of patients | *P* value | n (%) of lesions | *P* value | n (%) of lesions > 1 cm | *P* value |
|---|---|---|---|---|---|---|
| CT/ MRI | 7 (70) | - | 9 (45) | - | 7 (78) | - |
| SRS | 3 (30) | - | 3 (15) | - | 3 (38) | - |
| CT/ MRI+ SRS | 7 (70) | - | 9 (45) | - | 7 (78) | - |
| $^{11}$C-5-HTP PET | 1 (10) | * < 0.05 | 3 (15) | * 0.11 | 1 (11) | * 0.13 |
| EUS | 10 (100) | * 0.25 | 17 (85) | * < 0.05 | 8 (89) | * 1 |

Abbreviations: CT, computed tomography; MRI, magnetic resonance imaging, SRS, somatostatin receptor scintigraphy; $^{11}$C-5-HTP PET, $^{11}$C-5-hydroxytryptophan positron emission tomography; EUS, endoscopic ultrasound.
* $^{11}$C-5-HTP PET and EUS, compared with CT/MRI+ SRS.

EUS did not detect 3 solid lesions, and 2 solid lesions were only visualized with CT of which 1 turned out to be a ~3 cm serous cystadenoma at surgery. Another lesion was only visualized with $^{11}$C-5-HTP PET.

Of the 9 solid lesions > 1 cm, 8 were detected with EUS, 1 with $^{11}$C-5-HTP PET, 7 with CT/MRI, 3 with SRS and 7 with CT/MRI+ SRS (Table 2). Seven patients had pancreatic solid lesions visualized on the conventional imaging techniques CT/MRI+ SRS, in which EUS found 6 additional lesions. $^{11}$C-5-HTP PET detected 2 additional lesions in these patients, but missed 8 that were identified with conventional imaging.

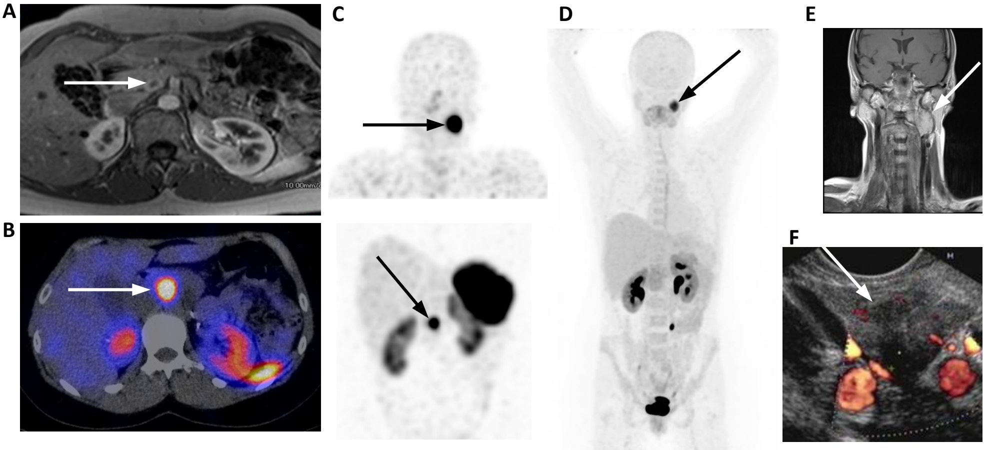


***Figure 3.*** ***A*** *Axial image of abdominal MRI (T1 weighted with contrast),* ***B*** *axial image of SRS fused with low-dose CT* ***C*** *SRS coronal SPECT image of head and abdominal region,* ***D*** *coronal maximum intensity projection of $^{11}$C-5-HTP PET,* ***E*** *coronal image MRI image of head and neck region and* ***F*** *EUS image of the pancreas. On abdominal MRI, 1 pancreatic lesion was found, corresponding with 1 focal lesion on SRS. Moreover on SRS, a focal lesion was visualized in the neck region. $^{11}$C-5-HTP PET only showed a lesion in the neck at the same location. MRI of the neck confirmed a paraganglioma. With EUS, the 17 mm pancreatic solid lesion was identified. Cell material obtained by EUS-FNA confirmed the diagnosis of a NET.*

However, following resection, 2 of these 8 solid lesions that were $^{11}$C-5-HTP PET negative turned out to be serous cystadenomas.

Of the 15 patients without pancreatic solid lesions on CT/MRI plus SRS, none had focal $^{11}$C-5-HTP uptake in the pancreas. In 3 of these patients, 4 solid lesions were found with EUS: all were < 1 cm.

Seven patients had elevated tumor markers, of which 3 patients had only pancreatic cysts, 1 patient had multiple cysts and 1 pancreatic solid lesion < 1 cm detected with EUS, 1 patient had 4 pancreatic solid lesions detected with $^{11}$C-5-HTP PET, EUS and/or CT, and 2 patients had pancreatic cysts and NETs based on histology.

## Extra-pancreatic lesions with nuclear imaging

$^{11}$C-5-HTP PET detected 15 extra-pancreatic focal lesions in 7 patients (Table 3) (Figure 3). Most lesions corresponded with a hemangioblastoma in the central nervous system (6 lesions in 4 patients) and metastases of an earlier resected renal cell cancer (6 lesions in one patient). Of the 15 $^{11}$C-5-HTP PET positive lesions, SRS was positive in 3 lesions of 2 patients. In addition, SRS detected a cerebellar focal lesion corresponding with a hemangioblastoma on MRI, which was not seen with $^{11}$C-5-HTP PET.

**Table 3.** Extra-pancreatic lesions visualized in seven patients with $^{11}$C-5-HTP PET

| Patient | Location | $SUV_{max}$ | Diagnosis | Other imaging |
|---|---|---|---|---|
| A | Neck | 15.8 | Paraganglioma | MRI, SRS |
| | Prevertebral | 6.4 | Paraganglioma, LN | - |
| B | Kidney (6 lesions) | 4.0-10.4 | * RCC | ¶ CT |
| C | Eye | 3.4 | Retinal angioma | Opthalmoscopy, SRS |
| | Cerebellum | 6.9 | Hemangioblastoma | MRI, SRS |
| D | Cerebellum | # | Hemangioblastoma | MRI |
| E | Liver | 1.3 | Serous cystadenoma | CT |
| F | Cerebellum (2 lesions) | 4.3-5.1 | Hemangioblastoma | MRI |
| G | Cerebellum | # | Hemangioblastoma | MRI |

Abbreviations: LN, lymph node; RCC, renal cell cancer; MRI, magnetic resonance imaging; SRS, somatostatin receptor scintigraphy; CT, computed tomography
* indicates that diagnosis was histological confirmed
¶ indicates that lesions were visualized retrospectively
# $SUV_{max}$ could not be calculated, since uptake was too low for a reliable measurement

# Discussion

In this head-to-head comparison of EUS and $^{11}$C-5-HTP PET relative to standard pNET screening with CT/MRI and SRS in VHL patients, EUS was superior for pancreatic solid lesion detection. $^{11}$C-5-HTP PET had no value in this screening setting. We have shown for the first time that EUS is an excellent method for pancreatic solid lesion detection in VHL disease. EUS can be executed without radiation exposure of the patient, and it allows obtaining cytology for NET confirmation. Therefore, EUS can be of additive value for pancreas imaging in VHL patients.

With EUS we could also identify various lesion characteristics. Most often pancreatic solid lesions were hypoechoic, homogeneous, had an iso-elastic consistency and were hypervascular based on power Doppler. Based on EUS combined with power Doppler, these characteristics might help to identify the characteristics of pNETs. Besides solid lesions, we also detected serous cystadenomas with EUS. Serous cystadenomas of the pancreas include microcystic serous cystadenoma, serous oligocystic and ill-demarcated adenomas as well as macrocystic serous cystadenoma.[20]

In our series, most cysts were macrocystic serous cystadenomas, recognized by an anechoic appearance. On EUS, 3% of the cysts had a classic honeycomb structure, which is characteristic for serous microcystic cystadenomas. In our study, 2 lesions with a solid appearance on EUS and CT/MRI suspicious of pNET were shown to be serous cystadenomas by means of histology. Overdiagnosis of pNET in VHL has also been reported by others.[6, 8-9, 12] In our study, one lesion turned out to be a serous cystadenoma, which was clearly hypervascular based on EUS combined with power Doppler. This indicates that a hypervascular nature of pancreatic solid lesions in VHL does not exclude the existence of a serous cystadenomas. Others also reported cases of pancreatic serous cystadenomas having hypervascular appearances on anatomical imaging.[21-23]

To avoid unnecessary surgery, making a distinction between pNET and serous cystadenoma is warranted in VHL disease. EUS potentially allows cytology to be obtained by FNA. However, we obtained adequate material in only 2 out of 7 lesions. This may partly be due to the fact that 3 of the 7 lesions were < 10 mm. In a retrospective study in 15 patients using EUS FNA for confirmation of the diagnosis pNET, the yield was 53%.[24] Similar to our series, samples were often hemorrhagic with a low cell yield.[24] Other retrospective series reported higher accuracy rates of 90-93%, but it is unclear how patients were selected in these studies.[25-26] Instead of obtaining cytological material, it is also possible to obtain tissue samples by EUS-guided fine needle tissue acquisition. In a recent prospective study, 30 patients with pancreatic lesions suspected of sporadic pNET underwent fine-needle tissue acquisition with a 19 Gauge needle, without complications.[27] In 93% of patients with lesion size ranging from 7 to 100 mm, the NET diagnosis could be confirmed.[27] In VHL disease, obtaining tissue samples instead of cell material might also improve the yield.

In general, pNETs have the ability to produce hormones or amines, which provides various options for specific imaging by using this metabolic pathway. In 18 patients with advanced NETs, $^{11}$C-5-HTP PET was superior for lesion detection compared to CT.[28] In addition, we showed that $^{11}$C-5-HTP PET is a more sensitive technique compared to $^{18}$F-DOPA PET and SRS in patients with advanced pNET.[15] Adding CT resulted in a slight improvement of sensitivity.[15] However, in the current VHL study, $^{11}$C-5-HTP PET showed no added value for early detection of primary pNETs in VHL patients.

Besides pancreatic lesions, $^{11}$C-5-HTP PET found 15 other VHL manifestations, including hemangioblastomas, renal cell carcinomas and paraganglioma. Like pNETs, paragangliomas are able to take up and decarboxylate amine precursors.[29] This property has not been identified in renal cell carcinomas and hemangioblastomas. Nevertheless, in both tumor types immunohistochemical studies showed positivity for specific neuroendocrine markers, including neuron specific enolase and synaptophysin,[30-31] indicating presence of neuroendocrine properties of these cells. This might clarify visualization with $^{11}$C-5-HTP PET.

The presence of somatostatin receptor subtype 2 on NET cells is essential for tumor imaging with SRS.[32] In our study, the value of SRS was limited, since only 15% of pancreatic solid lesions could be visualized. Another study showed a SRS patient-based positivity of 59% in 27 VHL patients with pNETs with a median size of 30 mm (range 10-80 mm).[33] An explanation for the lower yield of SRS in our study could be that the median size of the solid pancreatic lesions was ~3–fold smaller compared to the study of Corcos et al.[33] Altogether, this suggests that SRS is not useful for pNET screening in VHL disease.

In our series, 2 out of 4 patients with a cytologically/histologically confirmed NET had elevated serum chromogranin A or plasma pancreatic polypeptide levels. In total, 7 patients had elevated tumor markers, which were marginally increased in 6 patients (not more than 2 times the upper limit of normal). The biological and analytical variations of these markers are not known, making it difficult to interpret these findings. Moreover, false-positive values can occur in a variety of clinical conditions. Elevated chromogranin A levels can occur due to use of proton pump inhibitors, renal or hepatic insufficiency, and elevated pancreatic polypeptide levels due to high age, diarrhea or gut inflammation.[16, 34] In a large series of 108 VHL patients with pNETs in which the serum tumor markers insulin, glucagon, pancreatic polypeptide and vasoactive intestinal peptide were evaluated, none were indicative for pNET in VHL.[8] This indicates that measurement of these tumor markers is likely of no value.

The current available VHL guidelines recommend for adults yearly abdominal imaging by CT [6] or yearly transabdominal ultrasound and MRI at least every other year.[10] However, the sensitivity of transabdominal ultrasound is low and CT has the disadvantages of radiation exposure and use of iodine-containing contrast. MRI does not include radiation exposure, but requires gadolinium-containing contrast, which can be nephrotoxic.[35] Therefore, transabdominal ultrasound combined with EUS might replace them. The invasive character of EUS is a disadvantage by both clinicians and patients. However in general EUS in combination with conscious sedation is well tolerated.[36]

Our findings illustrate that EUS is of additional value in VHL patients for early pancreatic solid lesion detection. Apart from its high sensitivity, EUS can be combined with FNA to obtain cytology for NET confirmation. EUS may moreover identify different lesion characteristics, it is in general a well-tolerated procedure and it can be executed without radiation exposure and use of contrast agents. Therefore, we suggest to use EUS in the surveillance of VHL disease.

**Acknowledgments** We would like to thank Drs D.J. Gouma and D. O'Toole for their contributions as members of the external monitoring committee.

**Funding** Supported by a Grant of the Dutch Cancer Society (RUG 2008-4188).

# References


1. Yao JC, Eisner MP, Leary C, et al. Population-based study of islet cell carcinoma. Ann Surg Oncol 2007;14:3492-3500.
2. Zhou J, Enewold L, Stojadinovic A, et al. Incidence rates of exocrine and endocrine pancreatic cancers in the United States. Cancer Causes Control 2010;21:853-861.
3. Latif F, Tory K, Gnarra J, et al. Identification of the von Hippel-Lindau disease tumor suppressor gene. Science 1993;260:1317-1320.
4. Maher ER, Iselius L, Yates JR, et al. Von Hippel-Lindau disease: a genetic study. J Med Genet 1991;28:443-447.
5. Wilding A, Ingham SL, Lalloo F, et al. Life expectancy in hereditary cancer predisposing diseases: an observational study. J Med Genet 2012;49;264-269.
6. Lonser RR, Glenn GM, Walther M, et al. Von Hippel-Lindau disease. Lancet 2003;361:2059-2067.
7. Hammel PR, Vilgrain V, Terris B, et al. Pancreatic involvement in von Hippel-Lindau disease. The Groupe Francophone d'Etude de la Maladie de von Hippel-Lindau. Gastroenterology 2000;119:1087-1095.
8. Blansfield JA, Choyke L, Morita SY, et al. Clinical, genetic and radiographic analysis of 108 patients with von Hippel-Lindau disease (VHL) manifested by pancreatic neuroendocrine neoplasms (PNETs). Surgery 2007;142:814-818.
9. Neuzillet C, Vullierme MP, Coulevard A, et al. Difficult diagnosis of atypical cystic pancreatic lesions in von Hippel-Lindau disease. J Comput Assist Tomogr 2010;34:140-145.
10. The VHL handbook (http://www.vhl.org/handbook/vhlhb4.php#Suggested) (access date: 10 January 2013).
11. http://www.nccn.org/professionals/physician_gls/pdf/neuroendocrine.pdf (access date: 10 January 2013).
12. Kitano M, Millo C, Rahbari R, et al. Comparison of 6-18F-fluoro-L-DOPA, 18F-2-deoxy-D-glucose, CT and MRI in patients with pancreatic neuroendocrine neoplasms with von Hippel-Lindau disease. Surgery 2011;150:1122-1128.
13. Rösch T, Lightdale CJ, Botet JF, et al. Localization of pancreatic endocrine tumors by endoscopic ultrasonography. N Engl J Med 1992;326:1721-1726.
14. Sundin A, Eriksson B, Bergström M, et al. Demonstration of [11C]-5-hydroxy-L-tryptophan uptake and decarboxylation in carcinoid tumors by specific positioning labeling in positron emission tomography. Nucl Med Biol 2000;27:33-41.
15. Koopmans KP, Neels OC, Kema IP, et al. Improved staging of patients with carcinoid and islet cell tumors with 18F-dihydroxy-phenyl-alanine and 11C-5-hydroxy-tryptophan positron emission tomography. J Clin Oncol 2008:26;1489-1495.
16. Modlin IM, Gustafsson BI, Moss SF, et al. Chromogranin A–Biological function and clinical utility in neuroendocrine tumor disease. Ann Surg Oncol 2010;17:2427-2443.
17. Reznek RH. CT/MRI of neuroendocrine tumours. Cancer imaging 2006;S163-S177.

18. Balon HR, Goldsmith SJ, Siegel BA, et al; Society of Nuclear Medicine. Procedure guideline for somatostatin receptor scintigraphy with (111)In-pentetreotide. J Nucl Med 2001;42:1134-1138.
19. Iglesias-Garcia J, Larino-Noia J, Abdulkader I, et al. EUS elastography for the characterization of solid pancreatic masses. Gastrointest Endosc 2009;70:1101-1108.
20. Compton CC. Serous cystic tumors of the pancreas. Semin Diagn Pathol 2000;17:43-55.
21. Gabata T, Terayama N, Yamashiro M, et al. Solid serous cystadenoma of the pancreas: MR imaging with pathologic correlation. Abdom Imaging 2005;30:605-609.
22. Takeshita K, Kutomi K, Takada K, et al. Unusual imaging appearances of pancreatic serous cystadenoma: correlation with surgery and pathologic analysis. Abdom Imaging 2005;30:610-615.
23. Gerke H, Silva R, Jensen CS. Hypervascular pancreatic tumor diagnosed as a serous cystadenoma by EUS-guided Trucut biopsy. Gastrointest Endosc 2006;64:273-274.
24. Voss M, Hammel P, Molas G, et al. Value of endoscopic ultrasound guided fine needle aspiration biopsy in the diagnosis of solid pancreatic masses. Gut 2000;46:244-249.
25. Ardengh JC, de Paulo GA, Ferrari AP. EUS-guided FNA in the diagnosis of pancreatic neuroendocrine tumors before surgery. Gastrointest Endosc 2004;60:378-384.
26. Figueiredo FA, Giovannini M, Monges G, et al. Pancreatic endocrine tumors: a large single-center experience. Pancreas 2009;38:936-940.
27. Larghi A, Capurso G, Garnuccio A, et al. Ki-67 grading of nonfunctioning pancreatic neuroendocrine tumors on histologic samples obtained by EUS-guided fine-needle tissue acquisition: a prospective study. Gastrointest Endosc 2012;76:570-577.
28. Orlefors H, Sundin A, Ahlström H, et al. Positron emission tomography with 5-hydroxytryprophan in neuroendocrine tumors. J Clin Oncol 1998;16:2534-2541.
29. Eisenhofer G. Screening for pheochromocytomas and paragangliomas. Curr Hypertens Rep 2012;14:130-137.
30. Becker I, Paulus W, Roggendorf W. Histogenesis of stromal cells in cerebellar hemangioblastomas. Am J Pathol 1989;134:271-275.
31. Ronkainen H, Soini Y, Vaarala MH, et al. Evaluation of neuroendocrine markers in renal cell carcinoma. Diagn Pathol 2010;5:28.
32. Teunissen JJ, Kwekkeboom DJ, Valkema R, et al. Nuclear medicine techniques for the imaging and treatment of neuroendocrine tumours. Endocr Relat Cancer 2011;18:S27-S51.
33. Corcos O, Coulevard A, Giraud S, et al. Endocrine pancreatic tumors in von Hippel-Lindau disease: clinical, histological and genetic features. Pancreas 2008;37:85-93
34. Oberg K. Circulating biomarkers in gastroenteropancreatic neuroendocrine tumours. Endocr Relat Cancer 2011;18:S17-S25.
35. Perazella MA. Current status of gadolinium toxicity in patients with kidney disease. Clin J Am Soc Nephrol 2009;4:461-469.
36. Bonta PI, Kok MF, Bergman JJ, et al. Conscious sedation for EUS of the esophagus and stomach: a double-blind, randomized, controlled trial comparing midazolam with placebo. Gastrointest Endosc 2003;57:842-847.

**Supplemental Table 1.** EUS characteristics of pancreatic solid lesions (n=17) and cysts (n=139)

| Characteristics | Solid lesions (n) | Cystic lesions (n) |
|---|---|---|
| Localization: | | |
| Pancreatic head | 11 | 56 |
| Pancreatic body-tail | 6 | 83 |
| Lesion size | | |
| > 1 cm | 7 | 47 |
| ≤ 1 cm | 10 | 92 |
| Relation pancreatic duct | | |
| Yes | 6 | 5 |
| No | 11 | 74 |
| Unknown | 0 | 60 |
| Echogenic pattern | | |
| Hyperechoic | 0 | 0 |
| Hypoechoic | 17 | 0 |
| Anechoic | 0 | 139 |
| Ultrasonographic texture | | |
| Homogeneous | 11 | 133 |
| Heterogeneous | 6 | 6 |
| Power Doppler signal | | |
| Positive | 10 | * |
| Negative | 7 | * |
| Elastography | | |
| Rigid | 2 | * |
| Iso-elastic | 11 | * |
| Unknown | 4 | * |
| Honeycomb structure | | |
| Yes | * | 4 |
| No | * | 135 |

*Indicates that characteristic is not applicable

Note that the patient in which almost the total pancreas was replaced by cysts, has not been evaluated for cystic lesion characteristics.

# Chapter 4

## Endoscopic ultrasound is superior for detection of pancreatic lesions compared to standard imaging in Multiple Endocrine Neoplasia type 1 patients

Sophie J. van Asselt
Adrienne H. Brouwers
Hendrik M. van Dullemen
Eric J. van der Jagt
Alfons H.H. Bongaerts
Ido P. Kema
Klaas P. Koopmans
Gerlof D. Valk
Henri J.L.M. Timmers
Wouter W. de Herder
Richard A. Feelders
Paul Fockens
Wim J. Sluiter
Elisabeth G.E. de Vries
Thera P. Links

***Submitted***

# Abstract

**Objectives** In Multiple Endocrine Neoplasia type 1 (MEN1), pancreatic neuroendocrine tumors (pNET) are the leading MEN1-related cause of death. Therefore, early detection is warranted. The best imaging technique for detection of pNETs in MEN1 is unknown. We performed a head-to-head evaluation of endoscopic ultrasound (EUS) and $^{11}$C-5-hydroxytryptophan positron emission tomography ($^{11}$C-5-HTP PET), compared to the recommended screening techniques in MEN1 patients.

**Design** We conducted a cross sectional study in 41 patients at a tertiary care university medical center. Patients with proven MEN1 mutation or with one MEN1-manifestation and a mutation carrier as 1$^{st}$ grade family member, with recent screening by abdominal computed tomography (CT) or magnetic resonance imaging (MRI) and somatostatin receptor scintigraphy (SRS) were eligible. Patients underwent both linear EUS and $^{11}$C-5-HTP PET. Patient- and lesion-based positivity was calculated for all imaging techniques.

**Results** In 35 out of the 41 patients, 107 pancreatic lesions were detected in total. EUS detected 101 pancreatic lesions in 34 patients, $^{11}$C-5-HTP PET detected 35 lesions in 19 patients, and CT/MRI+ SRS 32 lesions in 18 patients ($P$ <.001). $^{11}$C-5-HTP PET performed similar to CT/MRI+ SRS, and better compared to SRS only (13 lesions in 12 patients), both at a patient- and lesion-based level ($P$ < .05).

**Conclusions** EUS is superior to CT/MRI+ SRS for pancreatic lesion detection in MEN1 patients. In this setting $^{11}$C-5-HTP PET is not useful. We recommend EUS as first choice pancreas imaging technique in MEN1 patients.

# Introduction

Pancreatic neuroendocrine tumors (pNETs) are rare, with an incidence of 1-10 per 1 million in the general population.[1-2] pNETs can occur sporadically and as part of the hereditary multiple tumor syndromes Multiple Endocrine Neoplasia type 1 (MEN1) and von Hippel-Lindau disease. The prevalence of individuals with MEN1 is estimated at 1-10 per 100,000 in the general population.[3] MEN1 is characterized by a mutation in the *MEN1* gene located on chromosome 11q13. A mutation in this tumor suppressor gene can lead to endocrine tumors in various organs including the parathyroid gland, pituitary gland and pancreas. The prevalence of pNETs in MEN1 is 30-75%.[3-4] Non-functional pNETs are most common. pNETs can also produce hormones, and are called functional tumors if symptoms are present. Insulinomas and gastrinomas are the most frequent functional tumors in MEN1, of which gastrinomas are more often located in the duodenum than in the pancreas.[3] pNETs can have malignant potential and surgery is the only curative treatment.

Screening is performed for early detection of pNETs.[4-5] The 2001 expert-based MEN1 International Screening Guideline advised annual biochemical tests, including fasting glucose and insulin, starting at 5 years of age.[4] Additionally, at the age of 20 years, glucagon, pancreatic polypeptide, chromogranin A and pro-insulin are recommended annually together with somatostatin receptor scintigraphy (SRS) and abdominal computed tomography (CT) or magnetic resonance imaging (MRI) once every 3 years.[4] Despite screening, 28-46% of MEN1 patients die of a MEN1-associated manifestation, of which pNET is the leading cause of death.[6-8] Therefore, earlier detection of pNETs is warranted.

In a retrospective control study in patients without MEN1, EUS detected 82% of histological proven functional pNETs, which were not identified by trans-abdominal ultrasound and CT.[9] Several relatively small studies in MEN1 patients suggested that endoscopic ultrasound (EUS) is a sensitive method for early imaging of pNETs.[10-14] Given the lack of evidence, no screening modality for pNET is currently preferred in MEN1 patients; the recently revised MEN1 guideline recommends either CT, MRI or EUS annually.[5]

In addition to EUS, imaging with $^{11}$C-5-hydroxytryptophan positron emission tomography ($^{11}$C-5-HTP PET) is potentially interesting for detection of pNETs in MEN1. $^{11}$C-5-HTP is a precursor of serotonin, which can be decarboxylated by pNET cells to $^{11}$C-serotonin.[15] $^{11}$C-5-HTP PET in combination with CT is the most sensitive method for imaging of advanced pNET, compared to CT combined with SRS or $^{18}$F-6-fluoro-L-dihydroxyphenylalanin ($^{18}$F-DOPA) PET.[16]

To evaluate the imaging strategies EUS and $^{11}$C-5-HTP PET for detecting pNETs, we performed a prospective head-to-head study of these strategies compared to the recommended conventional screening techniques CT/MRI and SRS in MEN1 patients. Since tumor markers are part of the current MEN1 guideline, we also evaluated serum chromogranin A and gastrin, and plasma glucagon and pancreatic polypeptide.

# Patients and methods

## Patients

In this prospective study, treating physicians in the MEN1 centers at the University Medical Centers of Rotterdam, Utrecht, Nijmegen and Groningen referred patients to the University Medical Center Groningen for study participation. Patients were included between February 2009 and August 2011. Eligible were those with genetically proven MEN1 or patients with clinically proven MEN1 with a 1st grade family member with genetically confirmed MEN1, with an age of ≥18 years. Standard MEN1 screening had to be performed at the patients' own MEN1 center. This screening included SRS within 6 months, abdominal CT or MRI and serum/plasma tumor marker assessment including serum chromogranin A and gastrin, and plasma glucagon and pancreatic polypeptide within 4 months before inclusion in the study.

Excluded were pregnant patients and patients known with alcohol abuse and/or chronic pancreatitis. This study was approved by the Medical Ethics Committee of Groningen, and all patients gave written informed consent. The study was registered in the Dutch trial register under http://www.trialregister.nl/trialreg/index.asp (NTR1668).

## Conventional screening

### *CT/MRI*

Depending on the preference of the treating physician, patients underwent abdominal CT or MRI. CT scans were performed with a multidetector CT scanner, before and after intravenous (IV) administration of iodine-containing contrast agent. MRI scans were performed in T1 and T2-weighted sequences, with and without IV administration of gadolinium-containing contrast agent. The reconstruction interval varied between 0.75-5.0 mm. CT and MRI scans were reviewed by a radiologist (EJvdJ) blinded for the clinical information. In case of discrepancy between the radiologist of the referral and the research center, a second radiologist (AHHB) reviewed these scans, and consensus between both radiologists was reached after discussion.

### *SRS*

According to guidelines of the Dutch Nuclear Medicine Association, 24 hours after administration of ~200 MBq $^{111}$In-pentetreotide (Octreoscan; Mallinckrodt, Petten, the Netherlands) IV, planar total-body and 3D SPECT images were obtained using standard methods as described previously.[17] SRS scans were reviewed by a nuclear medicine physician (AHB) blinded for clinical information. In case of discrepancy between the nuclear medicine physician of the referral and the research center, a second nuclear medicine physician (KPK) reviewed the SRS, and after discussion between both nuclear medicine physicians, consensus was reached.

### *Tumor markers*

Assessment methods of tumor markers differed between centers. Serum chromogranin A,[18] plasma pancreatic polypeptide,[19] serum gastrin [20] and plasma glucagon [21-22] were assessed with commercially available radioimmunoassays as described previously. Serum gastrin was also determined with an immunometric assay.[23] At one center, gastrin and pancreatic polypeptide were assessed with in-house radioimmunoassays. Since the use of proton pump inhibitors can lead to spurious elevation of chromogranin A and gastrin levels,[24-25] patients on proton pump inhibitors were excluded from analysis of these levels. To compare results obtained with various assays, ratios were calculated by dividing the value with the upper limit of normal. Ratio > 1 of one of the four tumor markers in one patient was defined as overproduction.

In patients with symptoms of an insulinoma (symptoms consistent with hypoglycemia, low plasma glucose concentration when symptoms are present, relief of symptoms when plasma glucose level is raised), a 72 hour fast test was performed at the referral center.[26]

## EUS and $^{11}$C-5-HTP PET

If possible, EUS and $^{11}$C-5-HTP PET were performed on the same day. EUS was performed with a linear ultrasound endoscope (FG-34UX, Pentax GmbH, Hamburg, Germany) and a scanner system (EUB-525, Hitachi Ultrasound BV, Reeuwijk, the Netherlands). The endoscope had a 60º forward oblique viewing video camera, a 120º scanning ultrasound transducer with a 105º field of view, and a 2.0 mm working channel. The scanning frequency could be switched between 5 and 10 MHz. Presence of vascularity was assessed with power Doppler, and elasticity or rigidity of lesions were qualitatively assessed with elastography.[27] Patients underwent EUS with conscious sedation. EUS was performed by one endoscopist (HMvD) blinded for all other imaging. Number and location of pancreatic lesions were recorded on a standardized record form. Fine needle aspiration (FNA) was performed with a 22 or 25 G needle with a stylet (Sono Tip II 22 and 25 Gauge Medi-Globe GmbH, Germany) when cytological confirmation of a NET was desirable by the referred physician and/or the lesion was > 1 cm. A cytotechnologist was present during the FNA procedure for on-site assessment of the obtained material. All procedures were videotaped and photographs were obtained for all visualized lesions. For validation, videotapes of 22 non-selectively chosen lesions were reviewed by a second endoscopist (PF).

$^{11}$C-5-HTP PET scans were performed as described previously [15] either on an ECAT HR+ PET camera (n=12) or on a Siemens Biograph mCT camera (PET/CT 64 slices) (Siemens, Knoxville, TN) (n=29). PET scans were independently and randomly interpreted by two nuclear medicine physicians (AHB, KPK) blinded for all clinical information and other imaging. Number and location of positive lesions were listed on a standardized record form. In discrepant cases, consensus was reached between both physicians.

The results of the four imaging modalities were discussed in a multidisciplinary team, consisting of a radiologist (EJvdJ), nuclear medicine physician (AHB), gastroenterologist (HMvD), endocrinologist (TPL) and the clinical trial doctor (SJvA). The pancreatic lesions found on both EUS and $^{11}$C-5-HTP PET were matched with CT/MRI+ SRS.

## Statistical analysis

To demonstrate additional or new lesions in 12.5% of the patients with EUS and/or $^{11}$C-5-HTP PET, 39 patients were needed for a statistically meaningful comparison. McNemar's test was used for comparison with 80% power and 5% two-sided significance levels. Analysis was performed at the level of individual patients and lesions. Since EUS only images the pancreatic region, EUS and $^{11}$C-5-HTP PET were compared with CT/MRI, SRS and CT/MRI+ SRS for the pancreatic region only. The percentage of detected pancreatic lesions was calculated for all four imaging techniques by using a composite reference standard. This standard included the four imaging outcomes. McNemar's test was used to compare the yield of the four imaging techniques. A $P$ value <.05 was considered statistically significant. All authors had access to the study data and had reviewed and approved the final manuscript.

# Results

## Patient characteristics

In total 41 MEN1 patients were recruited for study participation. Characteristics of the included MEN1 patients are shown in table 1. The 41 patients carried 19 different MEN1 mutations (Supplementary Table 1).

**Table 1.** Patient characteristics (n=41)

| Characteristics | Value |
|---|---|
| Sex: Female/Male (n of patients) | 27/14 |
| Median age in years (range) | 44 (18-67) |
| Earlier pancreatic surgery: yes/no (n of patients) | 7/34 |
| Enucleation (n of patients) | 2 |
| Lymph node dissection (n of patients) | 1 |
| PPPD* (n of patients) | 1 |
| Pancreatic tail resection (n of patients) | 3 |
| Use of proton pump inhibitor: yes/no (n of patients) | 11/30 |
| Imaging: CT/MRI (n of patients) | 23/18 |

Abbreviations: PPPD, pylorus preserving pancreaticoduodenectomy; CT, computed tomography; MRI, magnetic resonance imaging.

## MEN1 conventional screening

With conventional screening, ≥ 1 pancreatic lesions were detected by CT/MRI in 14 patients (34%), by SRS in 12 patients (29%) and by CT/MRI+ SRS in 18 patients (44%). Of the 23 patients with CT and the 18 with MRI, 9 (39%) and 6 (33%) patients had positive imaging for pancreatic lesions, respectively. In total, 32 pancreatic lesions were detected with CT/MRI (24 lesions) and SRS (13 lesions).

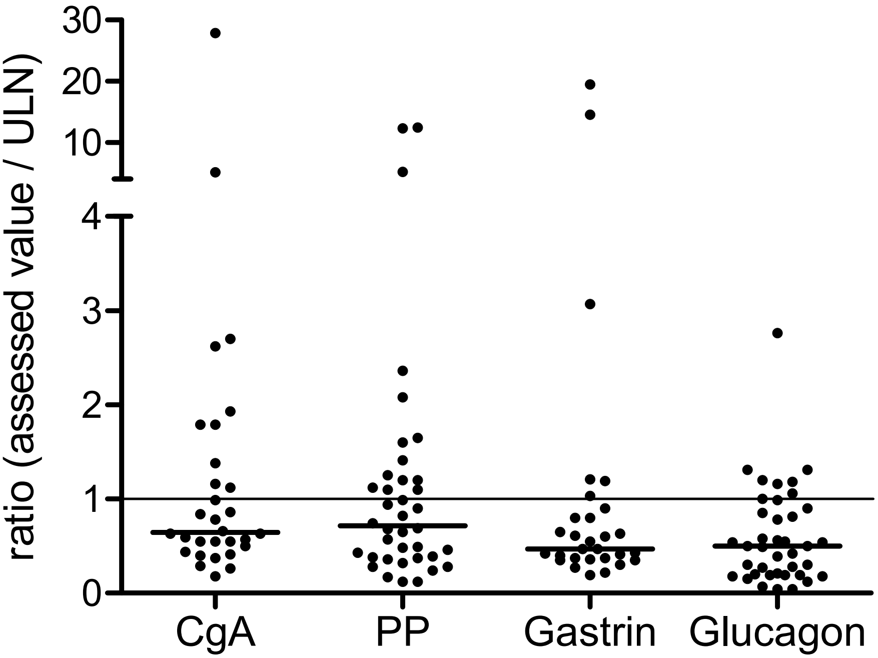


***Figure 1**. The y-axis shows the ratios of the tumor marker values for on the x-axis chromogranin A (n=30), pancreatic polypeptide (n=38), gastrin (n=29) and glucagon (n=39). Abbreviations: CgA, chromogranin A; PP, pancreatic polypeptide; ULN, upper limit of normal*

Of the 41 patients, 11 used proton pump inhibitors and were excluded from chromogranin A and gastrin analysis; 10 patients had elevated serum chromogranin A levels, 14 had elevated plasma pancreatic polypeptide levels, 6 had elevated serum gastrin levels, and 7 patients had elevated plasma glucagon levels (Figure 1). In 59% of the patients, levels were marginally elevated, being 1-2 times the upper limit of normal. Combining the 4 tumor markers resulted in 22 patients with elevated tumor markers, of whom 10 had a pancreatic lesion on CT/MRI and/or SRS.

## EUS

With EUS, 101 pancreatic lesions were detected in 34 patients (83%) with a mean size of 9.1 ± 7.5 mm. Different lesion characteristics were identified (Table 2). Most lesions were homogeneous, hypoechoic and iso-elastic, and 42% of lesions were hypervascular. Of all lesions, 15 (15%) were cystic; 9 lesions had a thickened wall, which was hypervascular in 5 lesions (Figure 2). EUS was positive in the 18 patients with pancreatic lesions on CT/MRI+ SRS. In 11 of these patients (61%), EUS detected 31 additional lesions. In the 23 patients without pancreatic lesions on CT/MRI+ SRS, EUS was positive in 16 patients (70%) and revealed 43 lesions. A second EUS expert (PF) reviewed 22 videotapes of lesions with sizes ranging from 2.5-25.8 mm. The presence of pancreatic lesions was confirmed in all cases.

In 10 patients, FNA was obtained for 12 lesions, with a median of 3 passes (range 1-4) per lesion. In 6 lesions the cytological diagnosis NET could be confirmed. The remaining samples did not yield enough cell material for a diagnosis. One patient was hospitalized because of abdominal pain after the FNA procedure due to acute pancreatitis. Plasma C-reactive protein was 114 mg/L (upper limit of normal 10 mmol/L) and plasma amylase was 82 U/L (upper limit of normal 220 U/L) and on the CT, infiltration of mesenterial fat close to the pancreatic head was seen. The patient recovered with conservative treatment within 6 days.

**Table 2.** Characteristics of pancreatic lesions detected with EUS

| EUS characteristics | Total n (%) of lesions |
|---|---|
| Location | 101 (100) |
| Pancreatic head | 46 (46) |
| Pancreatic body-tail | 55 (55) |
| Morphology | 101 (100) |
| Solid | 86 (85) |
| Cyst | 6 (6) |
| Cyst with a thick wall | 9 (9) |
| Margins | 93 (100) |
| Sharp | 68 (73) |
| Unsharp margins | 25 (27) |
| Echogenic pattern | 100 (100) |
| Hyperechoic | 2 (2) |
| Hypoechoic | 83 (83) |
| Anechoic | 15 (15) |
| Ultrasonographic texture | 94 (100) |
| Homogeneous | 69 (73) |
| Heterogeneous | 25 (27) |
| Power Doppler signal | 88 (100) |
| Positive | 37 (42) |
| Negative | 51 (58) |
| Elastography | 73 (100) |
| Rigid | 19 (26) |
| Iso-elastic | 54 (74) |
| Halophenomena | 95 (100) |
| Yes | 16 (17) |
| No | 79 (83) |

Abbreviation: EUS, endoscopic ultrasound

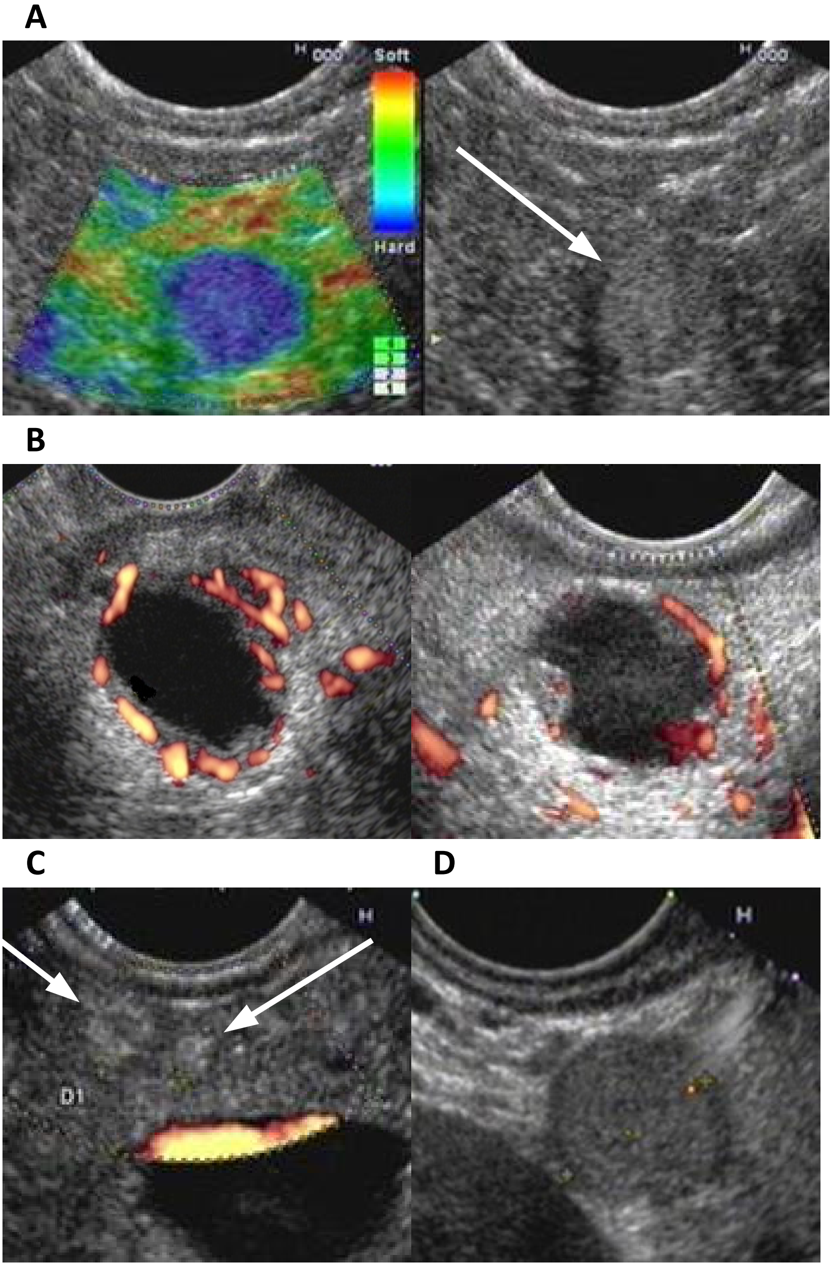


***Figure 2***. *EUS images of pancreatic lesions.* ***A*** *Elastography image of a pancreatic solid lesion (arrow). Blue color indicates rigidity.* ***B*** *Pancreatic cystic lesions with a thick hypervascular wall. Flow is present based on power Doppler, which indicates hypervascularity.* ***C*** *Two solid hyperechoic pancreatic lesions (arrows).* ***D*** *Pancreatic solid lesion with halo phenomena (black surrounding).*

## $^{11}$C-5-HTP PET

$^{11}$C-5-HTP PET showed uptake in the pancreas in 19 patients (46%) and detected 35 pancreatic lesions with focal increased uptake. In the 18 patients with pancreatic lesions on CT/MRI+ SRS, $^{11}$C-5-HTP PET detected 28 pancreatic lesions in 15 patients. In the 23 patients without pancreatic lesions on CT/MRI+ SRS, $^{11}$C-5-HTP PET was positive in 4 patients, and detected 7 pancreatic lesions.

## Surgery

Two patients underwent surgery. One patient with a pancreatic lesion on CT, SRS, $^{11}$C-5-HTP PET and EUS underwent a pancreatic tail resection of a 7.5 cm NET, confirmed with histology. The other patient with 6 lesions of 0.3-2.6 cm underwent subtotal pancreatectomy. All 6 were initially visualized with EUS, 4 with $^{11}$C-5-HTP PET, 2 with SRS and 1 with CT. The 2.6 cm lesion in the pancreatic head and multiple lesions in pancreatic body and tail showed NET at histology.

**Table 3.** Positive imaging for pancreatic lesions per pancreatic region

| **Pancreas** | **Total number (%) of lesions detected:** | | | | | |
|---|---|---|---|---|---|---|
| Location | CT/MRI | SRS | CT/MRI+SRS | $^{11}$C-5-HTP PET | EUS | Total |
| Head | 8 (17%) | 7 (15%) | 14 (29%) | 12 (25%) | 46 (96%) | 48 (100%) |
| Body-tail | 16 (27%) | 6 (10%) | 18 (31%) | 23 (39%) | 55 (93%) | 59 (100%) |

Abbreviations: CT, computed tomography; MRI, magnetic resonance imaging; SRS, somatostatin receptor scintigraphy; $^{11}$C-5-HTP, $^{11}$C-5-hydroxytryptophan positron emission tomography; EUS, endoscopic ultrasound

## EUS and $^{11}$C-5-HTP PET compared to MEN1 conventional screening

In 35 of 41 patients (85%), at least one of the imaging techniques was positive for a pancreatic lesion. At a patient-based level, EUS showed pancreatic lesions in more patients compared to CT, SRS and CT/MRI+ SRS (all $P$ <.001) (Table 3). $^{11}$C-5-HTP PET performed similar to CT/MRI and CT/MRI+ SRS, but was superior compared to SRS only ($P$ <.05). Regarding pancreatic lesions, 8 patients had 1 lesion, 9 patients had 2 lesions, 6 patients had 3 lesions, 4 patients had 4 lesions and 8 patients had 5 or more lesions. In total, 107 pancreatic lesions were detected: 48 were located in the pancreatic head and 59 in the pancreatic body-tail region (Table 3). Compared to CT/MRI, SRS and CT/MRI+ SRS, EUS found the most lesions (all $P$ <.001). This was also the case for lesions > 1 cm, (all $P$ <.01) (Table 4). In contrast, $^{11}$C-5-HTP PET performed similar to CT and CT/MRI+ SRS, but found more lesions compared to SRS only ($P$ <.05). At a patient- and lesion-based level (also lesions > 1 cm), EUS performed better compared to $^{11}$C-5-HTP PET ($P$ <.01). Figure 3 shows an example of a MEN1 patient with results of the four imaging techniques.

In total, 6 lesions were missed with EUS: 3 were detected with CT/MRI (1 lesion > 1 cm), 2 with $^{11}$C-5-HTP PET and 1 both with CT and $^{11}$C-5-HTP PET; 4 of the 6 lesions were located in the pancreatic tail.

Of the 35 patients with pancreatic lesions, 18 (51%) did have elevated tumor markers, of which 8 had less than 2-fold elevation of tumor markers, 4 between 2-fold and 3-fold, and 6 had > 3-fold elevation. Of the 6 patients without visualized pancreatic lesions, 4 (67%) also had elevated tumor markers, all with less than 2-fold elevation. Of these 4 patients, 2 had another MEN1-related manifestation: 1 patient had a pituitary macro-adenoma and 1 patient had a hyperparathyroidism, which can also be responsible for the elevated levels. Next to the pancreatic lesions, 15 extra-pancreatic lesions were found. (Supplementary Table 2).

**Table 4.** Positive imaging for pancreatic lesions in 35 patients

| Imaging Modality | Patients n (%) | *P* value | Lesions n (%) | *P* value | Lesions >1 cm n (%) | *P* value |
|---|---|---|---|---|---|---|
| CT/MRI | 14 (40) | - | 24 (22) | - | 17 (46) | - |
| SRS | 12 (34) | - | 13 (12) | - | 11 (30) | - |
| CT/MRI+SRS | 18 (51) | - | 32 (30) | - | 23 (62) | - |
| $^{11}$C-5-HTP PET | 19 (54) | 1* | 35 (32) | 0.74* | 19 (51) | 0.45* |
| EUS | 34 (97) | <0.001* | 101 (94) | <0.001* | 36 (97) | <0.01* |

* For $^{11}$C-5-HTP and EUS, discordance was calculated for the number of visualized lesions, compared to CT/MRI plus SRS.

Abbreviations: CT, computed tomography; MRI, magnetic resonance imaging; SRS, somatostatin receptor scintigraphy; $^{11}$C-5-HTP PET, $^{11}$C-5-hydroxytryptophan positron emission tomography; EUS, endoscopic ultrasound

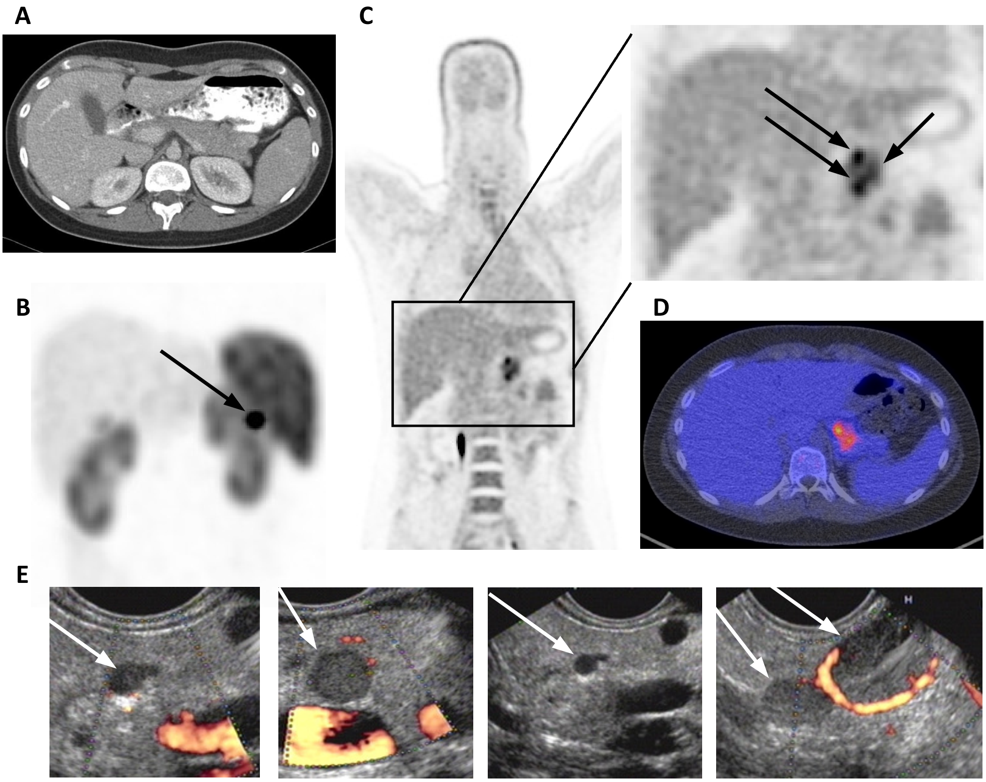

***Figure 3***. ***A*** *Axial image of CT scan,* ***B*** *maximum intensity projection image of SRS and* ***C*** *coronal image of* $^{11}$*C-5-HTP PET and* ***D*** *an axial fusion image of* $^{11}$*C-5-HTP PET with low-dose CT and* ***E*** *images of pancreatic lesions visualized with EUS. With CT no lesion was found and SRS showed 1 lesion located in the pancreatic tail. With* $^{11}$*C-5-HTP PET 3 lesions were visualized in the pancreatic body/tail region. However, EUS visualized 5 hypoechoic lesions: 4 in pancreatic body/tail region and 1 in the pancreatic head, with size ranging from 3.5-14 mm. The lesion of 14 mm showed a clear hypervascular wall with power Doppler.*

# Discussion

This is the first imaging study in MEN1 patients in which a prospective head-to-head comparison of EUS and $^{11}$C-5-HTP PET was performed relative to the standard screening for pNET detection. Compared to CT/MRI and SRS – separately or combined – EUS is superior for early detection of pancreatic lesions at both a patient and lesion-based level. In this screening setting, $^{11}$C-5-HTP PET is not useful.

Prominent in this study is the excellent performance of EUS. In our detailed analysis, most of the pancreatic lesions (83%) had a hypoechoic appearance on EUS. But not only solid lesions were detected; 15 lesions (15%) were cystic, with 9 having a thick, solid wall. Previously, cystic lesions were detected in 8% of MEN1 cases with EUS, but cysts with a thick wall were not described in that series.[13] In contrast to other studies which only looked at the echogenic pattern, we also checked for the presence of hypervascularity with power Doppler, which showed that 42% of pancreatic lesions were hypervascular. Moreover, differences were seen with elastography: most lesions had an iso-elastic consistency. Differences in EUS characteristics might reflect differences in growth behavior or malignant potential. In a retrospective EUS study with pNETs,[28] a univariate analysis of EUS findings showed that – in addition to larger size – heterogeneity and cystic changes are predictors of malignancy in pNET, which also might apply in MEN1 patients.

Until now MEN1 pancreatic imaging studies did not collect EUS and conventional imaging data prospectively. Moreover, not all standard screening imaging were available for a head-to-head comparison. However, the findings of the multicenter study in 90 MEN1 patients in which EUS was compared with MRI for pancreatic lesions is of interest.[29] In that study, 268 pancreatic lesions were detected with EUS and 158 with MRI. Of the 106 lesions ≥ 10 mm, 20 lesions (19%) were not detected by EUS, 19 of which were located in the pancreatic body-tail region. The authors therefore concluded that EUS and MRI are complementary and that both should be performed in the pancreas work-up for MEN1 patients.[29] In our study, EUS performed equally well in both the pancreatic head and body-tail region. This might be explained by the fact that EUS was performed in one center by an endoscopist who structurally mapped the pancreas. Only a linear scope was used with high quality devices. Since in the majority of cases EUS findings could not be confirmed by other imaging or pathologically, 22 EUS movies were reviewed by a second endoscopist at another academic center (PF). All lesions were considered as valid, which further supports EUS being superior compared to standard imaging.

In our study, EUS identified 101 lesions in 35 patients. Multiplicity of pancreatic lesions in MEN1 has also been confirmed by others in histological reports.[30-31] In pancreatic specimens of 28 MEN1 patients, the number of NETs (size > 5 mm) varied from 1–8 per patient.[31] Although cytological assessment was not performed in most pancreatic lesions in our study, the a priori chance of a present pNET is high in this patient group.

In one MEN1 imaging study for pNET screening, $^{11}$C-5-HTP PET was retrospectively evaluated in 16 patients and detected lesions in 6 (38%) patients, of which 2 lesions corresponded with CT.[12] In our study, $^{11}$C-5-HTP PET was of no value compared to standard screening. $^{11}$C-5-HTP PET detected only 51% of lesions > 1 cm, indicating that lack of detection is not only a result of the resolution of the PET camera. However, compared to SRS alone, $^{11}$C-5-HTP PET performed better, which indicates that SRS is not useful in the surveillance of MEN1. This outcome is in line with an earlier head-to-head comparison study in patients with advanced pNET, which showed $^{11}$C-5-HTP PET being superior to SRS.[16]

After the initial imaging, 2 patients had surgery, and NETs were histologically confirmed. Moreover, in 50% of the FNA procedures, the diagnosis NET could be confirmed. In previous retrospective study using EUS FNA for the diagnosis pNET, the yield was 53%.[32] Similar to Voss and colleagues,[32] our samples were often hemorrhagic, with only few cells available for cytology. In our study, one patient required hospitalization after the FNA procedure because of pancreatitis. In patients with pNETs, complications due to EUS guided FNA occurred in 1%.[33] Due to the risk of complications, it is questionable whether FNA in MEN1 patients is indicated, considering the high a priori chance of pNET. In the MEN1 setting, FNA could be reserved for a firm indication or whether diagnostic uncertainty exists.

To date, the value of the tumor markers chromogranin A, pancreatic polypeptide, gastrin and/or glucagon for screening of pNET is unknown. They are part of the MEN1 guidelines,[4-5] but without a known level of evidence. In our study, tumor markers were elevated in 51% of patients with pancreatic lesions on imaging, of which 44% had only marginally elevated levels (< 2 times the upper limit of normal). Moreover, 4 of the 6 patients without pancreatic lesions had marginally elevated levels; 2 of them had another MEN1-related manifestation. A large number of clinical conditions can cause false-positive levels, making interpretation difficult.[25-26, 34] Moreover, elevated chromogranin A levels were detected in 27% of patients with sporadic primary hyperparathyroidism or sporadic pituitary adenomas,[35] illustrating that chromogranin A can be elevated in the presence of other MEN1-related manifestations. In that same study, chromogranin A was elevated in 44% of MEN1 patients without NETs.[35] Overall, no clear data support that these markers are useful for pNET screening in MEN1.

pNET is the leading cause of MEN1-related death. To date, no markers are available that can predict malignant potential of pNET in MEN1. Size positively correlates with metastatic potential and is used as one of the most important arguments for pancreatic surgery. The MEN1 guideline recommends considering surgery for a lesion size ≥ 1 cm. However, no evidence exist concerning the best timing for surgery. Since EUS identified most lesions, follow-up with EUS will reveal insight into their growth velocity.[13] For smaller lesions are visualized, significant growth of pNETs can be detected. This may support surgery and may decline morbidity and mortality rates due to pNETs in MEN1.

Our study strongly supports EUS being superior for detection of pancreatic lesions in MEN1 patients compared to CT/MRI+ SRS and $^{11}$C-5-HTP PET. Based on our results, we suggest EUS as first choice imaging technique for pNET detection in MEN1.

**Acknowledgements** We would like to thank Drs D.J. Gouma and D. O'Toole for their contributions as members of the external monitoring committee.

**Funding** Supported by a Grant of the Dutch Cancer Society (RUG 2008-4188).

# References


1 Yao JC, Eisner MP, Leary C, et al. Population-based study of islet cell carcinoma. Ann Surg Oncol 2007;14:3492-3500.
2. Zhou J, Enewold L, Stojadinovic A, et al. Incidence rates of exocrine and endocrine pancreatic cancers in the United States. Cancer Causes Control 2010;21:853-861.
3. Pieterman CR, Vriens MR, Dreijerink KM, et al. Care for patients with multiple endocrine neoplasia type 1: the current evidence base. Fam Cancer 2011;10:157-171.
4. Brandi ML, Gagel RF, Angeli A, et al. Guidelines for diagnosis and therapy of MEN type 1 and type 2. J Clin Endocrinol Metab 2001;86:5658-5671.
5. Thakker RV, Newey PJ, Walls GV, et al. Clinical practice guidelines for Multiple Endocrine Neoplasia Type 1 (MEN1). J Clin Endocrin Metab 2012;97:2990-3011.
6. Doherty GM, Olson JA, Frisella MM, et al. Lethality of multiple endocrine neoplasia type 1. World J Surg 1998;22:581-586.
7. Dean PG, van Heerden JA, Farley DR, et al. Are patients with multiple endocrine neoplasia type I prone to premature death? World J Surg 2000;24:1437-1441.
8. Goudet P, Murat A, Binquet C, et al. Risk factors and causes of death in MEN1 disease. A GTE (Groupe d'Etude des Tumeurs Endocrines) cohort study among 758 patients. World J Surg 2010;34:249-255.
9. Rösch T, Lightdale CJ, Botet JF, et al. Localization of pancreatic endocrine tumors by endoscopic ultrasonography. N Engl J Med 1992;326:1721-1726.
10. Langer P, Kann PH, Fendrich V, et al. Prospective evaluation of imaging procedures for the detection of pancreaticoduodenal endocrine tumors in patients with Multiple Endocrine Neoplasia Type 1. World J Surg 2004;28:1317-1322.
11. Kann PH, Balakina E, Ivan D, et al. Natural course of small, asymptomatic neuroendocrine pancreatic tumours in Multiple Endocrine Neoplasia Type 1: an endoscopic ultrasound imaging study. Endocr Relat Cancer 2006;13:1195-1202.
12. Hellman P, Hennings, Akerström G, et al. Endoscopic ultrasonography for evaluation of pancreatic tumours in multiple endocrine neoplasia type 1. Br J Surg 2005;92:1508-1512.
13. Thomas-Marques L, Murat A, Delemer B, et al. Prospective endoscopic ultrasonographic evaluation of the frequency of nonfunctioning pancreaticoduodenal endocrine tumors in patients with multiple endocrine neoplasia type 1. Am J Gastroenterol 2006;101:266-273.
14. Lewis MA, Thompson GB, Young WF Jr. Preoperative assessment of the pancreas in multiple endocrine neoplasia type 1. World J Surg 2012;36:1375-1381.
15. Sundin A, Eriksson B, Bergström M, et al. Demonstration of [11C] 5-hydroxy-L-tryptophan uptake and decarboxylation in carcinoid tumors by specific positioning labeling in positron emission tomography. Nucl Med Biol 2000;27:33-41.
16. Koopmans KP, Neels OC, Kema IP, et al. Improved staging of patients with carcinoid and islet cell tumors with $^{18}$F-dihydroxy-phenyl-alanine and $^{11}$C-5-hydroxy-tryptophan positron emission tomography. J Clin Oncol 2008;26:1489-1495.

17. Balon HR, Goldsmith SJ, Siegel BA, et al. Procedure guideline for somatostatin receptor scintigraphy with (111)In-pentetreotide. J Nucl Med 2001;42:1134-1138.
18. Fiebrich HB, de Jong JR, Kema IP, et al. Total $^{18}$F-DOPA PET tumour uptake reflects metabolic endocrine tumour activity in patients with a carcinoid tumour. Eur J Nucl Med Mol Imaging 2011;38:1854-1861.
19. Walter T, Chardon L, Chopin-Laly X, et al. Is the combination of chromogranin A and pancreatic polypeptide serum determinations of interest in the diagnosis and follow-up of gastro-entero-pancreatic neuroendocrine tumours? Eur J Cancer 2012;48:1766-1773.
20. Suarez-Pinzon WL, Rabinovitch A. Combination therapy with a dipeptidyl peptidase-4 inhibitor and a proton pump inhibitor induces β-cell neogenesis from adult human pancreatic duct cells implanted in immunodeficient mice. Cell Transplant 2011;20:1343-1349.
21. Landstedt-Hallin L, Adamson U, Lins PE. Oral glibenclamide suppresses glucagon secretion during insulin-induced hypoglycemia in patients with type 2 diabetes. J Clin Endocrinol Metab 1999;84:3140-3145.
22. Deane AM, Chapman MJ, Fraser RJ, et al. The effect of exogenous glucagon-like peptide-1 on the glycaemic response to small intestinal nutrient in the critically ill: a randomised double-blind placebo-controlled cross over study. Crit Care 2009;13:R67.
23. Rice KS, Dickson G, Lane M, et al. Elevated serum gastrin levels in Jervell and Lange-Nielsen syndrome: a marker of severe KCNQ1 dysfunction? Heart Rhythm 2011;8:551-554.
24. Ito T, Cadiot G, Jensen RT. Diagnosis of Zollinger-Ellison syndrome: Increasingly difficult. World J Gastroenterol 2012;18:5495-5503.
25. Modlin IM, Gustafsson BI, Moss SF, et al. Chromogranin A–Biological function and clinical utility in neuro endocrine tumor disease. Ann Surg Oncol 2010;17:2427-2443.
26. http://www.uptodate.com/contents/hypoglycemia-in-adults-without-diabetes-mellitus-diagnostic-approach? (Access date: 1 July 2013)
27. Iglesias-Garcia J, Larino-Noia J, Abdulkader I, et al. EUS elastography for the characterization of solid pancreatic masses. Gastrointest Endosc 2009;70:1101-1108.
28. Ishikawa T, Itoh A, Kawashima H, et al. Usefulness of EUS combined with contrast-enhancement in the differential diagnosis of malignant versus benign and preoperative localization of pancreatic endocrine tumors. Gastrointest Endosc 2010;71:951-959.
29. Barbe C, Murat A, Dupas B, et al. Magnetic resonance imaging versus endoscopic ultrasonography for the detection of pancreatic tumours in multiple endocrine neoplasia type 1. Dig Liver Dis 2012;44:228-234.
30. Gauger PG, Doherty GM, Broome JT, et al. Completion pancreatectomy and duodenectomy for recurrent MEN-1 pancreaticoduodenal endocrine neoplasms. Surgery 2009;146:801-808.
31 Anlauf M, Schlenger R, Perren A, et al. Microadenomatosis of the endocrine pancreas in patients with and without the multiple endocrine neoplasia type 1 syndrome. Am J Surg Pathol 2006;30:560-574.
32. Voss M, Hammel P, Molas G, et al. Value of endoscopic ultrasound guided fine needle aspiration biopsy in the diagnosis of solid pancreatic masses. Gut 2000;46:244-249.

33. Atiq M, Bhutani MS, Bektas M, et al. EUS-FNA for pancreatic neuroendocrine tumors: a tertiary cancer center experience. Dig Dis Sci 2012;57:791-800.
34. Oberg K. Circulating biomarkers in gastroenteropancreatic neuroendocrine tumours. Endocr Relat Cancer 2011;18:S17-25.
35. Peracchi M, Conte D, Gebbia C, et al. Plasma chromogranin A in patients with sporadic gastro-entero-pancreatic neuroendocrine tumors or multiple endocrine neoplasia type 1. Eur J Endocrinol 2003;148:39-43.

# Supplementary data

**Supplementary Table 1.** Overview of mutations in the MEN1 patients

| Patients (n) | Mutation | Location | Type mutation |
|---|---|---|---|
| 2 | c.112delT (p.Ser38fs) | exon 2 | Frameshift |
| 1 | c.249_252del (p.Ile85fs) | exon 2 | Frameshift |
| 1 | c.322C>T (p.Arg108X) | exon 2 | Nonsense |
| 5 | c.358_360del (p.Lys120del) | exon 2 | In-frame deletion |
| 1 | c.506C>A (p.Ala169Asp) | exon 3 | Missense |
| 3 | c.517del (p.Leu173fs) | exon 3 | Frameshift |
| 2 | c.545T>C9 (p.Leu182Pro) | exon 3 | Missense |
| 3 | c.631del (p.Arg211fs) | exon 3 | Frameshift |
| 1 | c.810G>A (p.Trp270X) | exon 5 | Nonsense |
| 1 | c.965A>G (p.His322Arg) | exon 7 | Missense |
| 1 | c.1024G>C (p.Ala342Pro) | exon 7 | Missense |
| 2 | c.1074C>G (p.Tyr358X) | exon 8 | Nonsense |
| 3 | c.1099A>T (p.Lys367X) | exon 8 | Nonsense |
| 1 | c.1192C>T (p.Gln398X) | exon 8 | Nonsense |
| 3 | c.1430dupG (p.Glu478fs) | exon 10 | Frameshift |
| 4 | c.1561dup (p.Arg521fs) | exon 10 | Frameshift |
| 1 | c.1594C>T (p.Arg532X) | exon 10 | Nonsense |
| 1 | c.1677_16845dup8 (p.Lys562fs) | exon 10 | Frameshift |
| 5 | c.-110-?1848+?del (p.?) | whole gene | Deletion |

**Supplementary Table 2.** Overview of extra-pancreatic (suspicious) NET lesions

| **Location** | **Lesion visualized on imaging** | | | |
|---|---|---|---|---|
| | CT/MRI | SRS | $^{11}$C-5-HTP PET | EUS |
| Duodenum | Yes | No | No | No |
| Duodenum[#] | No | No | No | Yes |
| Duodenum[#] | No | No | No | Yes |
| Adjacent to pancreas LN | No | No | Yes | Yes |
| Adjacent to pancreas LN | No | No | No | Yes |
| Adjacent to pancreas LN | No | Yes | No | Yes |
| Adjacent to pancreas LN | Yes | Yes | No | No |
| Liver[^] | Yes | No | No | No |
| Liver | No | Yes | No | No |
| Liver | No | Yes | Yes | No |
| Omentum | Retrosp | No | Yes | No |
| Left adrenal gland | Yes | Yes | No | Yes |
| Pulmonary LN | Retrosp | No | Yes | No |
| Pulmonary LN | Retrosp | No | Yes | No |
| Pulmonary LN | Retrosp | No | Yes | No |

[#] Histological confirmed NET

[^] Classified as benign lesion based on imaging

Abbreviations: LN, lymph node; retrosp, retrospectively seen; CT, computed tomography; MRI, magnetic resonance imaging; SRS, somatostatin receptor scintigraphy; $^{11}$C-5-HTP, $^{11}$C-5-hydroxytryptophan PET; EUS, endoscopic ultrasound.

# Chapter 5

## $^{89}$Zr-bevacizumab PET visualizes disease manifestations in patients with von Hippel-Lindau disease

Sjoukje F. Oosting*
Sophie J. van Asselt*
Adrienne H. Brouwers
Alfons H.H. Bongaerts
Julia Steinberg
Johan R. de Jong
Marjolijn N. Lub-de Hooge
Anouk N.A. van der Horst-Schrivers
Annemiek M.E. Walenkamp
Eelco W. Hoving
Wim J. Sluiter
Bernard A. Zonnenberg
Elisabeth G.E. de Vries
Thera P. Links

***The first two authors contributed equally to this study.**

***Submitted***

# Abstract

**Purpose** Patients with von Hippel-Lindau (VHL) disease are at risk to develop benign and malignant vascular tumors. Local vascular endothelial growth factor (VEGF)-A production is supposed to play an important role in development of disease manifestations and is a treatment target for antiangiogenic therapy. The monoclonal antibody bevacizumab binds VEGF-A. We aimed to assess whether VHL-associated lesions can be visualized with $^{89}Zr$-bevacizumab positron emission tomography (PET) and to explore whether $^{89}Zr$-bevacizumab PET can differentiate progressive lesions from non-progressive lesions.

**Methods** Adult VHL patients with ≥ 1 measurable hemangioblastoma were eligible. $^{89}Zr$-bevacizumab, 37 MBq, was injected 4 days before the PET scan. Maximum standardized uptake values ($SUV_{max}$) were calculated. PET scans were fused with routine MRI of the central nervous system and abdominal MRI or CT. Progressive lesions were defined as new lesions, lesions that became symptomatic and lesions ≥ 10 mm that increased ≥ 10% and ≥ 4 mm on repeat anatomic imaging within 12 months.

**Results** Twenty-two patients were enrolled. $^{89}Zr$-bevacizumab PET visualized 59 VHL manifestations, 0-17 per patient, with a median $SUV_{max}$ of 8.5 (range 1.3 – 35.8). Detection rate for lesions ≥ 10 mm was 30.8%. Seven additional hotspots without substrate on baseline anatomic imaging were found, 2 were also detected with anatomic imaging during follow-up. Nine out of 25 progressive lesions were visible on PET ($SUV_{max}$ 0.9-8.9).

**Conclusion** VHL lesions can be visualized with $^{89}Zr$-bevacizumab PET with a striking heterogeneity in tracer accumulation. $^{89}Zr$-bevacizumab uptake does not predict progression within 12 months.

# Introduction

Von Hippel-Lindau (VHL) disease is an autosomal dominant inherited tumor syndrome caused by an inactivating germ line mutation in the *VHL* gene, located on chromosome 3p25. The estimated prevalence is 2-3 per 100,000 persons.[1-2] Inactivation or loss of the wild type *VHL* allele results in disease manifestations. Lack of functional VHL protein (pVHL) induces intracellular accumulation of the transcription factor hypoxia inducible factor 1 alpha (HIF1α) which activates cellular survival strategies for hypoxic circumstances. This leads to switching on angiogenesis via production of pro-angiogenic growth factors including vascular endothelial growth factor A (VEGF-A). VHL disease manifestations consist of hemangioblastomas of the central nervous system (CNS), retinal angiomas, renal cell carcinomas (RCC), pancreatic neuroendocrine tumors (pNET), pheochromocytomas, endolymphatic sac tumors of the middle ear, and cysts in kidneys, pancreas, epididymis and broad ligament. VHL mutation carriers often develop multiple disease manifestations that can severely affect quality of life. Moreover, VHL patients have a shorter life expectancy compared to the general population, with metastatic RCC as the leading cause of death.[3-4]

Guidelines for screening and surveillance of existing lesions advice frequent imaging, ocular examination, and blood and urine examination.[5-6] There is however currently no tool that predicts the behavior of a disease manifestation. Hemangioblastomas are often dormant for years but can suddenly start growing.[7]

Local concentrations of the key growth factor VEGF-A in VHL, may provide predictive information on biological behavior of VHL-associated lesions and provide information on the presence of a drug target. We developed the positron emission tomography (PET) tracer $^{89}$Zr-bevacizumab that binds VEGF-A and enables noninvasive whole body imaging and quantification. In patients with sporadic metastatic RCC, $^{89}$Zr-bevacizumab PET visualized tumor lesions including brain metastases, illustrating that the radioactive tracer can cross the blood brain barrier.[8]

The aim of the present feasibility study was to assess whether VHL-associated lesions can be visualized with $^{89}$Zr-bevacizumab PET and whether $^{89}$Zr-bevacizumab PET can differentiate progressive lesions from non-progressive lesions.

# Materials & methods

## Patients

Eligibility criteria included genetically proven VHL disease or clinically proven VHL [5] with a 1st grade family member with genetically confirmed VHL, age ≥ 18 years, participation in a surveillance program with routine anatomic imaging [5-6] and at least one measurable lesion located in the CNS. Pregnant patients were excluded. Treatment for VHL manifestations was recorded up to 12 months after $^{89}$Zr-bevacizumab PET imaging. The study was approved by the institutional review board and registered under http://www.clinicaltrials.gov (identifier: NCT00970970). All patients gave written informed consent.

## $^{89}$Zr-bevacizumab PET

Conjugation and labeling of bevacizumab (25 mg/mL, Roche) with $^{89}$Zr was performed as described earlier.[9-11] Whole-body PET images were acquired on a Siemens Biograph mCT (PET/CT 64 slices) from the upper legs to the head in 6-8 bed positions of 5 minutes acquisition time each and a final reconstruction resolution of ~10 mm. The first 3 patients underwent PET scans after 1 hr, and 2 and 4 days after the IV administration of $^{89}$Zr-bevacizumab (37 MBq, protein dose of 5 mg). The optimal scan timing with the highest lesion-to-background ratio was day 4. The next patients therefore underwent PET scanning 4 days after $^{89}$Zr-bevacizumab administration.

## Standard screening and surveillance

Patients underwent MRI of the CNS within 6 weeks prior to $^{89}$Zr-bevacizumab PET, and abdominal CT or MRI 3 months before till 3 months after $^{89}$Zr-bevacizumab PET. Follow-up anatomic imaging was carried out within 12 months of initial surveillance. MRI scans were performed with a 1.5 Tesla scanner in T1 and T2-weighted sequences, with and without intravenously (IV) administration of gadolinium-containing contrast agent. The reconstruction interval varied between 1 and 5 mm for CNS imaging and between 1.5 and 5 mm for abdominal imaging. CT scans were performed with a multidetector scanner, before and after IV administration of iodine-containing contrast agent and a maximum slice thickness of

5.0 mm. CNS and abdominal imaging were centrally reviewed by two radiologists (JS, and AHHB). Morphological aspect (cystic, solid, mixed) and maximal lesion diameters in transversal planes were recorded.

## Imaging analysis

The $^{89}$Zr-bevacizumab PET scans were compared with baseline MRI and/or CT scans in order to verify substrate for $^{89}$Zr-bevacizumab PET-positive lesions. Tracer uptake was quantified in VHL-associated lesions and healthy organs with AMIDE Medical Image Data Examiner software (version 0.9.1, Stanford University) by drawing 3D regions of interest.[12] Mean and maximum standardized uptake values ($SUV_{mean}$ and $SUV_{max}$) were calculated for healthy organs and VHL manifestations visualized on PET. Given the resolution of $^{89}$Zr-bevacizumab PET, we did a sub-analysis of lesions ≥ 10 mm.

For all lesions visualized on baseline CT/MRI except simple renal and pancreatic cysts, progression was recorded and compared with $^{89}$Zr-bevacizumab PET data. As a definition of progression for VHL manifestations and information on variability of measurements on repeat imaging is lacking, we took a conservative approach based on variability of lung tumor measurements on CT.[13] We considered lesions with a longest diameter of ≥ 10 mm that increased ≥ 10% and an absolute growth of ≥ 4 mm progressive, as well as new lesions visualized on the follow-up scan and lesions that became symptomatic.

## Plasma VEGF-A

VEGF-A levels were determined in plasma samples obtained immediately before $^{89}$Zr-bevacizumab administration with the Quantikine enzyme-linked immunosorbent assay kit (R&D Systems, Minneapolis, MN). Plasma VEGF-A was compared with $^{89}$Zr-bevacizumab PET results.

## Statistical analysis

The primary endpoint was the detection rate of $^{89}$Zr-bevacizumab PET for VHL-associated lesions. Spearman rank correlations served to calculate correlations. For comparison of unpaired data the Mann-Whitney test and for paired data the Wilcoxon signed rank test was used. A *P* value $<.05$ was considered statistically significant.

# Results

## Patient characteristics

Between November 2009 and April 2012, 22 patients were included, 13 male and 9 female patients with a median age of 42 years (range 23-66), for additional patient characteristics see Table 1.

**Table 1.** Patient characteristics

| Characteristic | Total population (n = 22) | |
|---|---|---|
| | No | % |
| **Sex** | | |
| Male | 13 | 59 |
| Female | 9 | 41 |
| **Age, years** | | |
| Median | 42 | |
| Range | 23 – 66 | |
| **Mutation** | | |
| c.-89-?_c.297+?del | 10 | 45 |
| c.500G>A | 5 | 23 |
| c.509T>A | 3 | 14 |
| c.490C>T | 1 | 5 |
| c.340+1G>A | 1 | 5 |
| c.241C>T | 1 | 5 |
| IVS1-59del46 (unclassified variant) | 1 | 5 |
| **History** | | |
| Hemangioblastoma | 22 | 100 |
| Retinal angioma | 15 | 68 |
| Renal cell carcinoma | 8 | 36 |
| Pancreatic NET | 5 | 23 |
| Pheochromocytoma | 4 | 18 |
| **Prior treatment** patients (procedures) | | |
| Craniotomy | 12 (28) | 55 |
| Spinal cord hemangioblastoma embolization | 2 (2) | 9 |
| Retinal laser/cryotherapy | 14 (19) | 64 |
| (Partial) nephrectomy | 8 (13) | 36 |
| Adrenalectomy | 4 (7) | 18 |
| (Partial) pancreatectomy | 2 (2) | 9 |

**Table 2.** VHL manifestations at routine imaging and $^{89}$Zr-bevacizumab PET per patient

| Patient | Sex (F/M) age (years) | VHL manifestations[a] at baseline anatomic imaging (N) | MRI/CT Lesions ≥ 10 mm | PET Lesions | $SUV_{max}$ Range |
|---|---|---|---|---|---|
| 1 | M 57 | CNS (5), pancreas (2) | 2 | 2 | 4.8 - 6.0 |
| 2 | F 23 | CNS (1) | 1 | 0 | |
| 3 | M 31 | CNS (8), kidney (1), epididymis[b] (1) | 3 | 1 | 12.2 |
| 4 | M 61 | CNS (4), kidney (8), pancreas (1) | 10 | 7 | 6.6 - 27.6 |
| 5 | F 61 | CNS (13), kidney (3), pancreas (1) | 9 | 8 | 2.4 - 28.3 |
| 6 | M 62 | CNS (3), pancreas (2) | 3 | 1 | 6.7 |
| 7 | F 36 | CNS (19), pancreas (2) | 3 | 3 | 1.3 - 2.8 |
| 8 | F 29 | CNS (10), pancreas (1) | 2 | 1 | 1.4 |
| 9 | M 33 | CNS (2), pancreas (2) | 1 | 1 | 4.3 |
| 10 | F 48 | CNS (9), kidney (4), pancreas (1) | 5 | 1 | 1.6 |
| 11 | F 29 | CNS (7) | 1 | 1 | 4.8 |
| 12 | F 38 | CNS (4), pancreas (1), adrenal gland (1) | 1 | 2 | 4.1 - 6.4 |
| 13 | M 63 | CNS (4), kidney (4), pancreas (1) | 3 | 0 | |
| 14 | F 46 | CNS (1), pancreas (1) | 1 | 0 | |
| 15 | F 60 | CNS (1), pancreas (1), liver (100), bone[c] (1) | 81 | 18 | 5.7 - 15.4 |
| 16 | M 26 | CNS (3) | 1 | 0 | |
| 17 | M 32 | CNS (8), kidney (2), pancreas (1) | 3 | 3 | 4.3 - 35.8 |
| 18 | M 31 | CNS (7) | 0 | 0 | |
| 19 | M 50 | CNS (55), epididymis[b] (1) | 5 | 7 | 2.7 – 9.0 |
| 20 | M 46 | CNS (1) | 1 | 0 | |
| 21 | M 66 | CNS (4) | 2 | 2 | 3.4 - 5.7 |
| 22 | M 35 | CNS (1), kidney (1) | 1 | 1 | 26.6 |

M=male, F=female, CNS=central nervous system, NA=not available

[a] excluding simple cysts,

[b] demonstrated on ultrasound,

[c] demonstrated on $^{11}$C-hydroxytryptophan (HTP) PET

## Routine anatomic imaging

In total 311 VHL associated lesions other than simple renal and pancreatic cysts were identified on baseline MRI and CT with a median of 7 per patient (range 1-102). In the CNS 170 lesions were detected, for details see Table 2 and Table 3. In total, 139 lesions were ≥ 10 mm. Furthermore, 130 simple cysts ≥ 5 mm were detected in the kidneys (range 0-46 per patient) and 126 in the pancreas (range 0-30).

**Table 3**. VHL manifestations at routine imaging and $^{89}$Zr-bevacizumab PET per organ

| Localization | MRI/CT Lesions (N) | (≥ 10 mm) | PET positive lesions (N) | SUV$_{max}$ median | (range) |
|---|---|---|---|---|---|
| Brain | | | | | |
| Cerebellum | 116 | (15) | 19 | 4.8 | (1.3 – 8.9) |
| Other | 4 | (1) | 1 | 6.1 | |
| Spine | 49 | (12) | 3 | 4.1 | (3.6 – 6.7) |
| Optical nerve | 1 | (1) | 1 | 2.4 | |
| Kidney | 23 | (19) | 12 | 22.2 | (6.6 – 35.8) |
| Pancreas | 17 | (11) | 3 | 6.0 | (4.3 – 10.3) |
| Adrenal gland | 1 | (0) | 1 | 6.4 | |
| Liver | 100 | (80) | 16 | 9.7 | (8.5 – 15.4) |
| Epididymis | * | | 2 | 10.6 | (9.0 – 12.2) |
| Iliac spine | ** | | 1 | 5.7 | |

* cystadenomas confirmed on ultrasound

** bone metastasis of pancreas neuroendocrine tumor confirmed on $^{11}$C-HTP PET

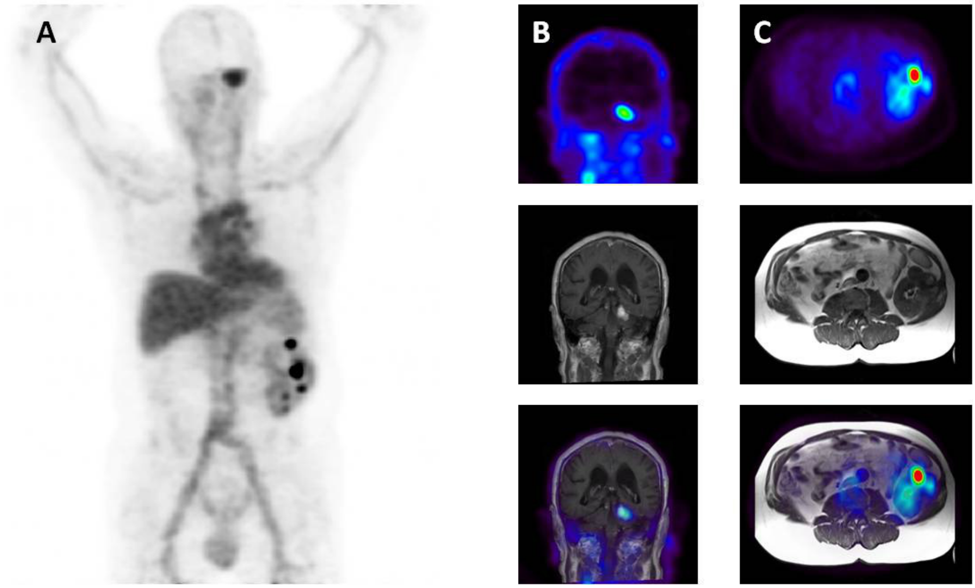


***Figure 1. A*** *$^{89}$Zr-bevacizumab PET scan of patient 4, demonstrating normal antibody distribution with tracer uptake in the blood pool and in the liver, and also uptake in a hemangioblastoma in the cerebellum (SUV$_{max}$ 8.3) and in 6 solid kidney lesions (SUV$_{max}$ 6.6 – 27.6).* ***B*** *Hemangioblastoma visualized by $^{89}$Zr-bevacizumab PET, MRI and the fusion image.* ***C*** *Kidney lesions visualized by $^{89}$Zr-bevacizumab PET, MRI and the fusion image.*

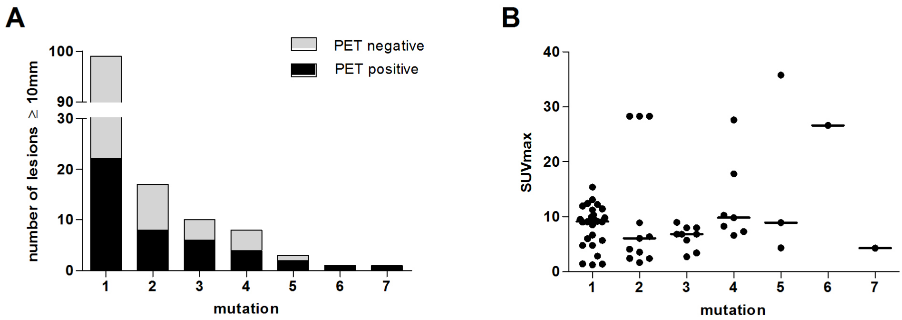


***Figure 2.*** *Number of PET positive VHL manifestations ≥ 10 mm according to* ***A*** *germline mutation and* ***B*** *SUV$_{max}$ for all PET positive VHL manifestations according to germline mutation: 1 = c.-89-?_c.297+? del, 2 = c.500G>A, 3 = c.490C>T, 4 = c.509T>A, 5 = c.340+1G>A, 6 = c.241C>T, 7 = IVS1-59del46.*

## $^{89}$Zr-bevacizumab PET

$^{89}$Zr-bevacizumab PET visualized 59 VHL-associated lesions, median 1 (range 0-17) per patient. In Figure 1 a representative patient is shown. Location of lesions detected with PET is summarized in Table 3. The PET scan demonstrated 7 additional hotspots without substrate on anatomic imaging, 3 in the kidney, 1 in the shoulder, 1 in the eye, 1 in the cerebellum and 1 in an adrenal gland. The last 2 lesions however, were detected also during follow-up on anatomic imaging. The smallest lesion detected on the PET scan was a hemangioblastoma measuring 4.0 mm on MRI. Out of 139 VHL manifestations ≥ 10 mm, 44 (30.8%) were visualized with $^{89}$Zr-bevacizumab PET. In Figure 2, SUV$_{max}$ and the proportion of PET positive lesions ≥ 10 mm are shown for the different germline mutations. Of the 59 PET positive VHL manifestations, 50 had a solid, 6 a cystic and 2 a mixed appearance on anatomic imaging, and 1 lesion could not be classified. No $^{89}$Zr-bevacizumab accumulation in simple renal and pancreatic cysts was demonstrated; 33 simple renal cysts appeared as cold spots.

Quantification of $^{89}$Zr-bevacizumab distribution revealed a strong correlation between SUV$_{max}$ and SUV$_{mean}$ for normal organs ($r = .99$, $P < .01$) and VHL lesions ($r = .97$, $P < .01$, Data Supplement). SUV$_{max}$ is less operator dependent and therefore reported. Normal organ distribution of $^{89}$Zr-bevacizumab was similar as for patients with neuroendocrine tumors and as reported for other antibody tracers [14-16] representing normal antibody distribution with relatively high uptake in the liver and the heart, the latter reflecting the blood pool, intermediate uptake in kidney and spleen and low uptake in lung, bone, muscle and brain (Figure 3A). Median SUV$_{max}$ of

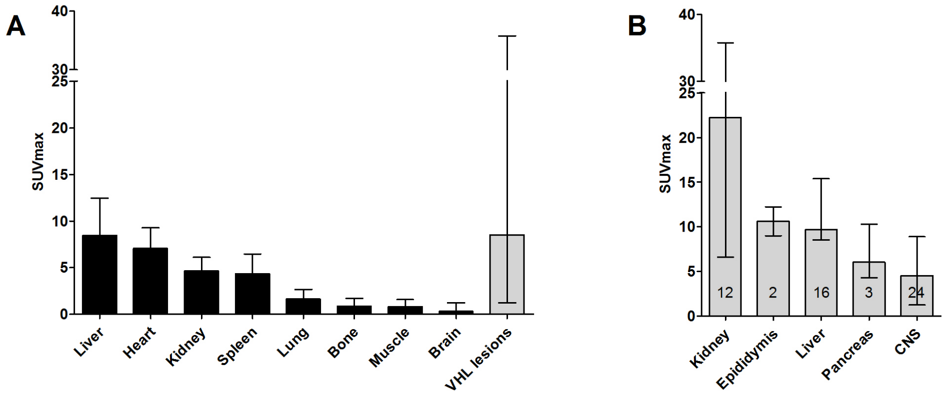


***Figure 3.** Quantification (median with range) of [89]Zr-bevacizumab distribution in 22 VHL patients in **A** normal organs and 59 VHL manifestations and in **B** VHL manifestations according to localization.*

VHL manifestations was 8.5 (range 1.3 – 35.8) with higher tracer uptake in kidney lesions (n = 12, median $SUV_{max}$ 22.2, range 6.6 – 35.8) than in CNS lesions (n = 24, median $SUV_{max}$ 4.5, range 1.3 – 8.9, $P$ <.0001, Figure 3B).

## Progressive lesions

Repeat abdominal imaging was available in 19 patients at a median of 349 days after baseline (range 196-642), and CNS imaging in 20 patients at a median of 319 days after baseline (range 90-540). Two hundred lesions were evaluable for progression. In total 25 lesions were progressive, of which 21 hemangioblastomas and 4 RCCs.

$^{89}$Zr-bevacizumab PET visualized 9 out of 25 (36%) progressive lesions and 27 out of 175 non-progressive lesions (15%), resulting in a positive predictive value (PPV) of 25% and a negative predictive value (NPV) of 90%. When limiting the analysis to lesions ≥ 10 mm at baseline, 7 out of 15 (43%) progressive lesions and 17 out of 35 (49%) non-progressive lesions were detected with PET, corresponding to a PPV of 29% and a NPV of 69%. Progressive and non-progressive lesions had a similar $SUV_{max}$ (median 4.8, range 0.9 – 8.9 versus 6.7, range 1.3 – 35.8, $P$ = .14).

**Table 4.** Treatment in the year after $^{89}$Zr-bevacizumab PET

| Patient | Sex(F/M) age (years) | Progressive lesions | Action |
|---|---|---|---|
| 1 | M 57 | Symptomatic HB | Craniotomy, resection |
| 2 | F 23 | None | Surveillance |
| 3 | M 31 | Symptomatic HB | Laminectomy, resection |
| 4 | M 61 | Symptomatic HB | Craniotomy, resection |
| 5 | F 61[a] | Multiple symptomatic inoperable HB | Bevacizumab/IFNα |
| 6 | M 62 | 2 new asymptomatic HB | Surveillance |
| 7 | F 36 | 3 new asymptomatic HB | Surveillance |
| 8 | F 29 | Symptomatic HB | Craniotomy, resection |
| 9 | M 33 | None | Surveillance |
| 10 | F 48[a] | Recurrent multifocal RCC Metastatic RCC | Resection,Bevacizumab/IFNα |
| 11 | F 29 | Growing asymptomatic HB | Surveillance |
| 12 | F 38 | None | Surveillance |
| 13 | M 63 | 1 new asymptomatic HB | Surveillance |
| 14 | F 46 | None | Surveillance |
| 15 | F 60 | Metastatic pNET, progression not assessed | Everolimus |
| 16 | M 26 | Growing asymptomatic HB | Surveillance |
| 17 | M 32 | None | Surveillance |
| 18 | M 31 | 1 new asymptomatic HB | Surveillance |
| 19 | M 50 | None | Surveillance |
| 20 | M 46 | Symptomatic HB | Laminectomy, resection |
| 21 | M 66 | None | Surveillance |
| 22 | M 35 | None | Surveillance |

M=male, F=female, HB=hemangioblastoma, IFNα=interferon alpha, RCC=renal cell carcinoma, pNET=pancreatic neuroendocrine tumor, NA=not available.
[a] Detailed case report in Data Supplement.

## Treatment

In the first year of follow-up, 8 patients were actively treated for VHL disease manifestations, 6 with surgery and 2 with systemic treatment, and 6 patients had asymptomatic progressive hemangioblastomas for which surveillance was intensified (Table 4 ). Two patients received bevacizumab treatment, one for metastatic RCC and one for progressive hemangioblastomas without local treatment options. In the first patient $^{89}$Zr-bevacizumab RCC uptake was similar to surrounding normal tissue, she died within 2 months of progressive disease. The second patient had intense $^{89}$Zr-bevacizumab uptake in hemangioblastomas and has continuing benefit after 27 months of treatment. These patients are described in more detail in the Data Supplement.

### Plasma VEGF-A

Baseline plasma VEGF-A levels were available for all, and follow-up levels for 14 out of 22 patients. Median plasma VEGF-A was 23.9 pg/mL (range: undetectable – 123.0) at baseline and 32.1 pg/mL (range: undetectable – 259.7) at follow-up. No correlation was found between baseline plasma VEGF-A and the total number of VHL manifestations, the number of PET positive lesions, $SUV_{max}$ or mean $SUV_{max}$. Furthermore, baseline and delta plasma VEGF-A did not differ between patients with progressive lesions and patients without.

## Discussion

This is the first study demonstrating that malignant and non-malignant manifestations of VHL disease can be visualized with $^{89}$Zr-bevacizumab PET. The detection rate for lesions ≥ 10 mm was 30.8%, indicating that in one third of the lesions the drug target VEGF-A is available and accessible. Despite the monogenetic pathogenesis, profound heterogeneity in tracer uptake by the lesions between and within patients was demonstrated which is partly determined by the type of manifestation. $^{89}$Zr-bevacizumab PET did not identify lesions that progressed within the next year, nor did plasma VEGF-A levels.

Abundant VEGF expression has been demonstrated by in situ hybridization and immunohistochemistry in a variety of VHL-associated lesions, including hemangioblastoma, retinal angioma, and RCC.[17-25] In contrast, VEGF mRNA was not detectable in normal brain,[18] and was 3-13 times lower in normal kidney than in RCC.[23] This corresponds with our imaging data that show virtually no $^{89}$Zr-bevacizumab accumulation in normal brain, intermediate uptake in normal kidney and high uptake compared to normal surrounding tissue in one third of disease manifestations. We did not perform biopsies to correlate imaging results with tissue VEGF-A concentration in the present study. However, in previous imaging studies with radiolabeled bevacizumab in 9 melanoma patients and 23 breast cancer patients, tumor tracer uptake correlated with tumor VEGF-A measurement by immunohistochemistry and enzyme-linked immunosorbent assay (ELISA) respectively,[11, 26] although in 5 RCC patients no correlation was found between $^{111}$In-bevacizumab uptake and VEGF-A concentration within primary tumors.[27]

VHL disease is clinically divided in type 1 (absence of pheochromocytoma) and type 2 (high risk of pheochromocytoma) and type 2 is further subdivided according to risk of RCC (2A: low, 2B: high, and 2C: pheochromocytoma only). Correlation between phenotype and genotype is complex; about 200 different germline mutations have been identified.[28] Type 1 appears to result from mutations that disrupt HIF1α degradation whereas in type 2 disease HIF1α regulation by pVHL is partly preserved.[28] Therefore, VEGF-A overexpression is probably much more pronounced and important for pathogenesis in type 1 disease then in type 2 disease and could explain heterogeneity of $^{89}$Zr-bevacizumab PET results between patients. Although the numbers of lesions are too small to draw conclusions, our results do not suggest important differences in the rate of PET positive lesions or in $SUV_{max}$ for the different germline mutations. Moreover, the capacity to target HIF for degradation and the degree of VEGF-A overexpression in a single disease manifestation is most likely a resultant of the type of the germline mutation and the second hit. The second hit differs across lesions, as has been demonstrated by analysis of deletion size in 16 disease manifestations of a single patient,[29] which could explain the intrapatient heterogeneity in $^{89}$Zr-bevacizumab uptake that we found. pVHL also has HIF-independent functions such as stabilization of microtubules, regulation of apoptosis, regulation of extracellular matrix assembly and maintenance of primary cilium. Loss of HIF-independent functions probably contributes to the development of disease manifestations.[28] Furthermore, additional mutations are involved in specific manifestations, as demonstrated by loss of chromosome 11 in 31 out of 36 VHL associated pheochromocytomas but in none of 7 VHL related hemangioblastomas, contributing to genomic intrapatient heterogeneity of VHL lesions.[30] In sporadic clear cell RCC, which is also characterized by *VHL* loss, additional mutations frequently exist.[31-32] In depth analysis of multiple tumor samples from 4 sporadic RCC patients also revealed striking mutational heterogeneity and a pattern of branched evolution.[33]

We found no difference in $^{89}$Zr-bevacizumab accumulation between progressive and non-progressive disease manifestations ≥ 10 mm. This contrasts with a small study of retinal angiomas of 3 VHL patients where the highest VEGF mRNA level was found in the patient with the most active disease.[34] Also in 50 patients with sporadic clear cell RCC who underwent nephrectomy, cytoplasmic VEGF expression correlated with tumor progression and tumor grade.[35]

Simple cysts in kidneys and pancreatic glands did not take up $^{89}$Zr-bevacizumab. Higher VEGF concentration were detected in the fluid of 2 renal cysts then in serum of 1 VHL patient.[36] Promotion of cyst formation may however be more dependent on loss of maintenance of the primary cilium than on activation of the VEGF pathway.[37]

We did not find a relation between plasma VEGF-A levels and PET imaging results. Also the number of lesions and presence of symptomatic or growing lesions was not related with plasma VEGF-A. This is in line with lack of a correlation between serum VEGF measurements and disease manifestations in 15 VHL patients, and the fact that serum VEGF did not differ significantly between VHL patients and healthy controls.[36] This may be explained by different VEGF-A splice variants in the circulation compared to the microenvironment of disease manifestations. The small variants, consisting of 121 and 165 amino acids ($VEGF_{121}$ and $VEGF_{165}$) are freely diffusible whereas the large variants $VEGF_{189}$ and $VEGF_{206}$ are bound to the extracellular matrix.[38] Imaging with $^{89}$Zr-bevacizumab, which binds to all splice variants, therefore potentially better reflects biology of disease manifestations than circulating VEGF-A.

VHL patients receive local treatment for symptomatic disease manifestations and lesions that pose a threat to functioning or have metastatic potential. Systemic treatment has been used as salvage strategy for unresectable or multiple progressive hemangioblastomas with high risk of severe morbidity from local treatment. There is no evidence based systemic therapy available but case reports, case series and small studies have been reported for antiangiogenic treatment with bevacizumab,[39] thalidomide [40-41] as well as the tyrosine kinase inhibitors semaxanib [42-46] and sunitinib.[47-48] Study results for vatalanib and for bevacizumab are awaited (www.clinicaltrials.gov identifiers: NTC00052013 and NTC01015300). Antiangiogenic therapy has resulted in improvement of symptoms, prolonged periods of disease stabilization, but rarely induces volume responses in hemangioblastomas. We treated two VHL patients with bevacizumab plus IFNα after participation in this imaging study. One patient, who received it for metastatic RCC and hardly showed $^{89}$Zr-bevacizumab accumulation in the tumor, did not respond and died of rapidly progressive disease after 2 months. The other patient was treated for multiple progressive unresectable hemangioblastomas with intense uptake on the PET scan. She experienced prolonged symptomatic improvement, and a decrease in hemangioblastoma size. These cases suggest that $^{89}$Zr-bevacizumab PET might offer a tool to select patients for anti-VEGF therapy, but this needs further evaluation in future studies.

In conclusion, $^{89}$Zr-bevacizumab PET can visualize different VHL manifestations but does not predict the behavior of a lesion. Striking heterogeneity between and within patients was found which may reflect different biology and might predict sensitivity to antiangiogenic treatment.

**Funding** This study is supported by a grant of the American VHL family alliance.

# References


1. Neumann HP, Wiestler OD. Clustering of von Hippel-Lindau syndrome: evidence for a complex genetic locus. Lancet 1991;337:1052-1054.
2. Maher ER, Iselius L, Yates JR, et al. Von Hippel-Lindau disease: a genetic study. J Med Genet 1991;28:443-447.
3. Wilding A, Ingham SL, Lalloo F, et al. Life expectancy in hereditary cancer predisposing diseases: an observational study. J Med Genet 2012;49:264-269.
4. Maher ER, Yates JR, Harries R, et al. Clinical features and natural history of von Hippel-Lindau disease. Q J Med 1990;77:1151-1163.
5. Lonser RR, Glenn GM, Walther M, et al. Von Hippel-Lindau disease. Lancet 2003;361:2059-2067
6. The VHL handbook (http://www.vhl.org/handbook/vhlhb4.php#Suggested) (access date: 10 December 2012)
7. Wanebo JE, Lonser RR, Glenn GM, et al. The natural history of hemangioblastomas of the central nervous system in patients with von Hippel-Lindau disease. J Neurosurg 2003;98:82-94.
8. Oosting SF, Brouwers AH, Van Es SC, et al. $^{89}$Zr-bevacizumab PET imaging in metastatic renal cell carcinoma patients before and during antiangiogenic treatment. J Clin Oncol 2012; 30: suppl; abstr 10581.
9. Verel I, Visser GW, Boellaard R, et al. $^{89}$Zr immuno-PET: comprehensive procedures for the production of $^{89}$Zr-labeled monoclonal antibodies. J Nucl Med 2003;44:1271-1281.
10. Nagengast WB, de Vries EG, Hospers GA, et al. In vivo VEGF imaging with radiolabeled bevacizumab in an ovarian tumor xenograft. J Nucl Med 2007;48:1313-1319.
11. Gaykema SB, Brouwers AH, Lub-deHooge MN, et al. $^{89}$Zr-bevacizumab PET imaging in primary breast cancer. J Nucl Med 2013;54:1014-1018.
12. Loening AM, Gambhir SS. AMIDE: a free software tool for multimodality medical image analysis. Mol Imaging 2003;2:131-137.
13. Oxnard GR, Zhao B, Sima CS, et al. Variability of lung tumor measurements on repeat computed tomography scans taken within 15 minutes. J Clin Oncol 2011;29:3114-3119.
14. Van Asselt SJ, Oosting SF, Brouwers AH, et al. Everolimus reduces $^{89}$Zr-bevacizumab tumor uptake in patients with neuroendocrine tumors. Accepted to J Nucl Med.
15. Dijkers EC, Oude Munnink TH, Kosterink JG, et al. Biodistribution of $^{89}$Zr-trastuzumab and PET imaging of HER2-positive lesions in patients with metastatic breast cancer. Clin Pharmacol Ther 2010;87:586-592.
16. Pandit-Taskar N, O'Donoghue JA, Morris MJ, et al. Antibody mass escalation study in patients with castration-resistant prostate cancer using $^{111}$In-J591: lesion detectability and dosimetric projections for $^{90}$Y radioimmunotherapy. J Nucl Med 2008;49:1066-1074.
17. Wizigman-Voos S, Breier G, Risau W, et al. Up-regulation of vascular endothelial growth factor and its receptors in von Hippel-Lindau disease-associated and sporadic hemangioblastomas. Cancer Res 1995;55:1358-1364.

18. Krieg M, Marti HH, Plate KH. Coexpression of erythropoietin and vascular endothelial growth factor in nervous system tumors associated with von Hippel-Lindau tumor suppressor gene loss of function. Blood 1998;92:3388-3393.
19. Vaquero J, Zurita M, Oya S, et al. Vascular permeability factor expression in cerebellar hemangioblastomas: correlation with tumor-associated cysts. J Neurooncol 1999;41:3-7.
20. Miyagami M, Katayama Y, Nakamura S. Clinicopathological study of vascular endothelial growth factor (VEGF), p53, and proliferative potential in familial von Hippel-Lindau disease and sporadic hemangioblastomas. Brain Tumor Pathol 2000;17:111-120.
21. Chan CC, Vortmeyer AO, Chew EY, et al. VHL gene deletion and enhanced VEGF gene expression detected in the stromal cells of retinal angioma. Arch Ophthalmol 1999;117:625-630.
22. Brown LF, Berse B, Jackman RW, et al. Increased expression of vascular permeability factor (vascular endothelial growth factor) and its receptors in kidney and bladder carcinomas. Am J Pathol 1993;143:1255-1262.
23. Takahashi A, Sasaki H, Kim SJ, et al. Markedly increased amounts of messenger RNAs for vascular endothelial growth factor and placental growth factor in renal cell carcinoma associated with angiogenesis. Cancer Res 1994;54:4233-4237.
24. Leung SY, Chan AS, Wong MP, et al. Expression of vascular endothelial growth factor in von Hippel-lindau syndrome associated papillary cystadenoma of the epididymis. Hum Pathol 1998;29:1322-1324.
25. Horiguchi H, Sano T, Toi H, et al. Endolymphatic sac tumor associated with a von Hippel-Lindau disease patient: an immunohistochemical study. Mod Pathol 2001;14:727-732.
26. Nagengast WB, Hooge MN, van Straten EM, et al. VEGF-SPECT with $^{111}$In-bevacizumab in stage III/IV melanoma patients. Eur J Cancer 2011;47:1595-1602.
27. Desar IME, Stillebroer AB, Oosterwijk E, et al. $^{111}$In-bevacizumab imaging of renal cell cancer and evaluation of neoadjuvant treatment with the vascular endothelial growth factor receptor inhibitor sorafenib. J Nucl Med 2010;51:1707-1715.
28. Richard S, Gardie B, Couvé S, et al. Von Hippel-Lindau: how a rare disease illuminates cancer biology. Semin Cancer Biol 2013;23:26-37.
29. Gläsker S, Sohn TS, Okamoto H, et al. Second hit deletion size in Von Hippel-Lindau disease. Ann Neurol 2006;59:105-110.
30. Lui WO, Chen J, Gläsker S, et al. Selective loss of chromosome 11 in pheochromocytomas associated with the VHL syndrome. Oncogene 2002;21:1117-1122.
31. Dalgliesh GL, Furge K, Greenman C, et al. Systematic sequencing of renal carcinoma reveals inactivation of histone modifying genes. Nature 2010;463:360-363.
32. Varela I, Tarpey P, Raine K, et al. Exosome sequencing identifies frequent mutation of the SWI/SNF complex gene PBRM1 in renal carcinoma. Nature 2011;469:539-542.
33. Gerlinger M, Rowan AJ, Horswell S, Larkin J, Endesfelder D, Gronroos E, et al. Intratumor heterogeneity and branched evolution revealed by multiregion sequencing. N Engl J Med 2012;366:883-892.

34. Liang X, Shen D, Huang Y, et al. Molecular pathology and CXCR4 expression in surgically excised retinal hemangioblastomas associated with von Hippel-Lindau disease. Opthalmology 2007;114:147-156.
35. Rioux-Leclercq N, Fergelot P, Zerrouki S, et al. Plasma level and tissue expression of vascular endothelial growth factor in renal cell carcinoma: a prospective study of 50 cases. Hum Pathol 2007;38:1489-1495.
36. Los M, Aarsman CJM, Terpstra L, et al. Elevated ocular levels of vascular endothelial growth factor in patients with von Hippel-Lindau disease. Ann Oncol 1997;8:1015-1022.
37. Thoma CR, Frew IJ, Hoerner CR, et al. pVHL and GSK3β are components of a primary clilum-maintanance signaling network. Nature Cell Biol 2007;9:588-595.
38. Park JE, Keller GA, Ferrara N. The vascular endothelial growth factor (VEGF) isoforms: differential deposition into the subepithelial extracellular matrix and bioactivity of extracellular matrix-bound VEGF. Mol Biol Cell 1993;4:1317-1326.
39. Omar AI. Bevacizumab for the treatment of surgically unresectable cervical cord hemangioblastoma: a case report. J Med Case Rep 2012;6:238.
40. Piribauer M, Czech T, Dieckmann K, et al. Stabilization of a progressive hemangioblastoma under treatment with thalidomide. J Neurooncol 2004;66:295-299.
41. Sardi I, Sanzo M, Giordano F, et al. Monotherapy with thalidomide for treatment of spinal cord hemangioblastoma in a patient with von Hippel-Lindau disease. Pediatr Blood Cancer 2009;53:464-467.
42. Aiello LP, Geaorge DJ, Cahill MT, et al. Rapid and durable recovery of visual function in a patient with von Hippel-Lindau syndrome after systemic therapy with vascular endothelial growth factor receptor inhibitor SU5416. Ophthalmology 2002;109:1745-1751.
43. Girmens JF, Erginay A, Massin P, et al. Treatment of von Hippel-Lindau retinal hemangioblastomas by the vascular endothelial growth factor receptor inhibitor SU5416 is more effective for associated macular edema than for hemangioblastomas. Am J Ophthalmol 2003;136:194-196.
44. Schuch G, de Wit M, Höltje J, et al. Case 2. Hemangioblastomas: diagnosis of von Hippel-Lindau disease and antiangiogenic treatment with SU5416. J Clin Oncol 2005;23:3624-3626.
45. Madhusudan S, Deplanque G, Braybrooke JP, et al. Antiangiogenic therapy for von Hippel-Lindau disease. JAMA 2004;291:943-944.
46. Richard S, Croisille L, Yvart J, et al. Paradoxical secondary polycythemia in von Hippel-Lindau patients treated with anti-vascular endothelial growth factor therapy. Blood 2002;99:3851-3853.
47. Jimenez C, Cabanillas ME, Santarpia L, et al. Use of tyrosine kinase inhibitor sunitinib in a patient with von Hippel-Lindau disease: targeting angiogenic factors in pheochromocytoma and other von Hippel-Lindau disease-related tumors. J Clin Endocrinol Metab 2009;94:386-391.
48. Jonasch E, McCutcheon IE, Waguespack SG, et al. Pilot trial of sunitinib therapy in patients with von Hippel-Lindau disease. Ann Oncol 2011;22:2661-2666.

# Supplementary data

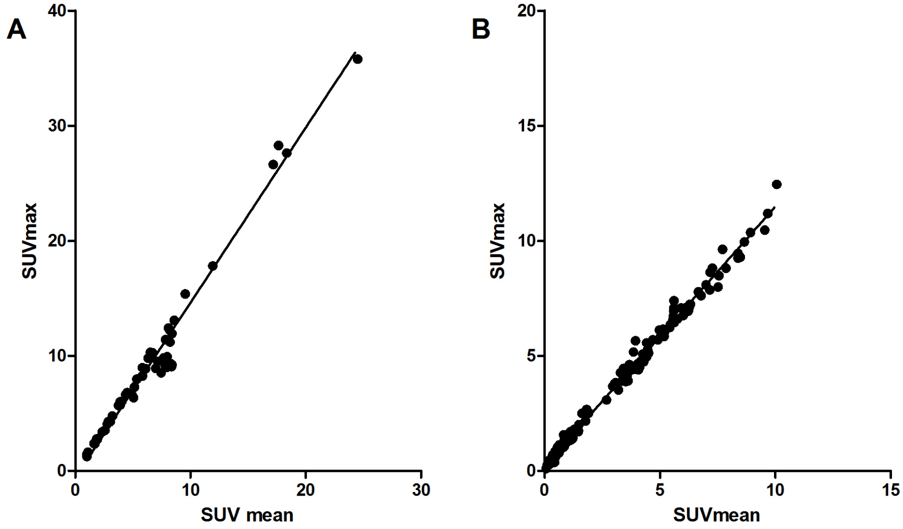


***Supplementary Figure 1***. *Correlation between* $SUV_{mean}$ *and* $SUV_{max}$ *for* ***A*** *VHL manifestations and* ***B*** *normal organs.*

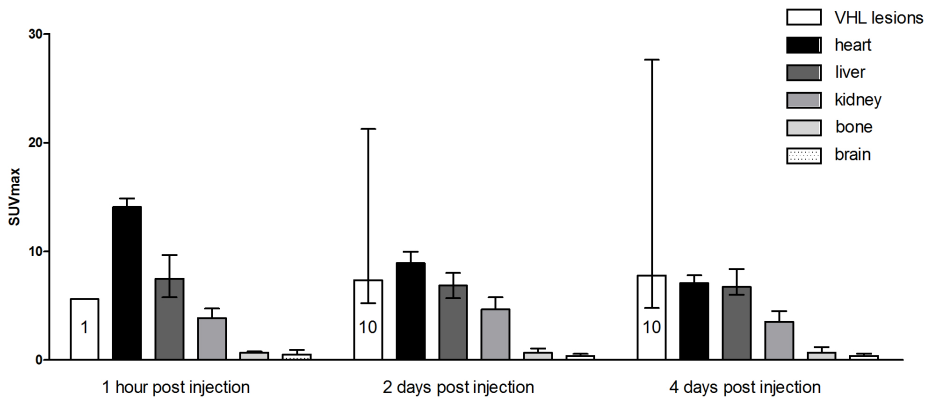


***Supplementary Figure 2.*** *Maximum standardized uptake value (median* $SUV_{max}$ *with range) of VHL-associated lesions and normal organs on serial PET scans of 3 VHL patients 1 hour, 2 days and 4 days after* $^{89}$*Zr-bevacizumab injection.*

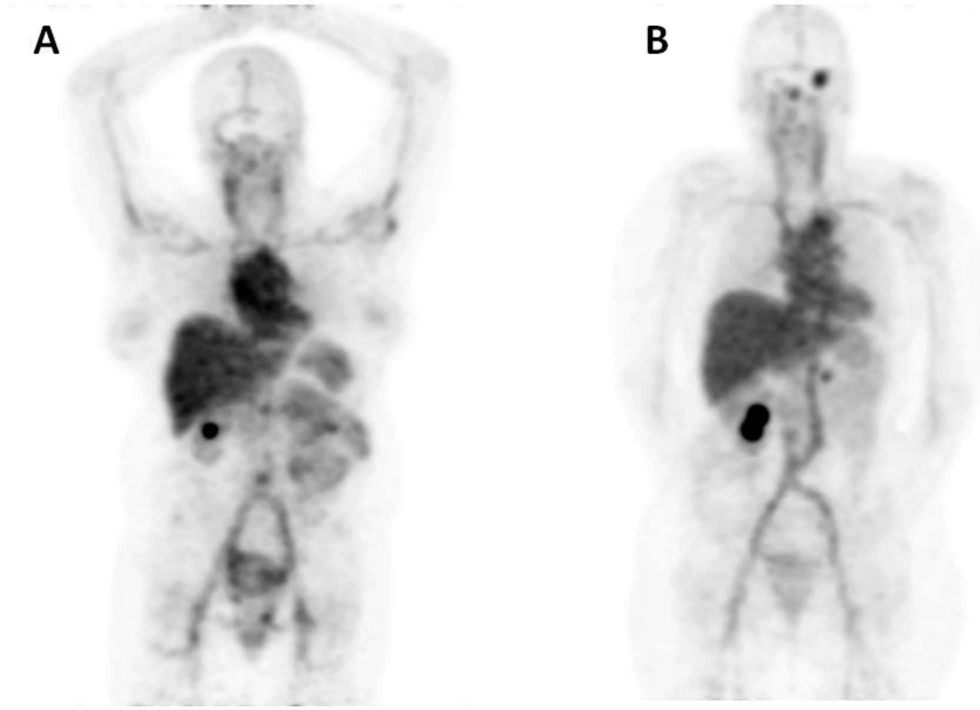


***Supplementary Figure 3. A*** *PET scan of patient A demonstrating a hotspot in the right kidney (no substrate on MRI) but no uptake above background in 4 RCCs localizations in the left kidney region.* ***B*** *PET scan of patient B showing tracer uptake in hemangioblastomas and right kidney.*

## Case reports

Patient A, a 48-year-old female patient with a c.500G>A mutation, had at trial entry a history of resected bilateral pheochromocytoma, treatment of retinal angioma, a resected cerebellar hemangioblastoma, a partial left nephrectomy for RCC and 4 progressive solid lesions growing from the left kidney remnant. Baseline MRI scans showed 14 VHL manifestations (5 ≥ 10 mm): 9 CNS lesions, 4 solid lesions in the left kidney and 1 solid pancreatic mass. Of these, only one cerebellar hemangioblastoma < 5 mm with a $SUV_{max}$ of 1.6 was visible on $^{89}$Zr-bevacizumab PET. The PET scan also demonstrated a hotspot in the right kidney but on MRI no substrate was found (Supplementary Figure 3A). The PET scan did not show focally increased uptake in recurrent RCC lesions from the left kidney remnant. Four weeks after the PET scan, a radical left tumor nephrectomy with a partial colon resection was performed because

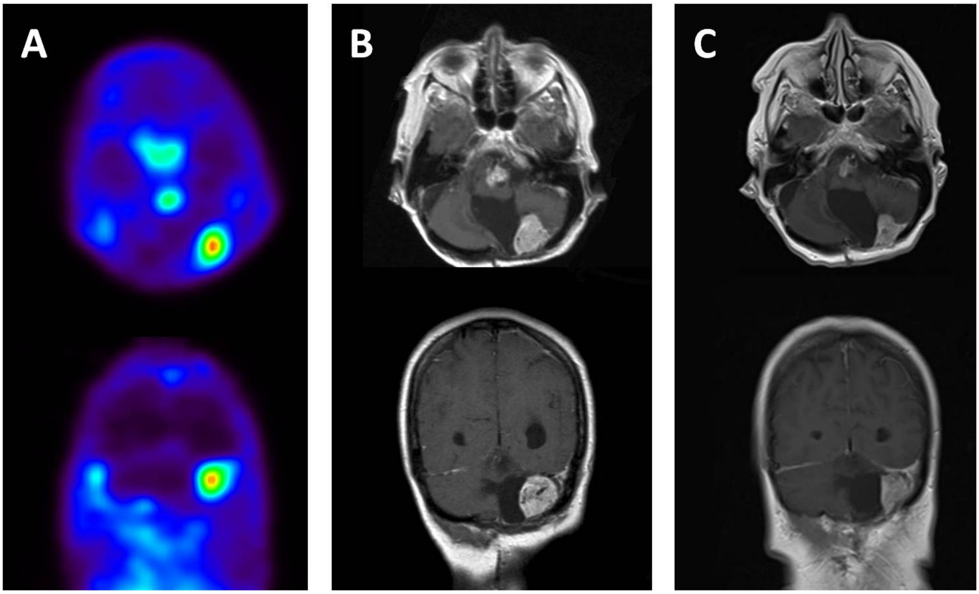


***Supplementary Figure 4. A** PET scan and **B** MRI scans of patient B demonstrating hemangioblastomas in the cerebellum and brain stem before and **C** after 3 months of bevacizumab treatment.*

of RCC infiltration. Six months later she presented with extensive local recurrence, ascites and liver metastases. She started standard RCC treatment with bevacizumab 10 mg/kg intravenously every 2 weeks plus INFα 3 times per week subcutaneously at a starting dose of 3 million units with the aim to increase the dose to 9 million units 3 times per week if tolerated. The patient died 2 months later of progressive RCC.

Patient B, a 61-year-old female patient with also a c.500G>A mutation, entered the trial with a history of bilateral retinal angiomas, 5 craniotomies for resection of hemangioblastomas, embolisation of a cervical spine hemangioblastoma, a radical left nephrectomy for RCC, a partial right nephrectomy and radiofrequency ablation for recurrent RCC. She suffered from ataxia, disturbed balance and diplopia. Baseline MRI scans revealed 13 CNS lesions (8 intracranial, 2 cervical, 2 thoracic and 1 optic nerve localization), 3 solid kidney lesions, and 1 pancreatic lesion suspect for pNET. Nine lesions were ≥ 10 mm, 8 lesions were visible on PET, with a median $SUV_{max}$ of 7.5 (range 2.4 – 28.3) including 5 CNS lesions (Supplementary Figure 3B). Five months after the $^{89}$Zr-bevacizumab PET scan, her condition deteriorated with dysartria and dysphagia and severe neuropathic pain in the neck, shoulders and arms. Progression of hemangioblastomas in the cerebellum, brain stem and cervical spine was demonstrated on MRI. Surgical or endovascular treatment was not possible, radiosurgery was deemed too dangerous because of the risk of transient increase in vascular permeability and edema. The patient received treatment with bevacizumab plus INFα according to the standard regimen for RCC.

Two weeks after the first bevacizumab dose, neuropathic pain had resolved completely. INFα was stopped after 8 weeks because of anorexia. Walking and speech improved a little over months. The MRI scan after 3 months of treatment showed a decrease in size of the hemangioblastomas in cerebellum and brain stem (Supplementary Figure 4) and of the kidney mass, whereas other lesions were unchanged. After 8 months of treatment she developed hydrocephalus because of growth of a cystic component of the cerebellar hemangioblastoma. An endoscopic third ventriculostomy was performed and bevacizumab was continued. Currently the patient has received 27 months bevacizumab treatment with clinical and radiological stable disease.

# Chapter 6

## Everolimus reduces $^{89}Zr$-bevacizumab tumor uptake in patients with neuroendocrine tumors

Sophie J. van Asselt
Sjoukje F. Oosting
Adrienne H. Brouwers
Alfons H.H. Bongaerts
Johan R. de Jong
Marjolijn N. Lub-de Hooge
Thijs H. Oude Munnink
Helle-Brit Fiebrich
Wim J. Sluiter
Thera P. Links
Annemiek M.E. Walenkamp
Elisabeth G.E. de Vries

*Accepted in Journal of Nuclear Medicine*

# Abstract

**Background** Everolimus increases progression free survival in patients with advanced neuroendocrine tumors (NETs). Currently, no biomarkers are available for early selection of patients who will benefit from everolimus. Everolimus can reduce VEGF-A production by tumor cells. Therefore, we aimed to investigate the effect of everolimus on tumor uptake of radioactive labeled VEGF-A antibody bevacizumab with positron emission tomography (PET) in NET patients.

**Methods** Patients with advanced progressive well-differentiated NET underwent $^{89}$Zr-bevacizumab PET scans before, and at 2 and 12 weeks during everolimus treatment. $^{89}$Zr-bevacizumab uptake was quantified by the maximum standardized uptake value ($SUV_{max}$). Tumor response and % change in sum of target lesion diameters was determined according to RECIST1.1 on CT 3-monthly.

**Results** In four of the 14 patients entered, no tumor lesions were visualized with $^{89}$Zr-bevacizumab PET. In the remaining patients, 19% of tumor lesions ≥ 1 cm known by CT were visualized. Tumor $SUV_{max}$ decreased during everolimus treatment with median -7% at 2 weeks ($P$ = .09) and median -35% at 12 weeks ($P$ < .001). $\Delta$ $SUV_{max}$ at 2 and 12 weeks correlated with % change on CT at 6 months ($r^2 = 0.51$, $P$ < .05, $r^2 = 0.61$, $P$ < .01, respectively).

**Conclusion** This study demonstrates variable $^{89}$Zr-bevacizumab PET tumor uptake in NET patients. $^{89}$Zr-bevacizumab tumor uptake diminished during everolimus treatment. Serial $^{89}$Zr-bevacizumab PET might be useful as early predictive biomarker of anti-VEGF directed treatment in NET patients.

# Introduction

Angiogenesis is a hallmark for tumor growth as well as for development of metastases.[1] Vascular endothelial growth factor A (VEGF-A) produced by tumors is one of the main factors responsible for angiogenesis. Currently, several anti-angiogenic therapies are available as anti-cancer agents, including VEGF-A antibodies, tyrosine kinase inhibitors (TKIs) and mTOR-inhibitors. Anti-angiogenic drugs are of interest in patients with well-differentiated neuroendocrine tumors (NETs)[2] as these tumors are hypervascular.[3-6] mTOR indirectly stimulates angiogenesis, but also induces mRNA translation of other genes important for cell survival and proliferation.[7]

Phase 3 trials have shown superior progression free survival in patients with advanced well-differentiated NETs treated with the VEGF-receptor TKI sunitinib or the mTOR inhibitor everolimus. Sunitinib resulted in a progression free survival benefit of 5.9 months in pancreatic NET (pNET) patients compared to placebo.[8] Two trials with everolimus, one in pNET patients and one in patients with NETs associated with carcinoid syndrome, showed a progression free survival benefit of 6.4 and 5.1 months respectively in favor of everolimus compared to placebo.[9-10]

As not all patients benefit of everolimus, biomarkers to select patients who will profit from treatment would be extremely helpful. An attractive candidate is VEGF-A. mTOR inhibition reduced VEGF-A excretion by NET tumor cell lines.[11] Additionally, in renal cancer xenografts, sensitivity to mTOR-inhibition correlated with reductions in tumor HIF-1α mRNA translation, VEGF-A expression and angiogenesis.[12] However, circulating VEGF-A in patients treated with anti-angiogenic drugs have not yet shown a clear predictive value.[13] Moreover in pNET patients, serum VEGF-A levels did not differ between patients treated with everolimus or placebo.[14] Therefore, it might be more relevant to determine the VEGF-A production at the site of the tumor lesions.

We have developed both single photon emission computed tomography (SPECT) and positron emission tomography (PET) radiopharmaceuticals to visualize VEGF-A non-invasively with the VEGF-A antibody bevacizumab coupled to a radionuclide.[15] We showed that everolimus lowered $^{89}$Zr-bevacizumab uptake in an ovarian cancer xenograft model. This coincided with lowered tumor VEGF-A levels.[16] Moreover, this approach is feasible in patients. $^{111}$In-bevacizumab SPECT could visualize all tumor lesions in melanoma patients.[17] Given the superior resolution and quantification options of PET we subsequently developed the PET tracer $^{89}$Zr-bevacizumab. We showed $^{89}$Zr-bevacizumab uptake in numerous tumor lesions in untreated renal cell cancer patients.[18]

Therefore, we decided to perform a feasibility study in which we used $^{89}$Zr-bevacizumab PET to investigate whether NET lesions in patients can be visualized and whether $^{89}$Zr-bevacizumab tumor uptake changes during everolimus therapy.

# Materials and methods

## Patients

Patients with advanced non-resectable well-differentiated (low or intermediate grade)[19-20] NET, ≥ 18 years of age, with an ECOG performance score of 0-2 [21] with adequate bone marrow, hepatic, and renal function, controlled lipid profile and glucose levels as well as radiological documentation of progressive disease over the past year and measurable lesions according to the response evaluation criteria in solid tumors (RECIST) version 1.1, were eligible.[22] Exclusion criteria were uncontrolled medical conditions, such as unstable cardiac disease, serious infections, as well as any psychological, familial, sociological or geographical conditions potential hampering compliance with the study. The study was approved by the local Medical Ethical Committee. All participants gave written informed consent. The study is registered on clinicaltrials.gov (NCT01338090).

## Everolimus treatment and patient monitoring

Treatment consisted of everolimus 10 mg orally once daily. In case of grade 3 toxicity, dose reductions were allowed to 5 mg every other day. Patients were treated until disease progression based on RECIST1.1, or intolerable toxicity. Progression free survival was defined as length of everolimus treatment until progressive disease according to RECIST1.1 or clinical progression. Before start of everolimus, after 11 days and every 4 weeks during treatment the patient visited the outpatient clinic for medical history, physical examination, and blood tests. Blood tests consisted of measurements of blood counts, renal and hepatic function, lipid profile, glucose and chromogranin A. Serum chromogranin A levels were determined as described earlier.[23] At 2 and 12 weeks, everolimus levels were measured in EDTA blood by liquid chromatography and tandem mass spectrometry, as described previously.[24] At baseline and 12 weeks, serum VEGF-A levels were determined with the Quantikine enzyme-linked immunosorbent assay kit (R&D Systems, Minneapolis, MN).

## $^{89}$Zr-bevacizumab PET/CT and CT

Conjugation and labeling of bevacizumab (25 mg/mL, Roche) was performed in UMCG cleanroom facilities under GMP conditions as described earlier.[16, 25] Four days prior to each $^{89}$Zr-bevacizumab PET scan, 37 MBq of $^{89}$Zr-bevacizumab (protein dose of 5 mg) was administered intravenously. Whole-body PET imaging was performed from upper legs to head in 6-8 bed positions of 5 minutes acquisition time each. All patients underwent $^{89}$Zr-bevacizumab PET scanning at baseline and after 2 weeks everolimus treatment. $^{89}$Zr-bevacizumab PET after 12 weeks everolimus treatment was performed only if tumor lesions could be visualized on earlier $^{89}$Zr-bevacizumab PET scans. At baseline and after 12 weeks, the PET scan was combined with a diagnostic CT of the chest and abdomen (Siemens Biograph mCT PET/CT, 4 detector rings, 64 slice CT, Siemens, Knoxville, TN). Staging after 6 months and every 3 months thereafter, was performed with a multislice CT scanner (Sensation 16 or 64 slice CT, Siemens). Diagnostic CT scans were performed before and after administration of intravenous contrast agent as a tri-phase scan, with maximal slice thickness of 5.0 mm.

## Image and data analysis

The image quality of 37 MBq $^{89}$Zr provides a resolution of ~10 mm on PET. Therefore, the total number of tumor lesions ≥ 10 mm on baseline CT scan was determined. $^{89}$Zr-bevacizumab PET was compared with the baseline CT scan. For lesions outside the field of view of the CT, other nuclear medicine imaging techniques were used for verification.

Tracer uptake was quantified in tumor lesions and organs with AMIDE Medical Image Data Examiner software (version 0.9.1, Stanford University) by drawing 3D regions of interest.[26] Mean and maximum standardized uptake values ($SUV_{mean/\ max}$) were calculated. If > 10 tumor lesions were visualized in one organ, then 10 were quantified. A high correlation was found between $SUV_{mean}$ and $SUV_{max}$ for healthy organs and tumor lesions (Pearson $r^2 = 0.99$ and $r^2 = 0.97$ respectively, $P < .0001$). Since it is less operator dependent, we present data as $SUV_{max}$. $\Delta$ $SUV_{max}$ of all tumor lesions, and $\Delta$ $SUV_{max}$ of the most intense ($^{89}$Zr-bevacizumab accumulating) tumor lesion per patient was assessed after 2 and 12 weeks. For patients individually, correlations were analyzed between baseline $SUV_{max}$ and $\Delta$ $SUV_{max}$, and the % change in sum of target lesion diameters on CT according to RECIST1.1. $\Delta$ $SUV_{max}$ was correlated with serum chromogranin A and VEGF-A as well as whole blood everolimus concentrations.

### Statistical analyses

In order to be able to study our primary endpoint: a change in $^{89}Zr$-bevacizumab uptake in tumor lesions between the baseline PET scan and the scans performed after 2 and 12 weeks, it was estimated that a minimum of 11 patients was needed to predict with 80% power (with 2-sided $\alpha = 0.05$) that there is a true difference in SUV ($\geq 1.25$ standard deviation) between the baseline scan and the scan after 2 and 12 weeks of treatment. Therefore, 14 patients were aimed for inclusion. The secondary endpoint was progressive disease according to RECIST1.1 on CT after 12 weeks of treatment. Data are presented as median and range, unless otherwise indicated. Pearson and Spearman rank correlation served to calculate correlations of parametric and non-parametric data respectively. For unpaired data, the Mann-Whitney test and for paired data the Wilcoxon signed rank test was used. With Kaplan Meier analysis the progression free survival was determined. SPSS version 18 was used for the statistical analyses. A $P$ value $< .05$ was considered statistically significant.

## Results

### Patient characteristics

Between April 2010 and February 2011, 14 patients were included. For the patient characteristics see Table 1. Six patients had serotonin producing NETs. Five of them already received somatostatin analogues, which was continued during everolimus treatment.

Currently, six patients are still on everolimus, with median treatment duration of 19 (range 14 - 21) months. Five patients stopped treatment because of disease progression: one after 6, 8, and 10 months and two after 12 months. Two patients discontinued because of toxicity: lingual angio-edema in one after 4 weeks of treatment and fatigue in the other after 3 months. One patient was lost to follow-up after 12 months (Table 2).

All of the 13 patients evaluable for tumors response experienced stable disease according to RECIST1.1, after 3 and 6 months. Progression free survival at 12 months was 64%, the median progression free survival is not yet reached.

**Table 1.** Baseline patient characteristics (N=14)

| | N (patients) |
|---|---|
| Age, years | |
| Median | 60 |
| Range | 43-67 |
| Gender | |
| Male | 7 |
| Female | 7 |
| ECOG Performance score | |
| 0 | 12 |
| 1 | 1 |
| 2 | 1 |
| Localization of the primary tumor | |
| Lung | 1 |
| Pancreas | 7 |
| Duodenal bulb | 1 |
| Small bowel | 3 |
| Unknown | 2 |
| NET WHO grading | |
| Grade 1 | 8 |
| Grade 2 | 6 |
| Peptide producing NET | |
| Chromogranin A producing | 12 |
| Serotonin producing | 6 |
| Gastrin producing | 1 |
| Prior treatment | |
| Surgery | 7 |
| Radiotherapy | 3 |
| Systemic therapy | 6 |
| - somatostatin analogue | 1 |
| - interferon α | 2 |
| - chemotherapy | 2 |
| - radioactive Lutetium octreotide/ MIBG | 2 |
| - sunitinib | 1 |

Abbreviations:
ECOG, Eastern Cooperative Oncology Group
MIBG, metaiodobenzylguanidine

**Table 2.** Imaging characteristics and treatment outcome per patient (N=14)

| Tumor Location | Functional NET | Number of metastases | | | Mean $SUV_{max}$ | | | Treatment duration | Best change CT target lesions |
|---|---|---|---|---|---|---|---|---|---|
| | | CT | PET | (%) | Baseline | 2 weeks | 12 weeks | (months) | (%) |
| Pancreas[a] | - | 82 | 34 | (41) | 10.9 | 10.3 | 6.7 | 21+ | -14 |
| Pancreas[b] | - | 7 | 0 | (0) | - | - | - | 1 | na |
| Pancreas | - | 26 | 1 | (4) | 5.5 | 5.6 | 4.8 | 21+ | -7 |
| Pancreas | - | 1 | 0 | (0) | - | - | - | 20+ | 13 |
| Pancreas | - | 39 | 11 | (31) | 5.1 | 4.5 | 3.6 | 10 | -4 |
| Pancreas | - | 27 | 4 | (15) | 2.9 | 2.8 | 2.7 | 14+ | -9 |
| Pancreas | - | 3 | 3 | (100) | 4.8 | 5.9 | 5.7 | 12 | 0 |
| Duodenum | Gastrin | 16 | 3 | (19) | 3.4 | 3.2 | 2.6 | 6 | -5 |
| Lung | Serotonin | 41 | 3 | (7) | 7.0 | 7.9 | 9.1 | 8 | -3 |
| Small bowel[b] | Serotonin | 2 | 0 | (0) | - | - | - | 3 | 11 |
| Small bowel[c] | Serotonin | 29 | 2 | (7) | 8.5 | 8.8 | 8.8 | 12 | 1 |
| Small bowel | Serotonin | 25 | 0 | (0) | - | - | - | 12 | -19 |
| Unknown | Serotonin | 15 | 1 | (7) | 10.4 | 8.6 | 7.7 | 18+ | -9 |
| Unknown | Serotonin | 14 | 1 | (7) | 8.6 | 4.9 | 2.6 | 16+ | -13 |

Abbreviation: na, not applicable

[a]VHL germline mutation carrier

[b]Taken off trial because of side effects

[c]Lost to follow-up at 12 months

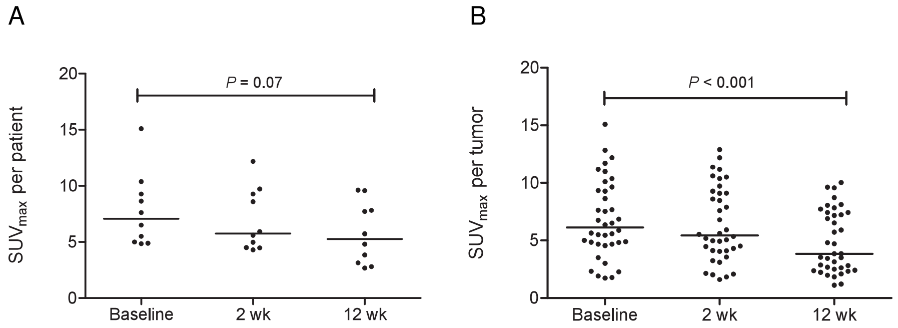


***Figure 1**. **A** SUV$_{max}$ in the most intense tumor lesion per patient and **B** in all tumor lesions at baseline, 2 weeks and 12 weeks. Horizontal bars represent median values.*

## Baseline $^{89}$Zr-bevacizumab PET

Four days after the tracer injection, typical antibody distribution [17, 27] of $^{89}$Zr-bevacizumab was visible in healthy tissues at baseline scan, as well as after 2 and 12 weeks. High $^{89}$Zr-bevacizumab uptake was present in the circulation (including the heart), kidneys, liver and spleen and low uptake in lung, muscle, bone and brain (Supplemental Figure 1).

In 10 patients $^{89}$Zr-bevacizumab PET visualized a total of 63 tumor lesions and in four patients, no tumor lesions were detected. $^{89}$Zr-bevacizumab PET detected 19 lesions in the bone, 36 in liver, 4 in the pancreas, 2 in the spleen, 1 in the bowel and 1 mediastinal lymph node. The median number of visualized lesions per patient was 3 (range 1 - 34) (Table 2), with a median SUV$_{max}$ of 5.8 (range 1.7 - 15.1). Seven lesions in four patients were located outside the field of view of CT. These lesions were confirmed bone metastases with other imaging techniques: 1 with $^{18}$F-Fluor-2-deoxy-D-glucose ($^{18}$F-FDG), 3 with $^{11}$C-5-hydroxytryptophan ($^{11}$C-5-HTP), 1 with $^{18}$F-dihydroxy-phenyl-alanine ($^{18}$F-DOPA) PET, and 2 with $^{99m}$Tc-oxidronate (bone scan). One lesion was located in the field of view, but not detected on CT: this lesion was confirmed with $^{11}$C-5-HTP PET. In all patients, baseline CT scan detected a total of 327 lesions ≥ 10 mm. In the 10 patients with tumor lesion uptake on $^{89}$Zr-bevacizumab PET 19% of lesions ≥ 10 mm showed uptake on $^{89}$Zr-bevacizumab PET.

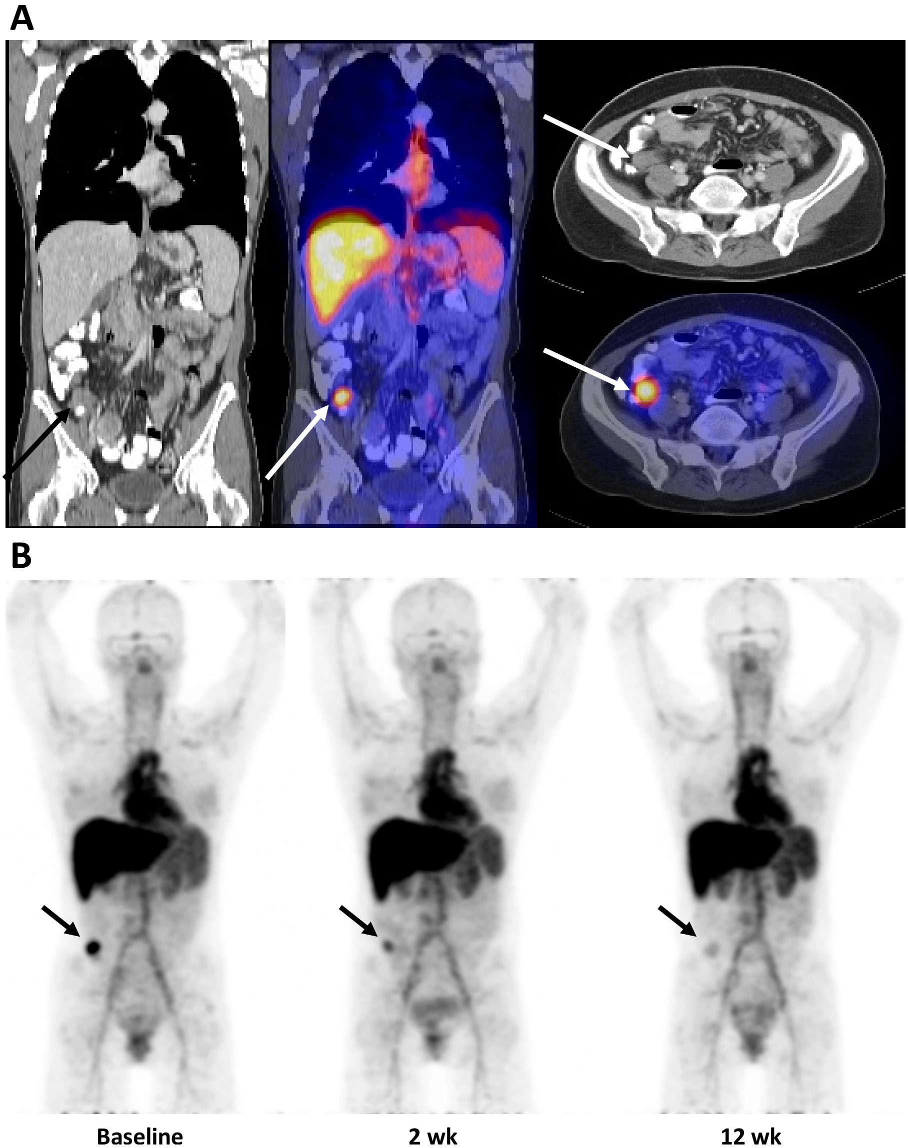


***Figure 2.*** *PET images 4 days after $^{89}$Zr-bevacizumab injection in a patient with metastatic midgut carcinoid.* ***A*** *Coronal and axial images of low dose CT and fusion images of PET and low dose CT shows increased tracer uptake in the abdominal tumor lesion.* ***B*** *Coronal PET images at baseline, 2 weeks and 12 weeks of everolimus treatment. Physiological $^{89}$Zr-bevacizumab uptake is present in the heart (blood pool), liver, spleen and circulation. At baseline, increased $^{89}$Zr-bevacizumab uptake was found in the tumor lesion located in the ileocecal angle. Tumor uptake was 43% lower at 2 weeks and 69% lower at 12 weeks while on everolimus.*

## Serial $^{89}$Zr-bevacizumab tumor uptake

In the 10 patients with a positive $^{89}$Zr-bevacizumab PET scan, seven patients showed a decrease of the tumor $SUV_{max}$, whereas in three patients the tumor $SUV_{max}$ increased (Supplemental Figure 2).

At a tumor lesion-based level, tumor $SUV_{max}$ decreased during everolimus treatment with median -7% at 2 weeks ($P$ = .09) and median -35% at 12 weeks ($P$ < .001) (Figure 1). Figure 2 shows an example of serial $^{89}$Zr-bevacizumab PET scans in a midgut NET patient. The change of tumor $SUV_{max}$ was not induced by changes in tumor size, as percentage change in tumor $SUV_{max}$ did not correlate with the percentage change in longitudinal tumor size on CT after 12 weeks ($r^2 = 0.072$).

## $^{89}$Zr-bevacizumab PET related to treatment outcome

The secondary objective was to explore if $^{89}$Zr-bevacizumab PET could early identify patients with progressive disease according to RECIST1.1 after 3 months. However, none of the patients experienced progressive disease after 3 and 6 months of everolimus treatment. Of the four patients without tracer uptake in tumor lesions, three were evaluable for response and experienced stable disease for 12 and 20+ months, while one discontinued everolimus after 3 months because of side effects. The 10 patients with a positive $^{89}$Zr-bevacizumab PET scan experienced stable disease ongoing for 6 to 21+ months (median 13). The seven patients with decrease in tumor $SUV_{max}$ experienced stable disease for 6 - 21+ months (median 16+). The three patients with an increase in tumor $SUV_{max}$ experienced stable disease for 8 and 12 months, and one patient was lost to follow-up (see also Table 2).

There was no correlation between baseline tumor $SUV_{max}$ and the % change in sum of target lesion diameters on CT according to RECIST1.1 after 6 months (Figure 3.). $\Delta$ $SUV_{max}$ after 2 and 12 weeks however correlated with the % change in sum of the target lesion diameters according to RECIST1.1 on CT after 6 months ($r^2 = 0.51$, $P < .05$, $r^2 = 0.61$, $P < .01$ respectively) (Figure 3).

## $^{89}$Zr-bevacizumab PET versus everolimus, chromogranin A and VEGF-A blood levels

Eleven patients were evaluable for whole blood everolimus levels at 2 and 12 weeks of therapy (median 13.4 µg/L, range 10.3 - 30.3 µg/L; median 15.6 µg/L, range 6.3 -

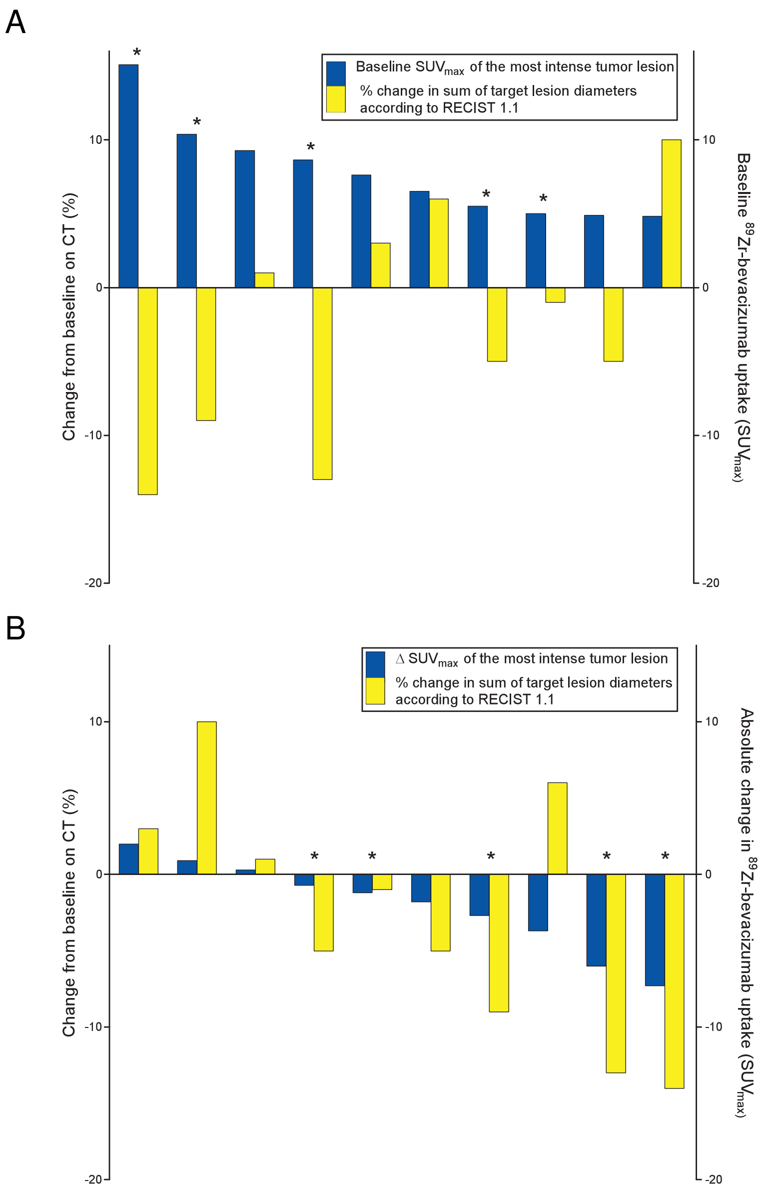


***Figure 3.*** *Waterfall plots of the 10 patients with visualized tumor lesions at $^{89}$Zr-bevacizumab PET.* ***A*** *Maximum baseline $SUV_{max}$ (dark bars) and the % change in sum of target lesion diameters according to RECIST1.1 on CT after 6 months (light bars).* ***B*** *Δ $SUV_{max}$ at 12 weeks of the most intense tumor lesion at baseline (blue bars) and % change in sum of target lesion diameters according to RECIST1.1 on CT after 6 months (yellow bars). (*indicates that the patient is still on everolimus).*

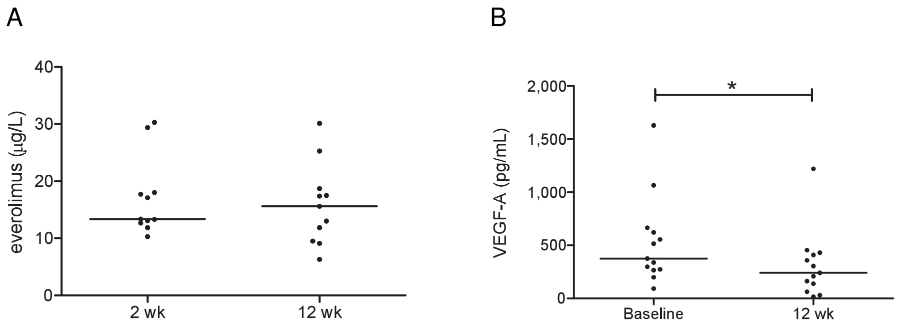


***Figure 4**. Horizontal bars represent median values. (* P < .05). **A** Whole blood everolimus levels after 2 weeks and 12 weeks of everolimus treatment (n = 11). **B** serum VEGF-A levels measured at baseline, 2 weeks and 12 weeks of treatment (n = 13).*

30.1 µg/L, respectively) (Figure 4). No correlation was found between everolimus levels and the change in $\Delta$ $SUV_{max}$ at 2 weeks and 12 weeks (data not shown).

Serum VEGF-A levels were lower at 12 weeks (median 240 pg/mL, range 16 - 1220) compared to baseline (median 375 pg/mL, range 92 - 1629) (n = 13) ($P < .05$). See also Figure 4. Percentage change in VEGF-A serum levels after 12 weeks did not correlate with change of $\Delta$ $SUV_{max}$ after 12 weeks (data not shown). Baseline median chromogranin A level was 821 µg/L (range 66 - 49,700 µg/L). In patients with elevated levels (> 100 µg/L), % change of serum chromogranin A levels after 3, 6, 9 and 12 months did not correlate with $\Delta$ $SUV_{max}$ after 12 weeks (data not shown).

# Discussion

This study shows that $^{89}$Zr-bevacizumab PET can visualize tumor lesions in patients with advanced well-differentiated NET. In 10 out of 14 patients, a total of 63 tumor lesions were visible, representing 19% of the lesions ≥ 1 cm on CT in these individuals. Everolimus treatment decreased $^{89}$Zr-bevacizumab tumor accumulation with 7% at 2 weeks (NS) and with 35% at 12 weeks. In addition, $\Delta$ $SUV_{max}$ correlated with % change in tumor size of target lesions on CT at 6 months.

The negative PET scans in four patients are remarkable, as a study with $^{111}$In-bevacizumab SPECT in stage III/IV melanoma patients and studies with $^{89}$Zr-bevacizumab PET in metastatic RCC patients and patients with early breast cancer demonstrated tumor lesions in all but one breast cancer patient.[17-18, 28] Tumor VEGF-A levels were not available in the current study, since no tumor biopsies were obtained at the moment of PET scanning. In stage III/IV melanoma patients, $^{111}$In-bevacizumab uptake clearly correlated with degree of VEGF-A tumor expression assessed by immunohistochemistry.[17] In addition, in patients with primary breast cancer $^{89}$Zr-bevacizumab uptake correlated with VEGF-A tumor levels measured with enzyme-linked immunosorbent assay (ELISA).[28]

The VEGF family consists of 4 different subtypes: VEGF-A, -B, -C and D. VEGF-A is considered to be the key player in tumor angiogenesis. VEGF-B is an inefficient factor for induction of angiogenesis. VEGF-C and D induce venous and lymphatic angiogenesis.[29] The involvement of different VEGF subtypes in NETs has been poorly investigated. In 50 low-grade gastrointestinal NET VEGF-A protein expression was strong in 32%, weak in 54% and absent in 14% of the tumors.[3] In 23 pNET patients VEGF-A and -C protein expression were studied. There was a limited VEGF-A protein expression in both the primary tumor (n=19) and liver metastases (n=7). Although VEGF-C expression was limited in primary tumors, liver metastases did show high expression.[30] In another study, expression of all VEGF subtypes was quantified with real-time polymerase chain reaction in 25 patients with ileal NETs. VEGF-A expression was similar between tumor lesions and healthy ileal mucosa. In contrast, VEGF-B and VEGF-D levels were higher in tumors compared to normal mucosa.[31] This might be one of the explanations why several of the NET lesions in our study did not show uptake of $^{89}$Zr-bevacizumab.

The heterogeneous baseline $^{89}$Zr-bevacizumab PET results may be an explanation for the fact that not all NET patients benefit of anti-angiogenic treatment with bevacizumab.[32-34] It might be of interest to perform a trial with $^{89}$Zr-bevacizumab PET before bevacizumab therapy to see whether this PET scan might be useful to select NET patients upfront. In that case, $^{89}$Zr-bevacizumab PET can be used to visualize presence of the drug target. However, in the current study we were interested in visualizing VEGF-A as an early read out of a downstream effect of mTOR inhibition, which might give insight in effect of treatment.

mTOR inhibition has pleiotropic antitumor effects, including reduction of tumor VEGF-A production. In the current study we did indeed find reduced $^{89}$Zr-bevacizumab tumor uptake after 2 and 12 weeks of everolimus treatment. Serial imaging results are in concordance with an ovarian cancer xenograft study, where 2 weeks of everolimus treatment decreased $^{89}$Zr-bevacizumab tumor uptake by 21.7% ± 4%, and corresponded with lower tumor VEGF-A protein levels and microvessel density in treated animals.[16] Not all patients with a positive $^{89}$Zr-bevacizumab PET before everolimus treatment showed a reduction in tumor uptake during everolimus treatment. This differential effect was not due to inadequate everolimus levels, as in all patients levels were comparable to those reported earlier in a phase 1 study.[35] A negative $^{89}$Zr-bevacizumab PET scan did not preclude benefit from treatment with everolimus. This is likely due to other antitumor effects of everolimus than reduction of VEGF-A.

Serum VEGF-A levels were 25% lower after 12 weeks of everolimus treatment, compared to baseline. In the RADIANT-3 study, serum VEGF-A levels were determined at baseline, 4, 8, and 12 weeks and did not change in pNET patients who received everolimus (n=207) or placebo (n=203).[14] These discrepant results may be the consequence of different assays. We observed no correlation between change in serum VEGF-A levels and tumor $\Delta$ $SUV_{max}$ after 2 and 12 weeks, suggesting that change in circulating VEGF-A does not reflect change of VEGF-A at tumor level. This may be explained by the fact that VEGF-A consists of different isoforms. $VEGF\text{-}A_{121}$ and $VEGF\text{-}A_{165}$ can diffuse freely, whereas $VEGF\text{-}A_{189}$ and $VEGF\text{-}A_{206}$ are attached to the extracellular matrix.[36] Moreover, serum VEGF-A levels contain VEGF-A released by platelets.[37]

Another useful imaging strategy to predict everolimus efficacy might be functional imaging with MRI, including diffusion weighted imaging (DWI) MRI and contrast-enhanced MRI. Tumor necrosis results in increased water permeability, which can be measured by DWI MRI. Contrast-enhanced MRI can quantify changes in tumor vascularity. In a retrospective study in 71 patients with advanced NETs who underwent intra-arterial chemo-embolization of liver metastases, DWI and contrast-enhanced MRI scans were performed at baseline and 4 weeks after therapy. The authors conclude that volumetric functional MRI criteria may act as biomarkers of early response.[38] An advantage of MRI is that it does not expose patients to radiation.

## Conclusion

In conclusion, this study demonstrates differences in $^{89}$Zr-bevacizumab tumor accumulation between and within patients with advanced well-differentiated NETs. This heterogeneity likely reflects differential VEGF-A pathway activity. Everolimus treatment reduced $^{89}$Zr-bevacizumab tumor accumulation without affecting normal organ distribution. A baseline $^{89}$Zr-bevacizumab PET scan cannot be used to select patients for everolimus treatment. Larger studies are needed to determine the predictive value of serial scans for efficacy of everolimus treatment, but read out of other downstream effects of mTOR inhibition might be more relevant in NETs.

**Acknowledgments** This study was supported by a research grant of Novartis, The Netherlands.

# References


1. Hanahan D, Weinberg RA. Hallmarks of cancer: the next generation. Cell. 2011;144:646-674.
2. Dong M, Phan AT, Yao JC. New strategies for advanced neuroendocrine tumors in the era of targeted therapy. Clin Cancer Res. 2012;18:1830-1836.
3. Zhang J, Jia Z, Li Q, et al. Elevated expression of vascular endothelial growth factor correlates with increased angiogenesis and decreased progression-free survival among patients with low-grade neuroendocrine tumors. Cancer. 2007;109:437-448.
4. Hobday TJ, Rubin J, Goldberg R, et al. Molecular markers in metastatic gastrointestinal neuroendocrine tumors. Proc Am Soc Clin Oncol. 2003;22:abstr 1078.
5. Terris B, Scoazec JY, Rubbia L, et al. Expression of vascular endothelial growth factor in digestive neuroendocrine tumours. Histopathology. 1998;32:133-138.
6. von Marschall Z, Scholz A, Cramer T, et al. Effects of interferon alpha on vascular endothelial growth factor gene transcription and tumor angiogenesis. J Natl Cancer Inst. 2003;95:437-448.
7. Meric-Bernstam F, Gonzalez-Angulo AM. Targeting the mTOR signaling network for cancer therapy. J Clin Oncol. 2009;27:2278-2287.
8. Raymond E, Dahan L, Raoul JL, et al. Sunitinib malate for the treatment of pancreatic neuroendocrine tumors. N Engl J Med. 2011;364:501-513.
9. Yao JC, Shah MH, Ito T, et al. RAD001 in advanced neuroendocrine tumors, Third (RADIANT-3) Study Group. Everolimus for advanced pancreatic neuroendocrine tumors. N Engl J Med. 2011;364:514-523.
10. Pavel ME, Hainsworth JD, Baudin E, et al. Everolimus plus octreotide long-acting repeatable for the treatment of advanced neuroendocrine tumours associated with carcinoid syndrome (RADIANT-2): a randomised, placebo-controlled, phase 3 study. Lancet. 2011;378:2005-2012.
11. Villaume K, Blanc M, Gouysse G, et al. VEGF secretion by neuroendocrine tumor cells is inhibited by octreotide and by inhibitors of the PI3K/AKT/mTOR pathway. Neuroendocrinology. 2010;91:268-278.
12. Thomas GV, Tran C, Mellinghoff IK, et al. Hypoxia-inducible factor determines sensitivity to inhibitors of mTOR in kidney cancer. Nat Med. 2006;12:122-127.
13. Shojaei F. Anti-angiogenesis therapy in cancer: Current challenges and future perspectives. Cancer Lett. 2012;320:130-137.
14. Yao JC, Tsuchihashi Z, Panneerselvam A, et al. Effect of everolimus treatment on markers of angiogenesis in patients with advanced pancreatic neuroendocrine tumours (pNET) – Results from the phase III RADIANT-3 study. Eur J Cancer. 2011;47:S463.
15. Nagengast WB, de Vries EG, Hospers GA, et al. In vivo VEGF imaging with radiolabeled bevacizumab in a human ovarian tumor xenograft. J Nucl Med. 2007;48:1313-1319.
16. van der Bilt AR, Terwisscha van Scheltinga AG, Timmer-Bosscha H, et al. Measurement of tumor VEGF-A levels with 89Zr-bevacizumab PET as an early biomarker for the

antiangiogenic effect of everolimus treatment in an ovarian cancer xenograft model. Clin Cancer Res. 2012;18:6306-6314.
17. Nagengast WB, Lub-de Hooge MN, van Straten EM, et al. VEGF-SPECT with 111In-bevacizumab in stage III/IV melanoma patients. Eur J Cancer. 2011;47:1595-1602.
18. Oosting SF, Brouwers AH, van Es SC, et al. 89Zr-bevacizumab PET imaging in metastatic renal cell carcinoma patients before and during antiangiogenic treatment. J Clin Oncol.2012;30 Available online: http://jco.ascopubs.org/gca?gca=ascomtg%3B30%2F15_suppl%2F10581&allch=&submit=Go
19. Rindi G, Klöppel G, Alhman H, et al. TNM staging of foregut (neuro)endocrine tumors: a consensus proposal including a grading system. Virchows Arch. 2006;449:395-401.
20. 20. Rindi G, Klöppel G, Coulevard A, et al. TNM staging of midgut and hindgut (neuro) endocrine tumors: a consensus proposal including a grading system. Virchows Arch. 2007;451:757-762.
21. Oken MM, Creech RH, Tormey DC, et al. Toxicity and response criteria of the Eastern Cooperative Oncology Group. Am J Clin Oncol. 1982;5:649-655.
22. Eisenhauer EA, Therasse P, Bogaerts J, et al. New response evaluation criteria in solid tumours: Revised RECIST guideline (version 1.1). Eur J Cancer. 2009;45:228-247.
23. Fiebrich HB, de Jong JR, Kema IP, et al. Total 18F-DOPA PET tumour uptake reflects metabolic endocrine tumour activity in patients with a carcinoid tumour. Eur J Nucl Med Mol Imaging. 2011;38:1854-1861
24. Koster RA, Dijkers ECF, Uges DRA. Robust, high-throughput LC-MS/MS method for therapeutic drug monitoring of cyclosporine, tacrolimus, everolimus and sirolimus in whole blood. Ther Drug Monit. 2009;31:116-125.
25. Verel I, Visser GW, Boellaard R, et al. 89Zr immuno-PET: comprehensive procedures for the production of 89Zr-labeled monoclonal antibodies. J Nucl Med. 2003;44:1271-1281.
26. Loening AM, Gambhir SS. AMIDE: a free software tool for multimodality medical image analysis. Mol Imaging 2003;2:131-137.
27. Dijkers EC, Oude Munnink TH, Kosterink JG, et al. Biodistribution of 89Zr-trastuzumab and PET imaging of HER2-positive lesions in patients with metastatic breast cancer. Clin Pharmacol Ther. 2010:87;586-592.
28. Gaykema SB, Brouwers AH, Lub-de Hooge MN, et al. 89Zr-bevacizumab PET imaging in primary breast cancer. J Nucl Med. 2013;54:1014-1018.
29. Li X, Eriksson U. Novel VEGF family members: VEGF-B, VEGF-C and VEGF-D. Int J Biochem Cell Biol. 2001;33:421-426.
30. Hansel DE, Rahman A, Hermans J, et al. Liver metastases arising from well-differentiated pancreatic endocrine neoplasms demonstrate VEGF-C expression. Mod Pathol. 2003;16:652-659.
31. Besig S, Voland P, Baur DM, et al. Vascular endothelial growth factors, angiogenesis, and survival in human ileal enterochromaffin cell carcinoids. Neuroendocrinology. 2009;90:402-415.
32. Yao JC, Phan A, Hoff PM, et al. Targeting vascular endothelial growth factor in advanced carcinoid tumor: a random assignment phase II study of depot octreotide with bevacizumab and pegylated interferon α-2b. J Clin Oncol. 2008;26:1316-1323.

33. Kulke MH, Chan JA, Meyerhardt JA, et al. A prospective phase II study of 2-methoxyestradiol administered in combination with bevacizumab in patients with metastastic carcinoid tumors. Cancer Chemother Pharmacol. 2011;68:293-300.
34. Chan JA, Stuart K, Earle CC, et al. Prospective study of bevacizumab plus temozolomide in patients with advanced neuroendocrine tumors. J Clin Oncol. 2012;30:2963-2968.
35. O'Donnell A, Faivre S, Burris HA 3rd, et al. Phase I pharmacokinetic and pharmacodynamic study of the oral mammalian target of rapamycin inhibitor everolimus in patients with advanced solid tumors. J Clin Oncol. 2008;26:1588-1595.
36. Park JE, Keller GA, Ferrara N. The vascular endothelial growth factor (VEGF) isoforms: differential deposition into the subepithelial extracellular matrix and bioactivity of extracellular matrix-bound VEGF. Mol Biol Cell. 1993;4:1317-1326.
37. Jelkmann W. Pitfalls in the measurement of circulating vascular endothelial growth factor. Clin Chem. 2001;47:617-623.
38. Gowdra Halappa V, Corona-Villalobos CP, Bonekamp S, et al. Neuroendocrine liver metastases treated by using intraarterial therapy: volumetric functional imaging biomarkers of early tumor response and survival. Radiology. 2013;266:502-51

# Supplementary data

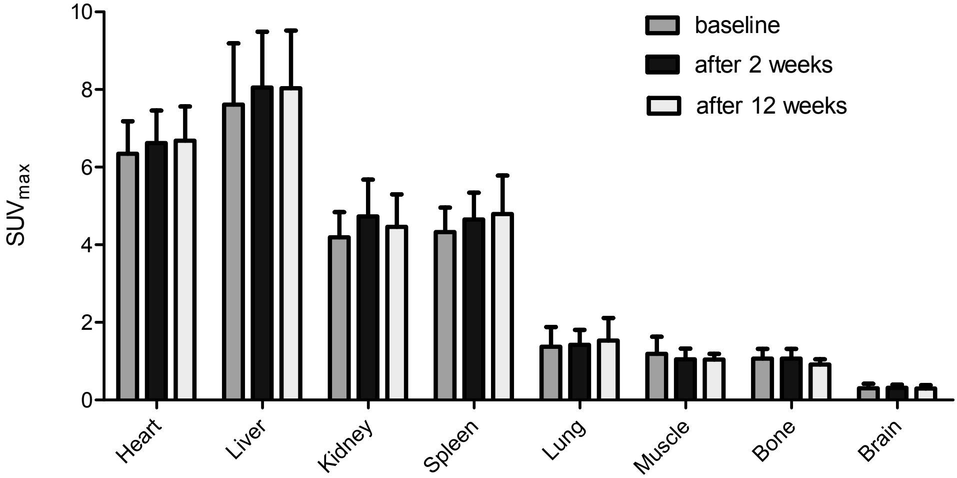


***Supplementary Figure 1**. $^{89}$Zr-bevacizumab healthy tissue uptake of all patients. All 14 patients underwent $^{89}$Zr-bevacizumab PET at both baseline and 2 weeks (spleen uptake n = 11; three patients had splenectomy). Ten of these 14 patients also underwent $^{89}$Zr-bevacizumab PET at 12 weeks (spleen uptake n = 8). Median and interquartile range are given.*

***Supplementary Figure 2. A** Each patient is represented by a separate line. Per patient values are given of the most intense tumor lesion visualized at baseline scan. $SUV_{max}$ values are shown at baseline, 2 weeks and 12 weeks. **B** shows the percentage change in $SUV_{max}$ of the most intense tumor lesion at baseline scan. **C–H** shows tumor uptake in patients in which $^{89}$Zr-bevacizumab PET visualized more than 1 tumor lesion. For most patients, the tracer uptake in tumor lesions shows the same direction of change in $SUV_{max}$ after 2 and 12 weeks.*

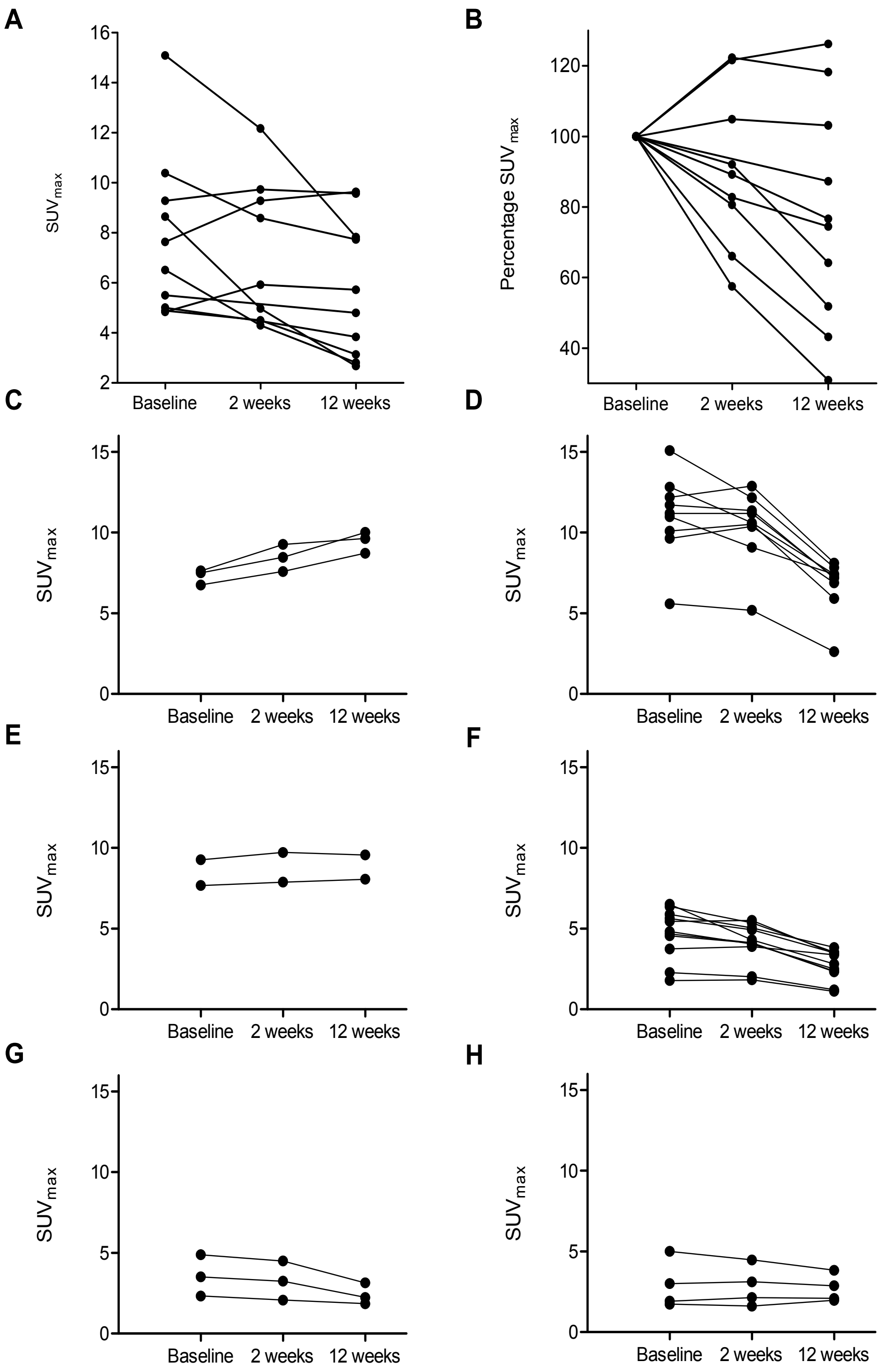


***Supplementary Figure 2.***

# Chapter 8

## Summary in Dutch

### (Nederlandse samenvatting)

# Nederlandse samenvatting

Neuroendocriene tumoren ontstaan uit (neuro)endocriene cellen. Deze cellen komen verspreid voor in het gehele lichaam. Neuroendocriene tumoren zijn zeldzaam en zijn voornamelijk gelokaliseerd in de long, pancreas, maag of dunne darm. Een belangrijke eigenschap van neuroendocriene tumoren is dat een deel van die tumoren peptiden kunnen produceren. Serotonine, pancreas polypeptide, en de hormonen glucagon, insuline en gastrine zijn hier voorbeelden van.

Door middel van weefselonderzoek kunnen neuroendocriene tumoren ingedeeld worden op basis van histologische karakteristieken. Goed-gedifferentieerde neuroendocriene tumoren hebben weinig delende cellen in vergelijking met slecht-gedifferentieerde neuroendocriene tumoren. Deze laatste groep heeft vaak een slechtere prognose. In dit proefschrift wordt met neuroendocriene tumoren alleen de goed-gedifferentieerde neuroendocriene tumoren bedoeld.

Patiënten met de erfelijke tumorsyndromen von Hippel-Lindau (VHL) of multipele endocriene neoplasie type 1 (MEN1) hebben een verhoogde kans op het ontwikkelen van neuroendocriene tumoren in het pancreas, met een respectievelijke prevalentie van 10-17% en 70%. VHL patiënten kunnen ook cysten in het pancreas ontwikkelen. Deze zijn altijd goedaardig. Naast pancreasneuroendocriene tumoren hebben VHL en MEN1 patiënten ook een verhoogde kans om tumoren te ontwikkelen op andere plaatsen in het lichaam. Een belangrijke doodsoorzaak bij VHL patiënten is nierkanker en hemangioblastomen (vaattumoren) in de kleine hersenen en het ruggenmerg. Bij één derde van de MEN1 patiënten is de doodsoorzaak MEN1-gerelateerd, waarbij pancreasneuroendocriene tumoren de doodsoorzaak nummer 1 is. Door de verhoogde kans op het ontwikkelen van deze verschillende tumoren, worden VHL en MEN1 patiënten periodiek onderzocht. Voor VHL patiënten wordt jaarlijkse een buikecho geadviseerd en tenminste om het jaar een MRI-scan. Voor de vroege opsporing van pancreasneuroendocriene tumoren is de internationale aanbeveling bij MEN1 patiënten om ieder jaar een CT-scan, MRI-scan of endoscopische echografie te verrichten.

Er zijn meerdere methoden om mensen te screenen op pancreasneuroendocriene tumoren. Echter, het is nog niet bekend welke techniek het beste is voor de vroege opsporing van pancreasneuroendocriene tumoren bij MEN1 en VHL patiënten. Met moleculaire beeldvorming is het mogelijk om bepaalde stofwisselingsprocessen in het lichaam in beeld te brengen. Specifieke eigenschappen van neuroendocriene tumorcellen kunnen hiervoor gebruikt worden. Neuroendocriene tumoren hebben de eigenschap om bouwstoffen zoals hydroxytryptofaan op te nemen, om te zetten in peptiden en op te slaan in de cel. De beeldvorming positron emissie tomografie (PET) met als tracer $^{11}$C-5-hydroxytryptophan ($^{11}$C-5-HTP) is gebaseerd op deze celeigenschap, waarmee neuroendocriene tumoren in beeld gebracht kunnen worden. Uit eerder onderzoek is gebleken dat $^{11}$C-5-HTP PET een gevoelige techniek is bij patiënten met pancreasneuroendocriene tumoren in een vergevorderd stadium.

De manier om patiënten met een neuroendocriene tumor te genezen is totale chirurgische verwijdering van de tumor. Bij vergevorderde en uitgezaaide ziekte is dit vaak niet meer mogelijk. Om klachten en toename van ziekte tegen te gaan kunnen patiënten in een palliatieve setting geopereerd worden en starten met een medicamenteuze behandeling gericht tegen de tumor. Voor neuroendocriene tumoren zijn moleculaire doelgerichte therapieën beschikbaar, die tumorgroei remmen, zoals octreotide. De tyrosinekinaseremmer sunitinib is gericht tegen de vasculaire endotheliale groei factor (VEGF) receptor en de proteïnekinaseremmer everolimus is gericht op het remmen van "mTOR".

Moleculaire beeldvorming met $^{89}$Zr-bevacizumab PET waarbij bevacizumab een antilichaam is gericht tegen VEGF-A kan de aanwezigheid dan wel afwezigheid van VEGF-A in het lichaam in beeld brengen. Dit is interessant omdat neuroendocriene tumoren vaak vaatrijk zijn en daarmee VEGF-A een mogelijk target is voor medicamenteuze behandeling. Daarnaast kan $^{89}$Zr-bevacizumab PET ook bruikbaar zijn bij VHL patiënten. Verlies van het functionele VHL-eiwit is de eerste stap bij de ontwikkeling van VHL manifestaties. Dit kan tot gevolg hebben dat VEGF-A verhoogd tot expressie komt in de tumor. Dit is mogelijk de reden dat VHL manifestaties vaak vaatrijk zijn. Op dit moment zijn er geen duidelijke biomarkers die het beloop van de ziekte in VHL-patiënten kunnen voorspellen.

In dit proefschrift hebben we gekeken naar de waarde van endoscopische echografie en $^{11}$C-5-HTP PET bij de vroege opsporing van pancreasneuroendocriene tumoren bij MEN1 en VHL-patiënten. Ook hebben we gekeken of $^{89}$Zr-bevacizumab PET bruikbaar is om ziektemanifestaties in beeld te brengen bij VHL-patiënten en patiënten met een gemetastaseerd neuroendocriene tumor om te kijken of dit te gebruiken is als voorspeller van respectievelijk tumor gedrag en effect van de behandeling.

**Hoofdstuk 1** geeft een introductie tot het proefschrift. In **hoofdstuk 2** hebben we de literatuur samengevat die beschikbaar is over de ontwikkeling van pancreascysten bij de ziekte VHL. De prevalentie van deze cysten is ongeveer 70% in VHL-patiënten. Dit maakt de ziekte VHL tot de enige erfelijke tumorsyndroom dat gekenmerkt wordt door zo'n hoge prevalentie van pancreascysten. Door bestudering van de ziekte VHL kan inzicht worden verkregen in de ontwikkeling van pancreascysten in het algemeen. We hebben in de literatuur zoekmachine PubMed gezocht naar Engelstalige literatuur over *in vitro* en *in vivo* studies over (pancreas) cyste ontwikkeling gerelateerd aan VHL. Relevante referenties van de geselecteerde artikelen werden ook bestudeerd. Bovendien hebben we ook gekeken naar klinische studies op het gebied van pancreascysten bij VHL.

Er waren geen studies beschikbaar met *VHL*-mutaties in pancreascellijnen, waardoor we genoodzaakt waren andere VHL-gerelateerde *in vitro* studies mee te nemen, waarvan de meesten in niercelkankercellijnen waren uitgevoerd. Naast de cellijnstudies waren er een aantal dierstudies beschikbaar waarbij geselecteerd verlies van het *VHL*-gen in het pancreas was bewerkstelligd met *Cre/Lox P* technologie. De belangrijkste uitkomst is dat bij het ontstaan van een VHL-gerelateerde cyste meerdere factoren een rol spelen op het niveau van de extracellulaire matrix en het cytoskelet. Bij de ontwikkeling van pancreascysten lijkt het verlies van cilia in de pancreasductaalcellen een belangrijke rol te spelen. VHL-patiënten hebben nauwelijks klachten van pancreascysten. Op basis van de beschikbare literatuur lijken deze cysten niet geassocieerd te zijn met maligniteit of endocriene en/of exocriene pancreasinsufficiëntie.

In **hoofdstuk 3** hebben we in VHL-patiënten de waarde van endoscopische echografie en $^{11}$C-5-HTP PET geëvalueerd versus de standaardbeeldvorming voor de detectie van solide pancreasafwijkingen, verdacht voor een neuroendocriene tumor. Patiënten ouder dan 18 jaar met een aangetoonde VHL-mutatie of één VHL-geassocieerde afwijking met een VHL-mutatie aangetoond in een eerstegraads familielid kwamen in aanmerking voor dit onderzoek. Patiënten uit het Universitair Medisch Centrum van Utrecht, Rotterdam en Groningen participeerden. Voorafgaand aan de studie werd een abdominale CT-scan of MRI-scan en een somatostatine receptor scintigrafie (SRS) verricht in het ziekenhuis waar ze werden gecontroleerd. Patiënten ondergingen in het UMCG endoscopische echografie en $^{11}$C-5-HTP PET. Het aantal en percentage positieve bevindingen op beeldvorming werden berekend op zowel patiëntniveau als laesieniveau. Hierbij werden de uitkomsten van het totaal van de vier beeldvormende technieken als referentie gehanteerd. Tussen februari 2009 en augustus 2011 werden 22 VHL-patiënten geïncludeerd. Tien patiënten (45%) hadden op anatomische beeldvorming solide pancreaslaesies. Endoscopische echografie was positief in 10 patiënten, $^{11}$C-5-HTP PET in één, CT/MRI in zeven, SRS in drie en CT/MRI+ SRS in zeven patiënten. Twintig solide pancreaslaesies werden opgespoord: 17 met endoscopische echografie, 3 met $^{11}$C-5-HTP PET, 9 met CT/MRI, 3 met SRS en 9 met CT/MRI+ SRS. Endoscopische echografie spoorde de meeste laesies op (*P*

< 0,05), met een mediane grootte van 9,7 mm (range 2,9-55). Bij endoscopische echografie waren de meeste solide laesies homogeen en hypo-echogeen van aard, iso-elastisch op basis van elastografie en hypervasculair op basis van power Doppler. Bovendien werden met endoscopische echografie ook pancreascysten gevisualiseerd bij 18 patiënten (81%) met een mediaan van 4 cysten (range 1-30) per patiënt. Deze studie heeft in VHL-patiënten laten zien dat endoscopische echografie de beste beeldvorming is voor detectie van pancreas solide laesies die verdacht zijn voor neuroendocriene tumoren. $^{11}$C-5-HTP PET is niet bruikbaar in deze setting.

In de studie beschreven in **hoofdstuk 4** hebben we bij MEN1 patiënten de waarde van endoscopische echografie en $^{11}$C-5-HTP PET geëvalueerd versus de standaardbeeldvorming voor de detectie van pancreasafwijkingen. Patiënten $\geq$ 18 jaar met een aangetoonde MEN1 mutatie of één MEN1 geassocieerde afwijking met een MEN1 mutatie aangetoond in een eerste graad familielid, konden participeren. Patiënten deden mee vanuit het Universitair Medisch Centrum van Utrecht, Nijmegen, Rotterdam en Groningen. Voorafgaand aan studiedeelname was een abdominale CT-scan of MRI-scan en SRS verricht. Patiënten ondergingen in het UMCG endoscopische echografie en $^{11}$C-5-HTP PET. Het aantal en het percentage positieve bevindingen op beeldvorming werden berekend op patiëntniveau en laesieniveau, waarbij de uitkomsten van het totaal van de vier verkregen beeldvormende technieken als referentie werden gehanteerd. Eenenveertig MEN1 patiënten werden geïncludeerd tussen februari 2009 en augustus 2011. Bij 35 (85%) patiënten werden 107 pancreaslaesies vastgesteld. Endoscopische echografie detecteerde 101 laesies bij 34 patiënten, $^{11}$C-5-HTP PET 35 laesies bij 19 patiënten en CT/MRI+ SRS 32 laesies bij 18 patiënten. Op endoscopische echografie waren de meeste solide laesies homogeen en hypo-echogeen van aard. Op basis van power Doppler waren 42% van de laesies hypervasculair. Vijftien (15%) laesies waren cysteus, waarvan 9 zich presenteerden met een verdikte wand. Endoscopische echografie vond meer laesies dan CT/MRI+ SRS ($P$ < .001). In tegenstelling, $^{11}$C-5-HTP PET scoorde evengoed als CT/MRI+ SRS, maar was beter dan SRS alleen ($P$ < .05). Deze studie heeft aangetoond dat in MEN1 patiënten endoscopische echografie de beste methode is voor de opsporing van pancreaslaesies. In deze setting heeft $^{11}$C-5-HTP PET geen toegevoegde waarde. Indien endoscopische echografie in de richtlijn wordt geïmplementeerd als eerste keus beeldvorming, zijn vervolgstudies nodig om vast te stellen of dit ook een verbetering geeft ten aanzien van de behandeling en de morbiditeit/mortaliteit.

Voor de ziekte VHL zijn er op dit moment geen biomarkers beschikbaar die ziekte-activiteit kunnen voorspellen. **Hoofdstuk 5** beschrijft een studie waarbij we gekeken hebben of het mogelijk is om met $^{89}$Zr-bevacizumab PET ziektemanifestaties te visualiseren in VHL-patiënten. De tweede doelstelling was te kijken of tumorgroei voorspeld kan worden door $^{89}$Zr-bevacizumab PET. Tussen november 2009 en april 2012 werden 22 patiënten geïncludeerd. $^{89}$Zr-bevacizumab PET detecteerde 59 afwijkingen in 16 patiënten met een mediane "maximum standardized uptake value" ($SUV_{max}$) van 8,5 (range 1,3-35,8). 30,8% van de afwijkingen groter dan 10 mm werden gedetecteerd. De meerderheid van PET positieve laesies (85%) had een solide karakter op de anatomische beeldvorming. Van de 25 laesies die progressief waren tijdens follow-up waren er 9 zichtbaar op $^{89}$Zr-bevacizumab PET. Deze studie heeft laten zien dat $^{89}$Zr-bevacizumab PET VHL-manifestaties kan visualiseren, waarbij opvallend is dat er sprake is van heterogeniteit tussen patiënten en binnen één patiënt als het gaat om $^{89}$Zr-bevacizumab positieve en negatieve laesies. Progressie van laesies kan niet voorspeld worden met $^{89}$Zr-bevacizumab PET. Vervolgstudies moeten uitwijzen of $^{89}$Zr-bevacizumab PET bruikbaar is om VHL-patiënten te selecteren voor anti-VEGF-A behandeling.

Neuroendocriene tumoren zijn vaak vaatrijk. Patiënten met progressieve gemetastaseerde neuroendocriene tumoren kunnen behandeld worden met everolimus, dat de progressievrije overleving verlengt. Everolimus geeft *in vitro* (in cellijnen) onder andere een lagere productie van VEGF-A. Er is op dit moment geen biomarker beschikbaar die kan voorspeller welke patiënt baat heeft bij de behandeling met everolimus. In **hoofdstuk 6** beschrijven we een studie waarin we hebben gekeken of tumorlaesies in patiënten met een gemetastaseerd neuroendocriene tumor gevisualiseerd kunnen worden met $^{89}$Zr-bevacizumab PET. Bovendien hebben we gekeken bij PET positieve laesies of de $^{89}$Zr-bevacizumab opname afnam tijdens behandeling met everolimus. Vier dagen na het intraveneus toedienen van de $^{89}$Zr-bevacizumab tracer werden PET-scans verricht vooraf, na 2 en na 12 weken behandeling met everolimus. CT-scans werden vooraf verricht en elke 3 maanden hierna, waarbij tumorstadiëring plaatsvond volgens RECIST1.1. In vier van de 14 patiënten waren er geen tumorlaesies zichtbaar met $^{89}$Zr-bevacizumab PET. In de resterende 10 patiënten (71%) was 19% van de tumorlaesies groter dan 1 cm zichtbaar op $^{89}$Zr-bevacizumab PET. De tumor $SUV_{max}$ nam af na 2 weken (mediaan -7%, $P$ = 0,09) en daalde nog verder na 12 weken (mediaan -35%, $P$ < 0,001) ten opzichte van baseline. Delta $SUV_{max}$ na 2 en 12 weken correleerde met de percentage verandering van de diameters van tumorlaesies gemeten volgens RECIST1.1 na 6 maanden (respectievelijk $r^2 = 0{,}51$, $P < .05$ en $r^2 = 0{,}61$, $P < .01$). Op basis van deze resultaten kunnen we concluderen dat in de meerderheid van patiënten met een gemetastaseerd neuroendocriene tumor een deel van de tumorlaesies zichtbaar is op $^{89}$Zr-bevacizumab PET. $^{89}$Zr-bevacizumab tumoropname neemt af ten tijde van de everolimus behandeling. Vervolgstudies zijn nodig om te kijken of moleculaire beeldvorming bruikbaar is als biomarker voor de behandelkeus van patiënten met een gemetastaseerde neuroendocriene tumor.

# Dankwoord

# Dankwoord

De zorg voor patiënten met neuroendocriene tumoren en/of een erfelijk tumorsyndroom als VHL en MEN1 behoeft bij uitstek een multidisciplinaire benadering. Het is dan ook onmogelijk om promotieonderzoek als dit uit te voeren zonder de hulp van mensen vanuit verschillende vakgebieden. Gezien de lage prevalentie van VHL en MEN1 is samenwerking met andere academische centra onontbeerlijk. Ik ben dan ook zeer dankbaar dat er zo'n grote groep mensen de afgelopen 4 jaar om mij heen is geweest, die dit promotieonderzoek mogelijk heeft gemaakt.

Allereerst wil ik de patiënten bedanken die deel hebben genomen aan de studies. Zonder patiënten die bereid zijn deel te nemen aan onderzoek was dit niet mogelijk geweest. Wat ik altijd heel bijzonder heb gevonden is de bereidheid van patiënten om naar Groningen te komen voor onderzoek, wat voor menigeen absoluut niet naast de deur was!

Veel dank gaat uit naar mijn 2 promotoren prof. dr. T.P. Links en prof. dr. E.G.E. de Vries.

Beste Thera, de eerste keer dat ik met jou eind 2008 kennis maakte voor de baan als arts-onderzoeker, had ik nooit kunnen bedenken dat dit allemaal mij te wachten zou staan! Met onze kamers dicht bij elkaar wist ik je altijd snel te vinden. Ik heb genoten van onze theemomenten, waarbij ons werkoverleg constructief was, maar er ook tijd was voor persoonlijke zaken. Jouw favoriete quote: "Het gaat niet alleen om het eindresultaat, maar ook om de weg ernaar toe", heb ik vaak gehoord op momenten dat het mij niet snel genoeg ging. Vaak had je praktische oplossingen voor de problemen die ik aandroeg, en vaker nog liet je me zelf met de oplossing komen.

Beste Liesbeth, de snelheid waarmee jij de manuscripten weer terugstuurt is nauwelijks te overtreffen. Jouw commentaar zorgde ervoor dat ik scherp werd en bleef, en kritisch werd op mezelf en anderen. Bovendien gingen de manuscripten er kwalitatief erg op vooruit. Door met jou samen op de vrijdag poli te doen heb ik in de kliniek veel van jou mogen leren en ervaring mogen opdoen waar ik nu nog steeds veel plezier van heb. Hierin is mij ook zo duidelijk geworden dat patiëntenzorg en wetenschappelijk onderzoek niet zonder elkaar kunnen.

Veel dank gaat ook uit naar mijn copromotoren dr. A.H. Brouwers en dr. H.M. van Dullemen.

Beste Adrienne, menig scan heb ik samen met jou bekeken en daar heb ik enorm van kunnen leren. Uren hebben we doorgebracht in de bekijkruimte om de veelheid aan scans te (her)beoordelen en te scoren waarbij jij onvermoeibaar leek te zijn. Als er praktische problemen waren wist jij altijd wel tijd te vinden om me structureel verder te helpen.

Beste Hendrik, jouw relaxte manier van werken maakte menigmaal dat mijn "problemen" verdwenen als sneeuw voor de zon. Bij jou is één probleem geen probleem. Ik heb het altijd als een feest ervaren om samen met jou op het endoscopiecentrum te werken, dat er uiteindelijk ook tot toe heeft geleid dat ik heb gekozen voor "het mooiste vak dat er is!"

Veel dank gaat uit naar de leden van de beoordelingscommissie: Prof. dr. B.H.R. Wolffenbuttel, prof. dr. R.A.J.O. Dierckx en prof. dr. C.J. Lips. Beste Bruce, Rudi en Kees, dank voor de tijd en energie die jullie hebben gestoken in het beoordelen van dit proefschrift.

Aan alle co-auteurs veel dank voor jullie bijdrage. In het bijzonder wil ik prof. dr. E.J. van der Jagt, drs. A.H.H. Bongaerts, drs J. Steinberg, dr. K.P. Koopmans, prof. dr. R.H. Giles, dr. W.J. Sluiter en dr. S.F. Oosting bedanken. Beste Eric, veel scans hebben de revue gepasseerd. Menig multidisciplinair overleg hebben we gehad, waarbij jouw radiologische kennis onontbeerlijk was. Beste Fons, onder het genot van klassieke muziek hebben we uren achter jouw pc doorgebracht, zowel voor patiëntenzorg als de wetenschappelijk projecten. Voor mij waren dit zeer leerzame momenten. Beste Julia, als enthousiaste neuroradioloog vanuit het Martiniziekenhuis heb jij alle VHL scans van het centraal zenuwstelsel beoordeeld. Het was zeer prettig met jou samen te werken. Beste Klaas Pieter, dank voor je hulp bij de beoordeling van de HTP PET scans. Beste Rachel, jouw biologische kennis was onmisbaar voor het schrijven van het review. Jij zit als geen ander in de wereld van VHL op cel en genetisch niveau. Beste Wim, ik kon met al mijn statistiekvragen bij jou terecht. Dank voor je uitleg en hulp die je gaf met veel geduld en humor. Beste Sjoukje, dank voor de prettige samenwerking in de VHL-image studie.

Veel dank ben ik ook verschuldigd aan de co-auteurs prof. dr. W.W. de Herder, dr. R.A. Feelders, dr. H.J. Timmers, dr. G.D. Valk en dr. B.A. Zonnenberg. Beste Wouter, Richard, Henri, Gerlof en Bernard, zonder jullie enthousiaste medewerking, inzet en verwijzing van patiënten waren de pancreasstudies niet mogelijk geweest. De vergaderingen die we in Utrecht hebben gehad waren constructief en zorgden ervoor dat ik weer verder kon.

Veel dank gaat uit naar de mensen die mij hebben geholpen in de logistiek. Ik ben in het bijzonder de planners en medisch nucleair werkers van de afdeling nucleaire geneeskunde en de planners van de afdeling maag-darm-leverziekten zeer erkentelijk. Dank voor de inzet om alles altijd zo goed mogelijk te stroomlijnen! Ook bedank ik Wanda Geilvoet en Cicilia van Rooijen voor al hun hulp om zo snel mogelijk de patiënteninformatie en scans vanuit Rotterdam en Utrecht naar Groningen te sturen.

Veel dank gaat uit naar de stichting KWF kankerbestrijding. Zonder de subsidie waardoor ik als arts-onderzoeker aangesteld kon worden, was het onderzoek doen niet mogelijk geweest.

Alle collega's van de afdeling Endocrinologie, kamergenoten en ex-kamergenoten wil ik graag bedanken voor de gezelligheid op de kamer, het samen lunchen/ koffie drinken en het kunnen delen van de frustraties en zegevieringen. Lieve Pauline, ik ben blij dat ik jou heb mogen leren kennen. Veel lief en leed hebben wij samen gedeeld. Beste Carlijn, ik mocht jou begeleiden tijdens jouw wetenschappelijke stage. Nu heb jij het stokje van mij overgenomen, waar ik alle vertrouwen in heb.

Veel dank gaat ook uit naar mijn collega-onderzoekers bij de Medische Oncologie. Dank voor de gezelligheid tijdens het werk, maar ook na het werk op de beruchte vrijdagmiddag Feithhuisborrels inclusief la Chouffe met een 'bitter royale'. Ook heb ik genoten van de weekendjes weg. Beste Rob, dank voor de persoonlijke gesprekken en jouw humor, waar ik altijd weer vrolijk van word.

Lieve vrienden en vriendinnen, jullie hebben er altijd voor gezorgd dat er tijd was voor andere dingen dan werken alleen. Genoten heb ik van onze eetafspraken en (salsa)feestjes. Lieve Astrid en Karst, mijn paranimfen. Ik ken jullie al sinds aanvang van de studie geneeskunde. Ondanks dat we daarna allen onze eigen weg zijn gegaan, bewandelen we hetzelfde traject. Voor jullie duurt het nog even tot de promotie, maar dat gaat ook zeker lukken. Dank voor de gezellige momenten, jullie nuchterheid en steun, de weekendjes weg, de onvoorwaardelijke vriendschap en dat jullie straks aan mijn zijde willen staan!

Lieve Ciska, wat kennen we elkaar al lang. Wat ben ik dankbaar voor onze vriendschap. Onze week samen in Barcelona zal ik niet snel vergeten. Ik heb bij jou altijd het gevoel alles te kunnen delen. Ook al lopen onze agenda's soms over, gelukkig is er vaak wel tijd om elkaar 'live' te zien en anders via Skype. Dank voor het vertrouwen dat jij altijd in mij hebt.

Marie Louise en Anaïs, mijn lieve en stoere zussen. Het is altijd weer een feest om met z'n drieën te zijn. Dank voor jullie gezelligheid en enthousiasme tijdens onze weekendjes samen. Onze band is onvoorwaardelijk.

Lieve pap en mam, jullie hebben altijd in mij geloofd, ook op de momenten dat het wat minder ging. Jullie hebben mij geleerd vertrouwen te houden en door te zetten. Ik ben erg dankbaar dat jullie er voor mij zijn, ik heb jullie voor altijd lief.

En dan tot slot, lieve Johan. Dankjewel dat jij er altijd voor mij bent, dat is voor mij van onschatbare waarde. Je bent een ongelooflijke steun geweest tijdens dit gehele traject. Het is voor mij een feest om samen met jou te zijn, en.. binnenkort zijn we met z'n drieën! Jij haalt het goede in mij naar boven en jij geeft mij de ruimte om te zijn wie ik wíl zijn. Als dat geen liefde is!

Sophie

# Color figures

# Chapter 3

A C D

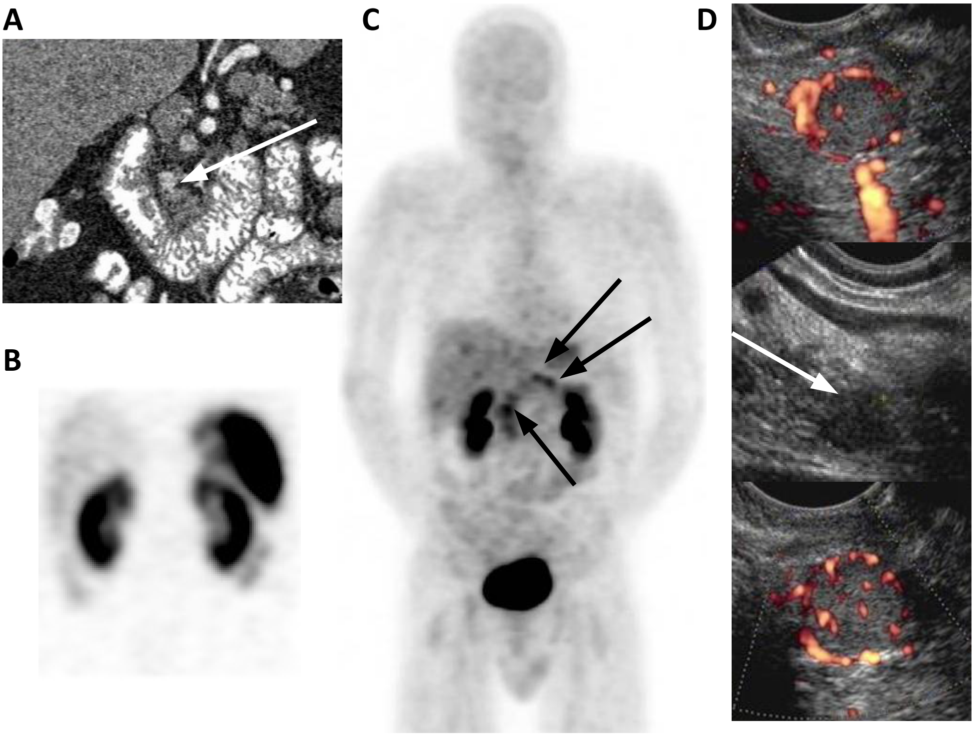

B

***Figure 2. A*** *Coronal images of CT scan,* ***B*** *SRS SPECT image,* ***C*** *maximum intensity projection image of $^{11}$C-5-HTP PET and* ***D*** *ultrasound images of pancreatic lesions visualized with EUS. In total 4 pancreatic solid lesions were detected. With CT, 1 lesion was found. The SRS was negative. $^{11}$C-5-HTP PET detected 3 lesions: 1 in the pancreatic head and 2 in the body-tail region. EUS detected 2 hypoechoic solid lesions in the pancreatic head and 1 in the body-tail region ranging 9.7-14.1 mm. Two solid lesions showed hypervascularity with power Doppler.*

***Color version of Chapter 3, Figure 2 on page 45***

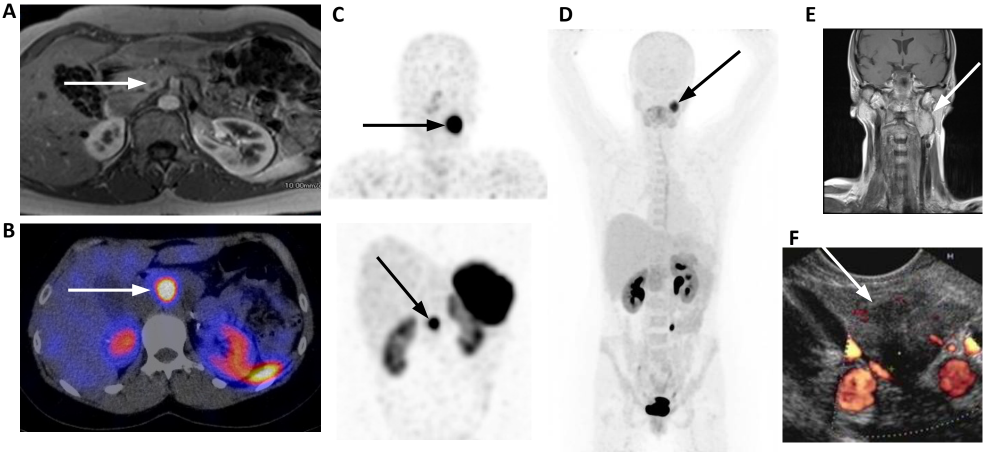


***Figure 3. A*** *Axial image of abdominal MRI (T1 weighted with contrast),* ***B*** *axial image of SRS fused with low-dose CT* ***C*** *SRS coronal SPECT image of head and abdominal region,* ***D*** *coronal maximum intensity projection of $^{11}$C-5-HTP PET,* ***E*** *coronal image MRI image of head and neck region and* ***F*** *EUS image of the pancreas. On abdominal MRI, 1 pancreatic lesion was found, corresponding with 1 focal lesion on SRS. Moreover on SRS, a focal lesion was visualized in the neck region. $^{11}$C-5-HTP PET only showed a lesion in the neck at the same location. MRI of the neck confirmed a paraganglioma. With EUS, the 17 mm pancreatic solid lesion was identified. Cell material obtained by EUS-FNA confirmed the diagnosis of a NET.*

***Color version of Chapter 3, Figure 3 on page 47***

# Chapter 4

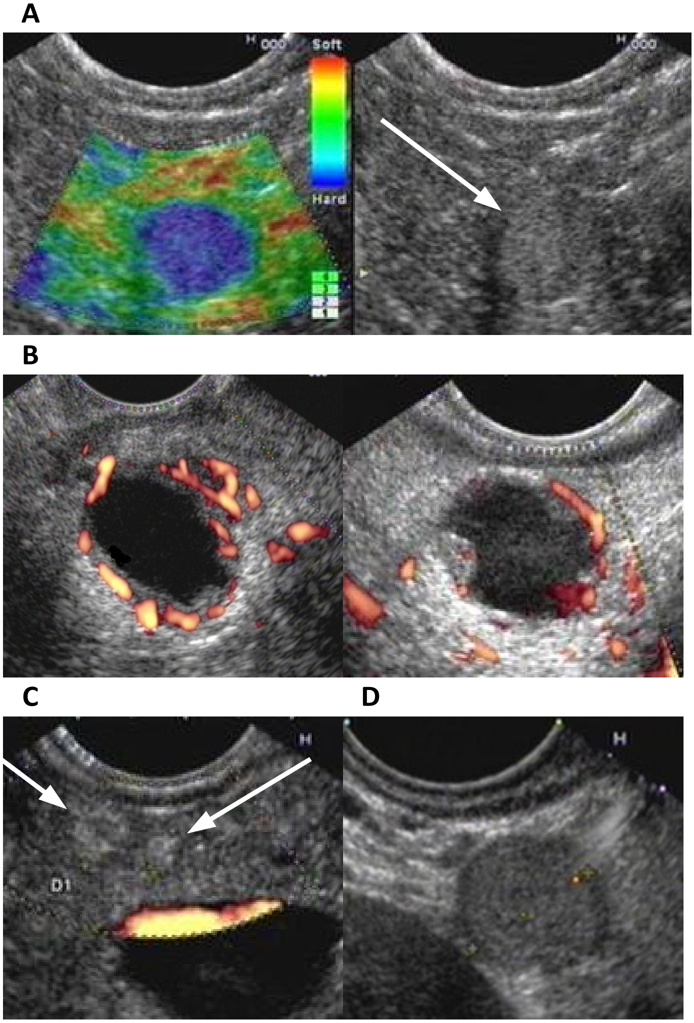


***Figure 2**. EUS images of pancreatic lesions. **A** Elastography image of a pancreatic solid lesion (arrow). Blue color indicates rigidity. **B** Pancreatic cystic lesions with a thick hypervascular wall. Flow is present based on power Doppler, which indicates hypervascularity. **C** Two solid hyperechoic pancreatic lesions (arrows). **D** Pancreatic solid lesion with halo phenomena (black surrounding).*

***Color version of Chapter 4, Figure 2 on page 64***

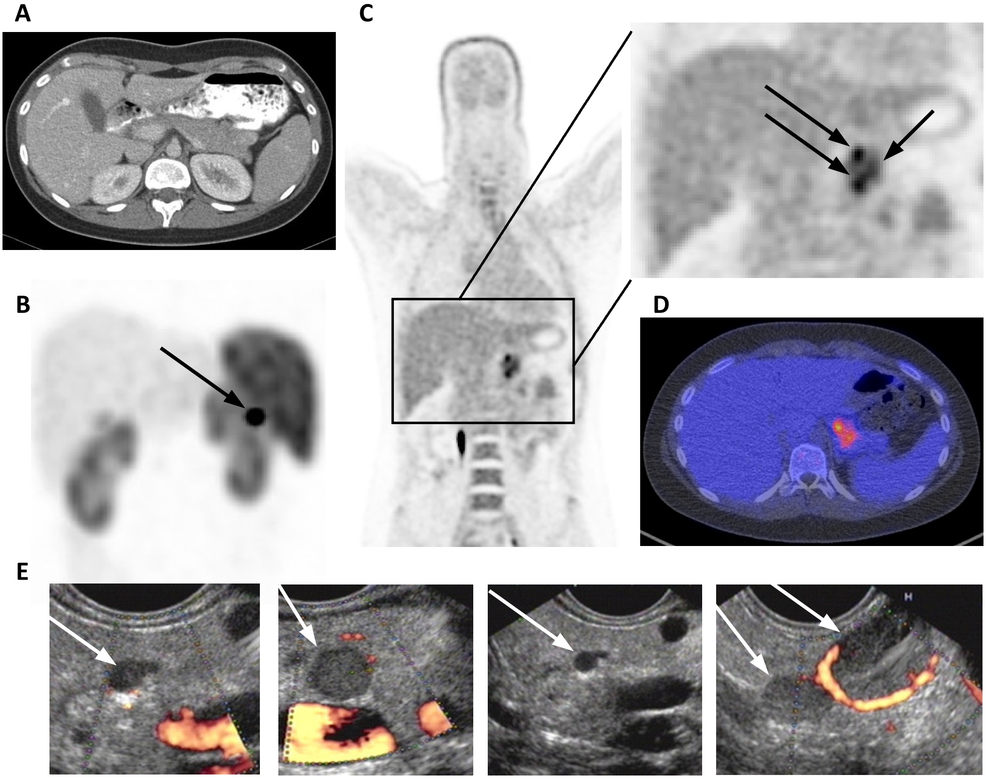


***Figure 3***. ***A*** *Axial image of CT scan,* ***B*** *maximum intensity projection image of SRS and* ***C*** *coronal image of* $^{11}$*C-5-HTP PET and* ***D*** *an axial fusion image of* $^{11}$*C-5-HTP PET with low-dose CT and* ***E*** *images of pancreatic lesions visualized with EUS. With CT no lesion was found and SRS showed 1 lesion located in the pancreatic tail. With* $^{11}$*C-5-HTP PET 3 lesions were visualized in the pancreatic body/tail region. However, EUS visualized 5 hypoechoic lesions: 4 in pancreatic body/tail region and 1 in the pancreatic head, with size ranging from 3.5-14 mm. The lesion of 14 mm showed a clear hypervascular wall with power Doppler.*

***Color version of Chapter 4, Figure 3 on page 67***

# Chapter 5

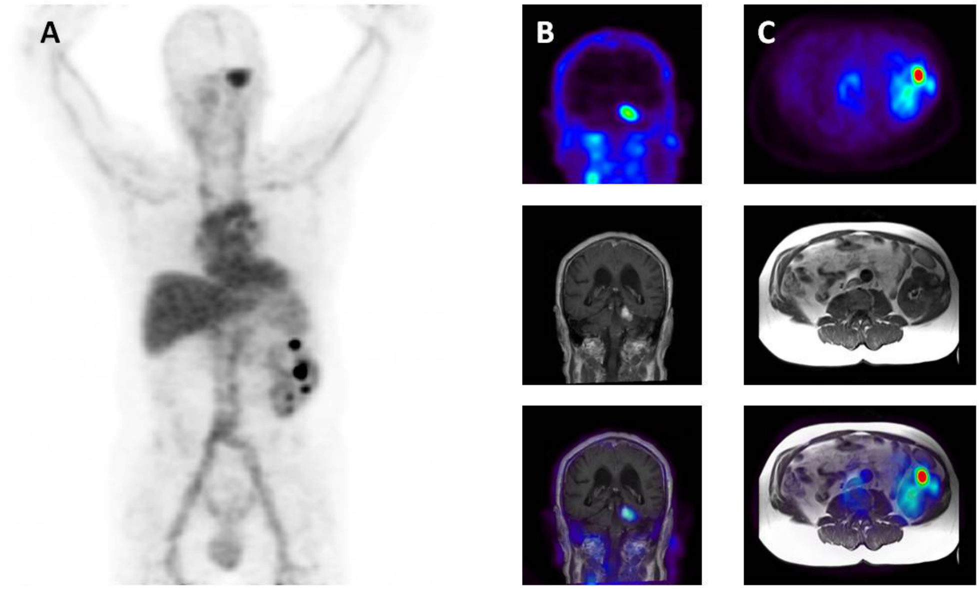


***Figure 1. A*** *$^{89}$Zr-bevacizumab PET scan of patient 4, demonstrating normal antibody distribution with tracer uptake in the blood pool and in the liver, and also uptake in a hemangioblastoma in the cerebellum ($SUV_{max}$ 8.3) and in 6 solid kidney lesions ($SUV_{max}$ 6.6 – 27.6).* ***B*** *Hemangioblastoma visualized by $^{89}$Zr-bevacizumab PET, MRI and the fusion image.* ***C*** *Kidney lesions visualized by $^{89}$Zr-bevacizumab PET, MRI and the fusion image.*

***Color version of Chapter 5, Figure 1 on page 84***

# Chapter 5 supplementary

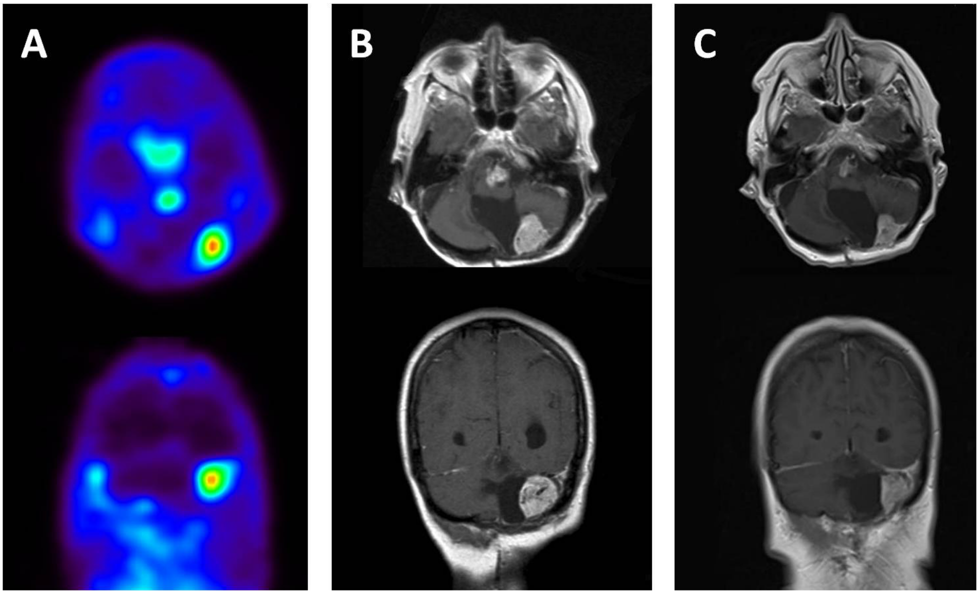


***Supplementary Figure 4. A*** *PET scan and* ***B*** *MRI scans of patient B demonstrating hemangioblastomas in the cerebellum and brain stem before and* ***C*** *after 3 months of bevacizumab treatment.*

***Color version of Chapter 5, Supplementary Figure 4 on page 97***

# Chapter 6

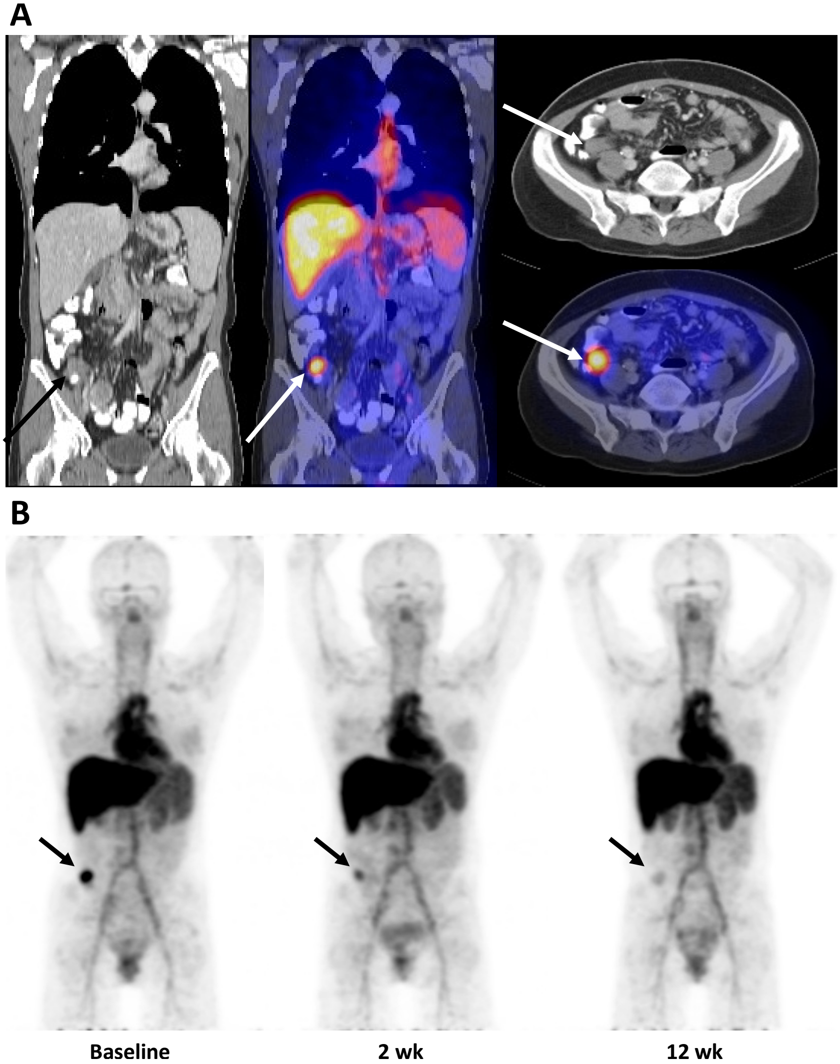


***Color version of Chapter 6, Figure 2 on page 108***

***Figure 2.*** *PET images 4 days after $^{89}$Zr-bevacizumab injection in a patient with metastatic midgut carcinoid.* ***A*** *Coronal and axial images of low dose CT and fusion images of PET and low dose CT shows increased tracer uptake in the abdominal tumor lesion.* ***B*** *Coronal PET images at baseline, 2 weeks and 12 weeks of everolimus treatment. Physiological $^{89}$Zr-bevacizumab uptake is present in the heart (blood pool), liver, spleen and circulation. At baseline, increased $^{89}$Zr-bevacizumab uptake was found in the tumor lesion located in the ileocecal angle. Tumor uptake was 43% lower at 2 weeks and 69% lower at 12 weeks while on everolimus.*